UCRL-53393
Distribution Category UC-35

Shaped-Charge Penetration in Concrete: A Unified Approach

Doctor of Engineering

Dissertation

by

Michael John Murphy

Manuscript date: January 14, 1983

LAWRENCE LIVERMORE LABORATORY
University of California • Livermore, California • 94550

Available from: National Technical Information Service • U.S. Department of Commerce
5285 Port Royal Road • Springfield, VA 22161 • $14.50 per copy • (Microfiche $4.50)

Shaped Charge Penetration in Concrete: A Unified Approach

By

MICHAEL JOHN MURPHY
B.S. (University of California, Berkeley) 1974
M.S. (University of California, Davis) 1975

DISSERTATION

Submitted in partial satisfaction of the requirements for the degree of

DOCTOR OF ENGINEERING

in

Engineering

in the

GRADUATE DIVISION

of the

UNIVERSITY OF CALIFORNIA

DAVIS

Approved:

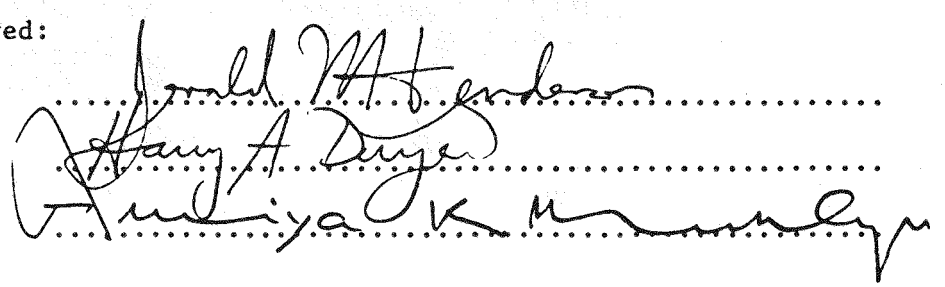

COMMITTEE IN CHARGE

Deposited in the University Library.....
Date Librarian

TABLE OF CONTENTS

ABSTRACT

A unified analytical approach to the solution of the shaped-charge penetration in concrete problem has been developed and is presented in this paper. The analytical model is correlated to three types of experiments that study the shaped-charge jet-formation process and resulting penetration phenomena. Hydrodynamic finite-element analysis of the explosive detonation, liner collapse, and jet formation process is compared to a flash x-ray experiment of the jet at 30, 35, 45, 60, and 90 μsec. Analytical predictions of the penetration-time history are compared to experiments where the penetration-time history is monitored. These experiments provide for a determination of the minimum jet velocity for penetration as a function of standoff. Finally, computer predictions of total penetration and hole profile are compared to experiments. These correlations provide for a determination of the jet-energy/target-hole-volume constant. The applicability of the computer model is shown by correlation to three sets of additional experimental data where the liner angle, liner thickness, and explosive type are varied. The following variations in the shaped charge design are studied:

1) 8% thick 6061-T6 aluminum liner with 75, 90, 105, and 120 degree cones and C-4 explosive;
2) 4% thick 6061-T6 aluminum liner with 100, 105, 110, 115, and 120 degree cones and octol explosive;

3) 105 degree 6061-T6 aluminum liner with 2, 4, 6, and 8% thick cones and octol explosive.

The method developed has been shown to be valid for a broad range of shaped-charge designs in concrete targets. Preliminary investigations, with other target materials show the method can be extended to a generalized shaped-charge design into any target as long as some basic target-material properties are known.

This work is dedicated to my wife, Jean for her love and support

ACKNOWLEDGEMENT

I take this opportunity to thank the many people who have helped make this work possible. I would like to thank my wife, Jean, who perservered throughout the study leading to this dissertation. I thank my parents, Jim and Madeline Murphy, for providing me the financial freedom to pursue my undergraduate studies and the encouragement to pursue this advanced degree. Special thanks go to Joseph Hershkowitz for his overall and technical guidance as well as his constant attention to detail that is required in accomplishing a complete study. Similarly, special thanks go to Mildred Rundquist for her long hours at the word processor and her attention to detail that is required in typing and editing a dissertation. My appreciation is extended to my thesis advisor, Jerald Henderson and thesis committee members Amiya Mukherjee and Harry Dwyer for giving me the freedom to approach this study on an independent basis while providing the guidance necessary to get it completed.

I would also like to thank the members of the Non-Nuclear Ordnance Program at the Lawrence Livermore National Laboratory for their time and efforts in making this study possible.

Franklin Walker	for providing the funds to pursue the study
Ronald Varosh	for his guidance and direction
Coleman Johnson	for providing the impetus necessary for getting hardware made on a "low priority" study

Vern Williamson	for drafting support
Dick Dunstan	for coordinating the delivery of the shaped charge and experimental hardware
Sparky Livensparger	for assembling the shaped charge and experimental hardware
Jack Davis	for the shaped charge high explosive assembly
Mark Accatino	for explosive testing support
Site 300 personnel	for support of remote testing of the shaped charges

Finally, I would like to thank several people at LLNL as well as the ME Department of LLNL for allowing me to pursue an advanced degree while working. My appreciation is extended to Gail Dennis of the ME Education Office for her expert coordination of affairs between U.C. Davis and myself and to her counterpart at U.C. Davis, Dianne Martin. To Steve Sackett for his conscientious editing of the many drafts and to John Hallquist for his customized versions of DYNA2D and ORION. I also thank the TID Graphics Department for their support in generating the report figures. A special thanks is extended to the TID Publications Services Department for their friendly assistance above the call of duty.

This work was performed under the auspices of the U.S. Department of Energy by the Lawrence Livermore National Laboratory under contract number W-7405-Eng-48.

NOMENCLATURE

V_0	jet material collapse velocity (cm/μsec)
ϕ	bending angle of liner during collapse (rads)
D	explosive detonation velocity (cm/μsec)
Vsp	jet stagnation point velocity (cm/μsec)
V_f	liner wall flow velocity (cm/μsec)
M_j	portion of the liner mass that forms the jet (g)
V_j	velocity of the portion of the jet associated with M_j (cm/μsec)
β	angle between the liner wall flowing into the stagnation point and the cone axis (rads)
P_s	stagnation pressure (Mbar)
ρ_j	jet density (g/cm^3)
V	jet velocity (cm/μsec)
U	penetration rate (cm/μsec)
ρ_t	target density (g/cm^3)
PEN	penetration (cm)
σ_j	characteristic jet strength (Mbar)
σ_t	characteristic target strength (Mbar)
E	jet energy ($g\text{-}cm^2/\mu sec$)
C	jet energy/hole volume constant (g/cm-μsec)
τ	target hole volume (cm^3)
ε	equivalent plastic strain

P	pressure (Mbar)
T	internal energy or temperature (^{o}K)
Y	yield strength (Mbar)
G	shear modulus (Mbar)
C_0 to C_6	empirical constants in aluminum material equation-of-state
Ei	initial internal energy of material
μ	relative volume of material
εi	initial plastic strain
Y_{max}	maximum allowable yield stress (Mbar)
A,B,R_1,R_2,ω	empirical constants for JWL high explosive equation-of-state
V	relative volume
P_{cj}	Chapman-Jouguet pressure (Mbar)
ε_{xx}	strain-rate in x direction
VO	spacial location of the virtual origin (cm)
TO	time that the virtual origin is formed (μsec)
TI	target impact time (μsec)
DP	incremental penetration (cm)
DT	time increment (μsec)
T	current time (μsec)
V_{min}	minimum jet velocity for penetration (cm/μsec)
DJ	portion of jet eroded during time DT (cm)
Zi	axial position of the i^{th} node (cm)

Vi	axial velocity of the i^{th} node (cm/μsec)
ER_i	virtual origin error for i^{th} node
V_{tip}	tip velocity of jet (cm/μsec)
V_{tail}	tail velocity of jet (cm/μsec)
DJLI	elemental portion of jet being considered for penetration (cm)
Vol	volume of hole created by jet element (cm^3)
SKE	kinetic energy of jet element ($g/cm-\mu sec^2$)
CTRGT	jet energy/hole volume constant ($g/cm-\mu sec^2$)
RADIUS	hole radius in target (cm)
SO	standoff distance from front surface of shaped charge to target
CD	charge diameters
η	jet penetration efficiency
DEPTH	empirical constant for determination of jet penetration efficiency
NEWDP	new incremental penetration depth
X%	represents liner thickness in percent of charge diameter

DEFINITIONS AND UNITS

liner angle	included angle of conical liner
liner thickness	thickness of liner, measured in percent of the shaped charge diameter
velocity gradient	refers to the velocity gradient between the shaped charge jet tip and tail
Lagrangian mesh	mesh is fixed with respect to materials and moves through space
Eulerian mesh	grid is fixed in space and the materials move through the fixed grid
velocity	cm/μsec
time	μsec (10^{-6} sec)
pressure	Mbar (10^{6} atmospheres)
atmosphere	14.5 psi
distance	cm
mass	g
density	g/cm^3
energy	$g\text{-}cm^2/\mu sec^2$
volume	cm^3
temperature	^oK

I. INTRODUCTION

SHAPED CHARGE PHENOMENOLOGY

The term "shaped charge" is generally used to describe a high explosive cylindrical charge with a lined or unlined cavity formed at one end. The most common shaped charge consists of a detonator-booster explosive train for initiation of a right circular cylinder of explosive which upon detonation collapses a metallic lined conical cavity at the opposite end of the detonator. The phenomenology of the explosive detonation, liner collapse, and resulting jet formation process is described in Fig. 1.

Upon initiation of the explosive, a spherical detonation wave propagates outward from the point of initiation. This high pressure shock wave propagates at the detonation velocity of the explosive (typically greater than 0.8 cm/μsec) and at a pressure level equal to the Chapman-Jouguet pressure (P_{cj} > 0.3 Mbar). As the detonation wave impinges upon the lined conical cavity the material is accelerated inward collapsing the cone. The collapse of the liner material on the centerline forces a portion of the liner to squirt out in the form of a jet with velocites as high as 1.2 cm/μsec. The final frame of Fig. 1 shows a fully formed jet.

Because of the extreme directionality of the energy residing in the jet, it is possible to deliver it to a specific location on a target. The pressure generated in the region of impact has been shown to be so great that the strength of the jet and target materials could be ignored, and therefore, these materials could be

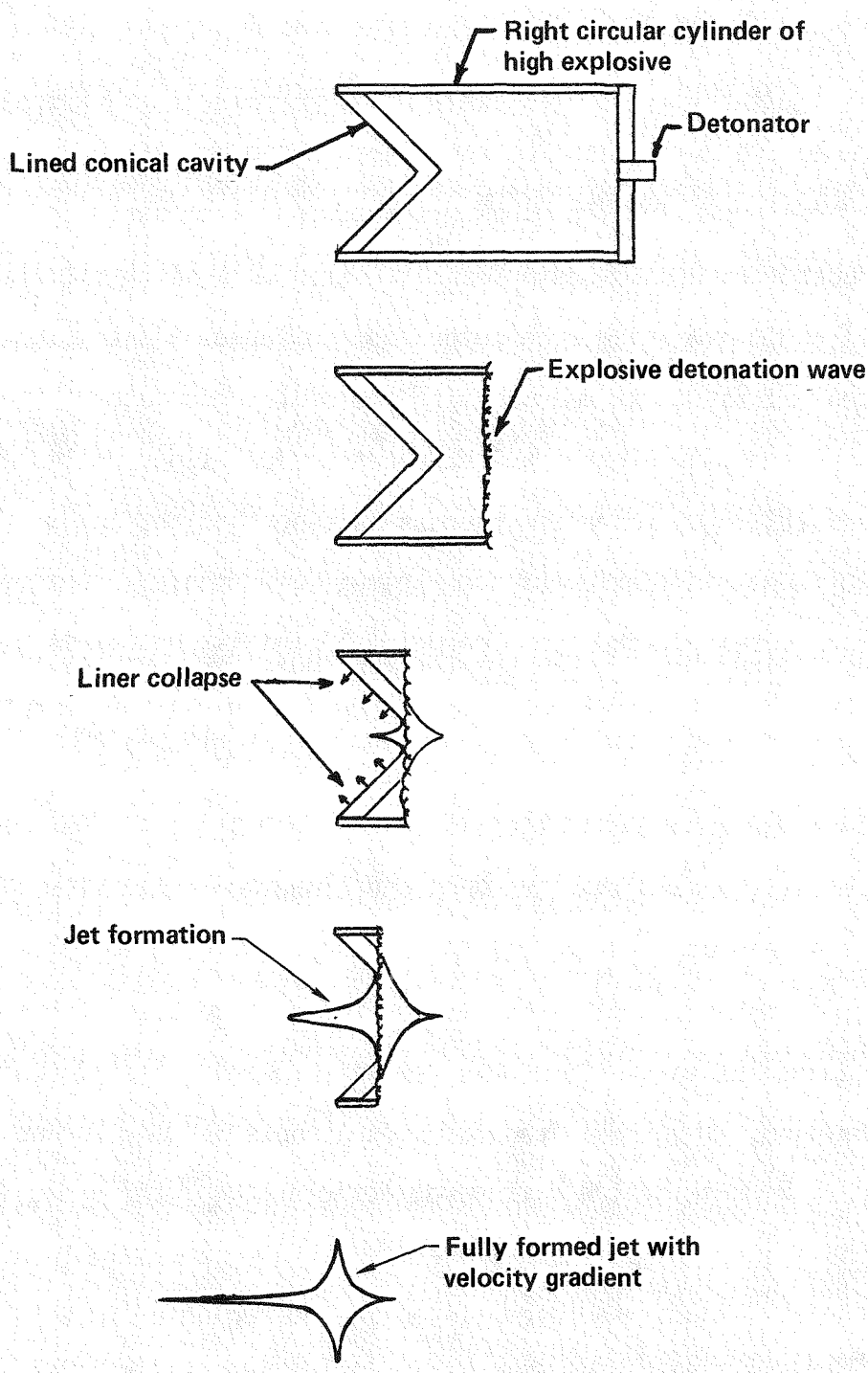

Fig. 1 Shaped charge phenomenology: Explosive detonation, liner collapse, and jet formation

treated as perfect fluids. In 1948, Birkoff, MacDougall, Pugh, and Taylor [1] showed that when the high velocity jet impinged upon the target material it produced pressures close to a million atmospheres (1 Mbar = 14.5 x 10^6 psi) which forced the target material to flow plastically out of the path of the jet. A description of this phenomena in the form of a piecewise penetration process is shown in Fig. 2.

Assume the jet is divided into n elements each of which will penetrate the target in a sequential manner. At initial impact, the first element penetrates the target, creating a hole, and eroding itself away in the process. This is similar to a jet of water creating a hole while penetrating a dirt embankment. The second element impacts the target at the bottom of the hole created by first element. Penetration continues until the jet is totally consumed while doing work on the target in creating the hole.

The overall process, from explosive detonation to total target penetration, occurs in under one-half millisecond (for short standoffs). Due to the extremely high pressures, short time durations, and generally harsh environment that exists in the jet/target interaction region, this is an exceedingly complex phenomena to describe analytically and diagnose experimentally. As early as the mid 1940's, however, experimentalists have shown that performance trends exist when certain shaped charge and target parameters are varied. Similarly, analysts have developed methods to predict the trends with the overall objective being to maximize depth of penetration in metallic targets. Generally, the analytical methods predict either the configuration of the jet without considering the target penetra-

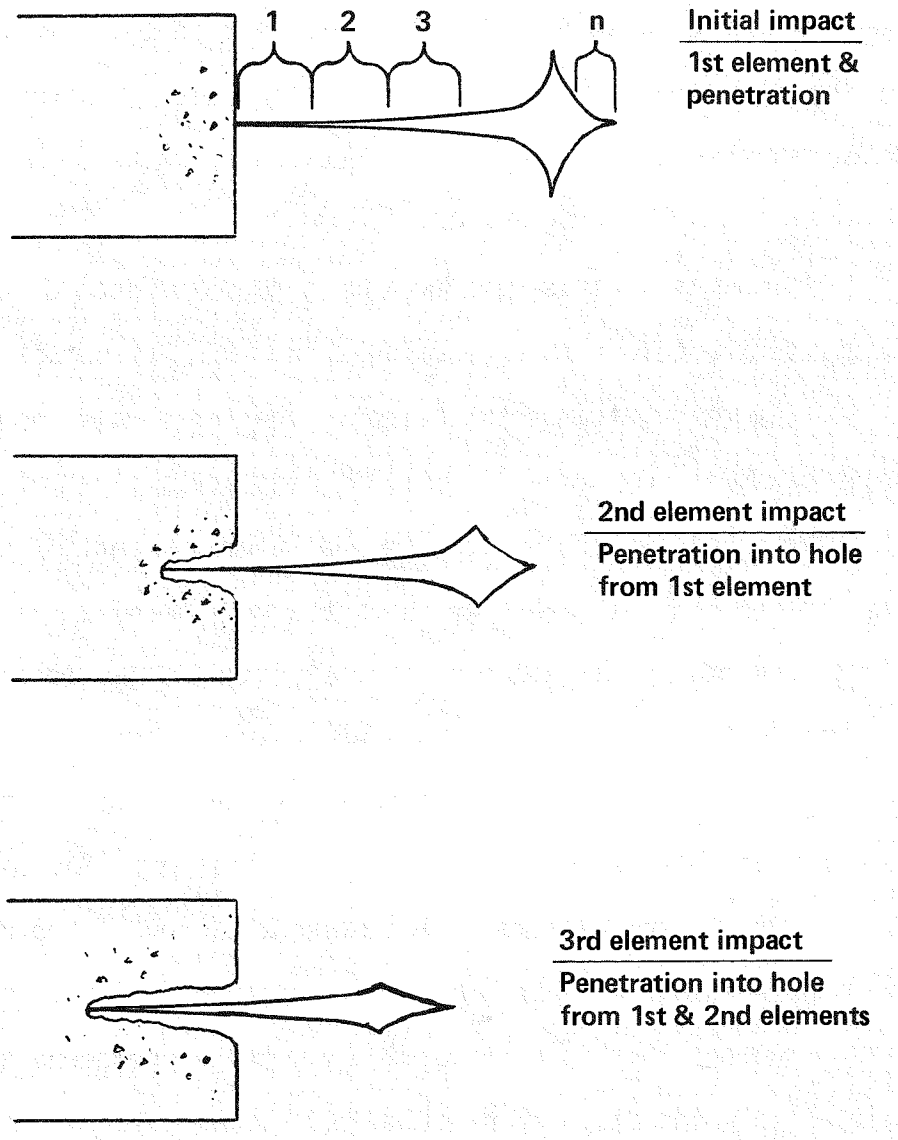

Fig. 2 Piecewise jet penetration process

tion process, or predict the target penetration assuming some prior knowledge of the jet configuration. Aside from a few specialized, empirically tuned codes for armor penetration, a unified approach predicting jet configuration and target penetration in concrete does not exist.

OBJECTIVE OF STUDY

This study was undertaken to determine if the shaped charge phenomenon could be modeled analytically with a unified approach (jet configuration and target penetration) for concrete targets. The overall objectives are to:

1) analytically describe the explosive detonation, liner collapse, and jet formation for a generalized shaped charge design;
2) analytically describe the jet penetration and corresponding hole profile in the concrete target.

Existing theories for penetration of shaped charge jets into homogeneous targets are extensive and well substantiated. For the concrete target, however, their application has not been shown. The basic hydrodynamic theory has not been experimentally verified for inhomogeneous, compressible, brittle materials with low strength. The intent of this project is to incorporate existing hydrodynamic theories into a computer model and experimentally verify them with test data in concrete targets.

APPROACH

The analytical approach being developed is a unified approach in that the computer method models both the explosive detonation, liner collapse, and jet formation process as well as the resulting target penetration for a generalized shaped charge design. The overall approach used to develop the analytical method is a combined experimental/analytical approach.

The emphasis is on analytical correlations to three types of experiments that describe the overall shaped charge penetration phenomena. First, the explosive detonation, liner collapse, and resulting jet formation process will be studied. Flash x-ray experiments which show the geometry of the jet while it is forming will be compared to hydrodynamic finite element predictions. These comparisons show the validity of the analytical technique for modeling the explosive detonation, liner collapse, and subsequent configuration of a fully formed jet. Second, analytical predictions of the penetration of the jet derived from the hydrodynamic analysis are compared to experiments where the penetration/time history is recorded. Finally, analytical predictions of the total penetration and hole profile are compared to experiments where the final geometry is measured.

The configuration of the shaped charge used is shown in Fig. 3. This is called a peripherally initiated shape charge because the detonation wave which collapses the liner originates from the outer surface of the explosive. Upon firing the detonator, a detonation wave propagates radially outward going around the inert foam wave shaper. Thus, peripheral initiation is achieved.

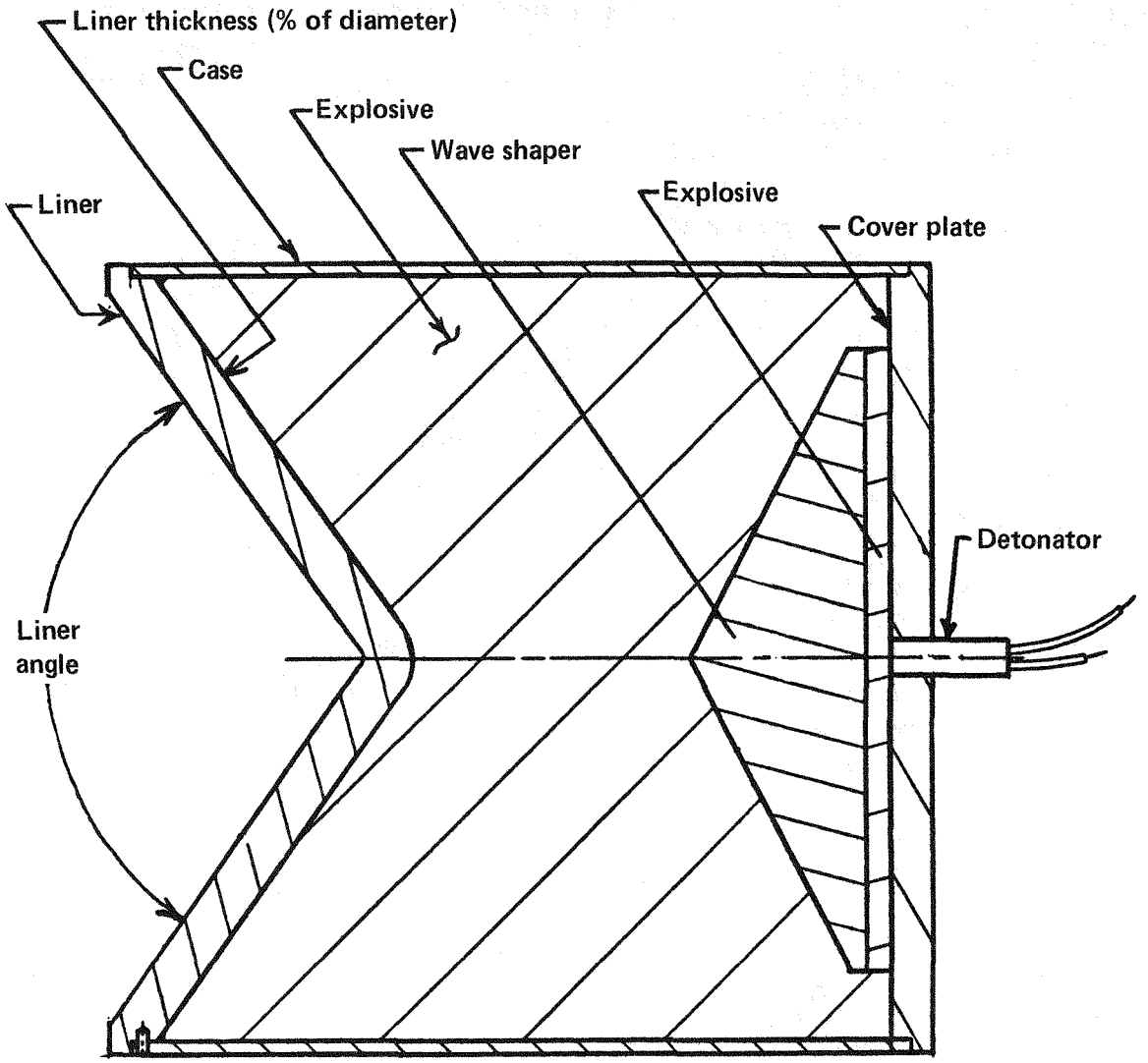

Fig. 3 Configuration of peripheral initiated shaped charge

II. THEORY

HISTORICAL OVERVIEW

The shaped charge has been called a number of things over the years since its first known reference as the "hollow charge principle" in 1792.[1] In its first application, mining engineers realized that some of the pressure generated by an explosive charge could be directed and concentrated on a localized area by hollowing out some explosive opposite to the area. Later references to this concept became known as the Munroe (1885) effect in England and the United States, the Neumann (1911) effect in Germany,[1] and the cumulation effect in Russia.[2,3] Rollings, et al.[2] state that there is no evidence that Munroe or Neumann discovered the lined cavity effect which Baum [3] has credited to Sukhreski in his systematic investigation of the cumulation effect. R. W. Wood (1936) is credited by Eichelburger [4] for recognizing the enhancement obtained by lining the hollow charge with a metal.

It wasn't until the 1940's that real advances in the design of shaped charges appeared. During World War II its primary usefulness was for penetration of hardened targets (armor, bunkers, fuel storage tanks). During this period the shaped charge was placed at the front end of a rocket propelled projectile (such as a bazoka). This projectile had a distinct advantage over ordinary projectiles because the depth of penetration was virtually independent of impact velocity. As reported by Simon and DiPersio [5] the shaped charge has also been employed for assorted peaceful purposes in the oil[6] and steel industries, in geophysical prospecting, mining,[7,8,9] quarrying, in salvage operations, boring holes in demolition

work,[10] breaking large rocks, as linear cutting charges for destruct devices in missiles,[11,12,13,14] and for hypervelocity impact studies.[15]

Generally, the methods developed to analytically model the shaped charge effect describe either the jet configuration resulting from the liner collapse and jet formation or the target penetration process. The following sections describe one-, two-, and three-dimensional theories used to develop the analytical models.

ONE DIMENSIONAL LINER COLLAPSE AND JET FORMATION THEORY

The first fairly complete discussion of the hydrodynamic theories of liner collapse and jet formation was presented in an article by Birkoff, MacDougall, Pugh and Taylor[1] in 1948. Their theories were based on a constant collapse velocity for the walls of the conical liner. However, it wasn't until 1952 that Pugh, Eichelburger, and Rostoker[16] showed that a variable collapse velocity resulting in a jet velocity gradient, satisfactorily explained why the jets were several times longer than the original steady-state theory would predict. This new theoretical technique was termed the Pugh, Eichelberger, and Rostoker (PER) theory of jet formation and has since been the workhorse for most one-dimensional computer models describing the jet formation process.

The result of applying the PER theory is presented in Fig. 4. Basically the theory shows that as the liner material is accelerated by the explosive detonation, it collapses on the charge axis, separating into a jet and slug region on either side of a "stagnation point". Knowing the geometry of the charge and the explosive

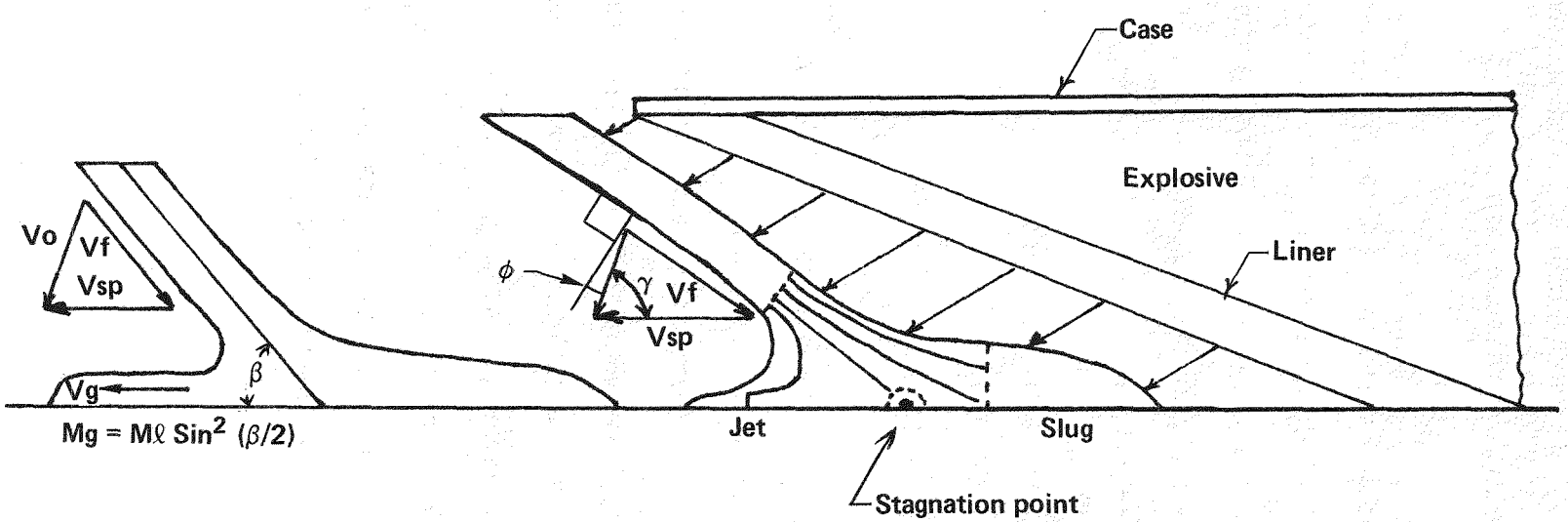

Fig. 4 One dimensional empirical model of explosive detonation, liner collapse, and jet formation

properties it can be shown that an elemental segment of the liner will be projected toward the axis at a velocity, V_0, with a bending angle ϕ according to the following relationship

$$V_0 = 2D \sin \phi/2 \qquad \text{II-1}$$

where D is the explosive detonation velocity. Using a coordinate system attached to the stagnation point and moving with velocity V_{sp} it is possible to determine the jet velocity. Denoting the velocity of the liner wall flowing into the stagnation point as V_f, and the angle between it and the cone axis as β, the jet velocity and mass equations are

$$V_j = V_f + V_{sp} \qquad \text{II-2}$$

$$M_j = M_L \sin^2(\beta/2) \qquad \text{II-3}$$

where V_j, is the jet velocity, M_j is the mass of the jet, and M_L is the mass of an elemental segment of the liner.

Although the PER method has a theoretical basis it requires a few empirical parameters before it can be applied. An implementation of this theory along with the specification of the required empirical parameters for a wide variety of armor penetrating shaped charges can be found in the BASC code written by J. T. Harrison.[17] The BASC code and empirical parameters have been written and defined for modeling shallow angle shaped charge penetration in metallic targets.

TWO AND THREE DIMENSIONAL METHODS FOR LINEAR COLLAPSE AND JET FORMATION

The two and three dimensional approach to the liner collapse and jet formation process basically consists of hydrodynamic finite element and finite difference techniques. These techniques can be broken down into Lagrangian or Eulerian formulations. In a Lagrangian formulation, the mesh describing the problem geometry and materials is fixed with respect to the materials and moves through space as deformations occur. With an Eulerian formulation, the grid is fixed in space and the materials move through the fixed grid. The Eulerian formulation has the advantage that the large deformations typical with shaped charges do not control the solution time of the problem. Diffusion at material boundaries, however, is a problem as the interface between materials is not explicitly defined. Conversely, with a Lagrangian formulation the definition of material boundaries is inherent to the method used and no diffusion occurs, but time step problems generally make it impossible to continue an analysis until the jet is fully formed. The time step in the Lagrangian system is calculated based on the minimum shock transit time through the smallest zone. As deformation occurs, many zones become stretched in one direction and compressed in the other driving the time step to an unacceptably low value.

With the advent of large computers like the CRAY-1 and fully vectorized programming,[18] along with advances in Lagrangian finite-element methods, it is now possible to calculate the explosive detonation, liner collapse, and jet formation process with a minimal amount of computer time (see Fig. 5). Figure 5(a) shows the

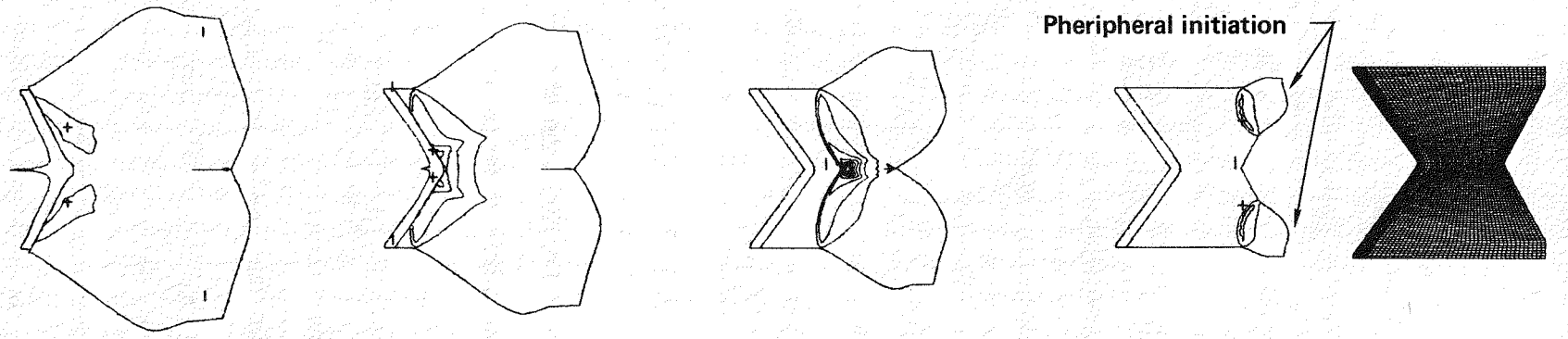

(a) Explosive detonation — contours of pressure

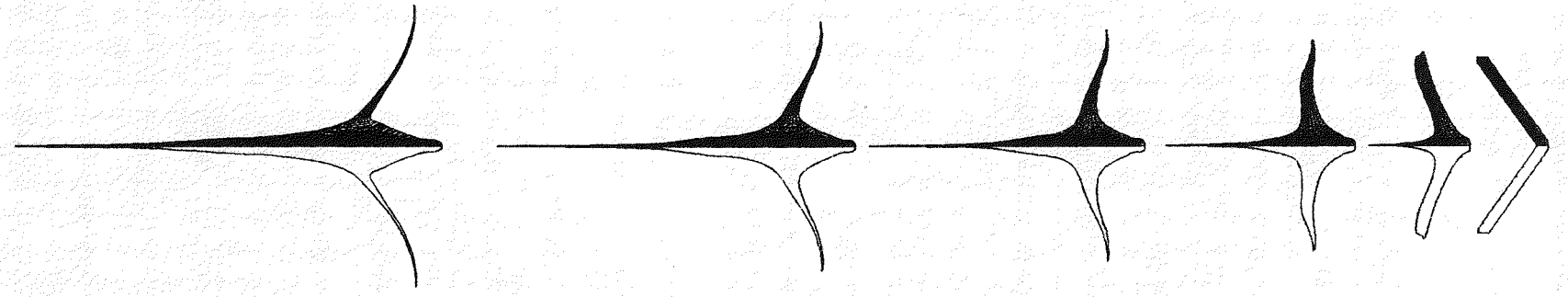

(b) Liner collapse and jet formation

Fig. 5 Two dimensional Lagrangian hydrodynamic analysis of explosive detonation, liner collapse, and jet formation

original finite element mesh and resulting pressure contours from pheripheral initiation of the explosive. As the explosive detonation wave impinges on the conical liner, the material is accelerated, collapsing on the axis of the charge. Figure 5(b) shows the subsequent total liner collapse and jet formation to the point where the kinetic energy of the jet has reached a maximum value.

ONE DIMENSIONAL PENETRATION AND HOLE PROFILE THEORIES

The penetration of a homogeneous, nonbrittle material by a shaped charge jet is similar to a jet of water impacting a bank of mud. The basic one dimensional theory of penetration of hypervelocity jets was developed independently by Pugh,[19] and Mott, Pack, and Hill[20] during World War II. This theory is based on the assumption that the pressure exerted on the target by the jet exceeds the yield strength of the target by at least an order of magnitude and thus Bernoulli's hydrodynamic theory can be utilized. Two basic assumptions are necessary to apply the hydrodynamic theory:

1) the target and jet behave as incompressible fluids during the penetration process;
2) flow is assumed to be at steady state when viewed from a frame of reference moving with the penetration velocity so that for the streamline along the axis of symmetry, the stagnation pressure,

   P_s, is given by:

$$P_s = \frac{1}{2}\rho_j(V - U)^2 = \frac{1}{2}\rho_t U^2 \qquad \text{II-4}$$

where

ρ_j = density of jet material

V = jet velocity

U = time rate of change of the depth of the hole (rate of penetration)

ρ_t = density of the target material

Assuming the penetrator has a constant velocity (no velocity gradient), one can solve for U, the penetration rate. Integrating yields the very idealized equation for penetration, PEN, in terms of the jet length, ℓ, and ratio of jet to target density.

$$PEN = \ell\sqrt{\rho_j/\rho_t} \qquad \text{II-5}$$

A description of the one dimensional Bernoulli hydrodynamic model of jet penetration is presented in Fig. 6. This figure shows a jet of length, ℓ, moving with constant velocity, V. The target penetration, U dt, comes at the expense of jet erosion, (V - U) dt, until the jet is totally consumed. Equation II-5 would indicate that the total penetration is:

1) proportional to the jet length (independent of jet velocity and target strength);
2) proportional to the square root of the jet density;
3) inversely proportional to the square root of the target density.

There are two important cases for which the simple theory outlined above is insufficient to fully account for the observed penetration.[20]

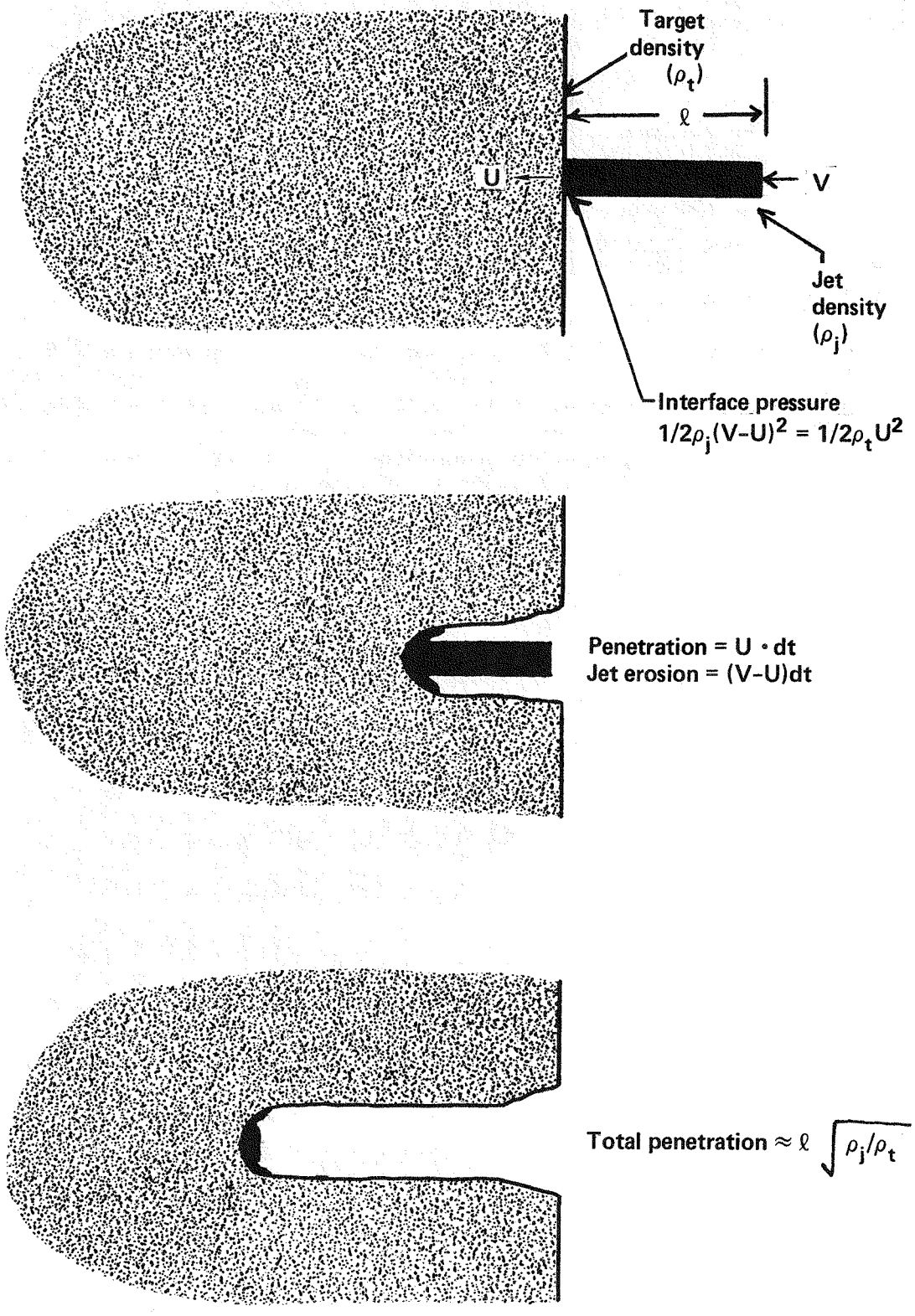

Fig. 6 One dimensional Bernoulli hydrodynamic model of jet penetration

1. From Eq. II-5 it would be expected that penetration into armor would be the same as into steel since their densities are equal. It is an experimental fact that the depth achieved in armor is definitely less than in steel. The difference may arise from the strength considerations that were neglected in Eq. II-4.
2. From Eq. II-5, the penetration by a given jet is inversely proportional to the square root of the density of the target. Predicted penetration in lead should be less than for steel, however, experiments on lead have resulted in penetration approximately double those which would have been predicted. Even when an adjustment in the ratios of penetration in lead and armor due to the strength differences is included, an excess of penetration is observed in lead. It is apparent that other significant parameters must be considered.

To account for the effect of the strength of the target and jet, an estimator for the target and jet strength is introduced. These additional parameters produce the following form of the hydrodynamic equation.

$$\frac{1}{2}\rho_j(V - U)^2 + \sigma_j = \frac{1}{2}\rho_t U^2 + \sigma_t \qquad \text{II-6}$$

where σ_j and σ_t are a characteristic strength of the jet and target. The following strength estimators have been proposed:

1) dynamic yield stress;[21,22,23]
2) Hugoniot elastic limit;[24]
3) Brinell hardness number.[25]

This equation can now account for the penetration differences in the mild steel and armor, but the modification doesn't help for lead.

Other experimentors have proposed different phases of the penetration phenomena to account for the periods when the basic hydrodynamic theory does not apply due to low jet velocities. These other phases of penetration will not be discussed here as the jet velocities being considered for this study are all in the hydrodynamic regime.

When applying the one-dimensional theories, it is possible to decouple the hole profile calculation from the associated penetration calculation. The two most basic methods of determining hole profile in the target are based on:

1) a linear relationship between target hole volume and the kinetic energy in the jet [26]
2) a relationship between the jet energy and spherical energy "sources" distributed along the line of penetration that produce radial expansion in the target material.[27]

In Feldman's[26] study of lead pellets and jets impacting steel targets, the jet KE per target unit volume is shown to be:

1) the same for jets and pellets;
2) independent of the densities of the pellets and targets as well as impact velocity in the range of 0.35 to 0.65 cm/μsec for the densities studied;
3) directly related to the Brinell hardness number of the target.

DiPersio, Simon, and Merendino[28] provide the equation

$$E = C\tau \qquad \text{II-7}$$

or

$$dE = C\, d\tau \qquad \text{II-8}$$

where dE is the kinetic energy of an incremental portion of the jet which produces the hole volume $d\tau$, and C is an empirical parameter relating the jet kinetic energy to the target hole volume.

A description of the one-dimensional Bernoulli penetration model with hole profile from spherical energy sources is presented in Fig. 7. This method considers the jet as a sequence of spherical energy sources introduced along the line of penetration. The energy sources interact with the target and one another creating a hole as the jet propagates.

The figure shows the initial source/target interaction at a depth, dP1, derived from the Bernoulli penetration method. As penetration continues, the source/source and source/target interaction region is shown for the first four jet energy sources. The final penetration and hole profile is shown for eight spherical jet/target interaction sources.

TWO AND THREE DIMENSIONAL METHODS FOR PENETRATION AND HOLE PROFILE

In general, the two and three dimensional methods apply finite element and finite difference techniques. However, Walters and Majerus[29] have developed a quasi two dimensional analytical model where jet and target flow in the axial and radial directions are taken into account, with the radial flow of the target material uncoupled from the axial flow of the penetrator. A graphical

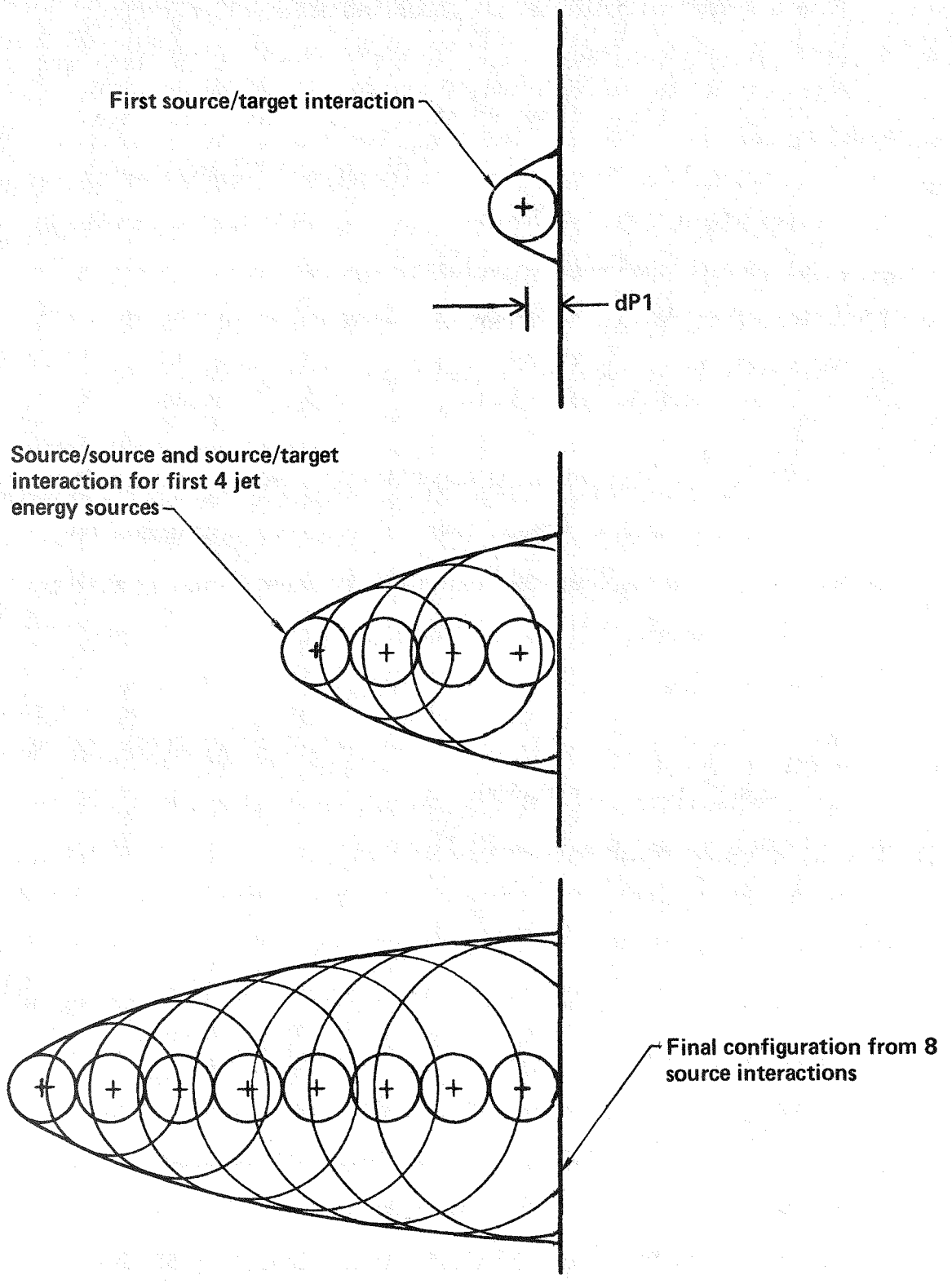

Fig. 7 One dimensional Bernoulli penetration with hole profile from spherical energy sources

representation of their method is presented in Fig. 8. Two regimes of flow are used to describe the localized interaction region between the target and penetrator. Regime A involves a fixed amount of penetrator material contained within the interaction region, moving axially with velocity, U, and displacing target material associated with depth, H. Regime B involves additional penetrator material (due to the relative velocity V - U) flowing in and out of the interaction region. Further refinements and options of the Walters and Majerus model presented above can be found in Refs. 30 through 34.

State-of-the-art hydrocode capabilities now make it possible to solve extremely complex two and three dimensional problems. An example of target response to high velocity penetration studied by Van Thiel and Edwards[35] is presented in Fig. 9. Their study used the coupled Eulerian-Lagrangian code, CHAMP.[36] CHAMP allows for Eulerian flow where material distortion is large and for a full Lagrange treatment further from the penetration path where grid distortions are small.

APPLICABILITY OF THEORY

A number of approaches to the description of the shaped charge phenomena have been discussed. Some involve simple models with empirical parameters to achieve correlation while others involve hydrocode analysis which requries only the configuration and materials of the problem. It is desirable to minimize empirical parameters due to the limitations of the applicability of the resulting analytical model as well as minimizing the excessive

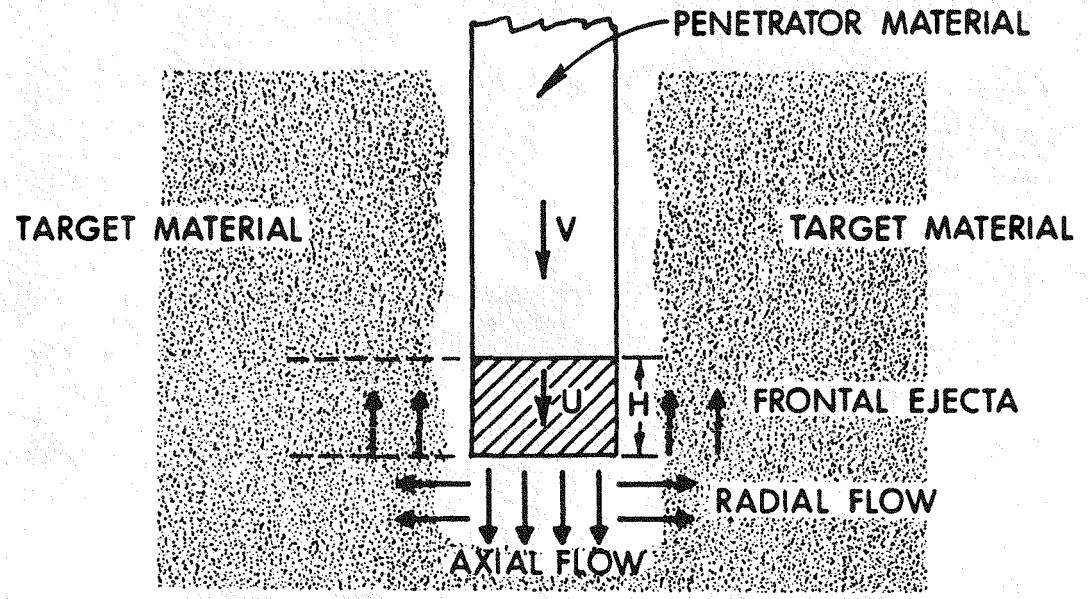

GENERAL TARGET AND PENETRATOR FLOWS FOR REGIME A

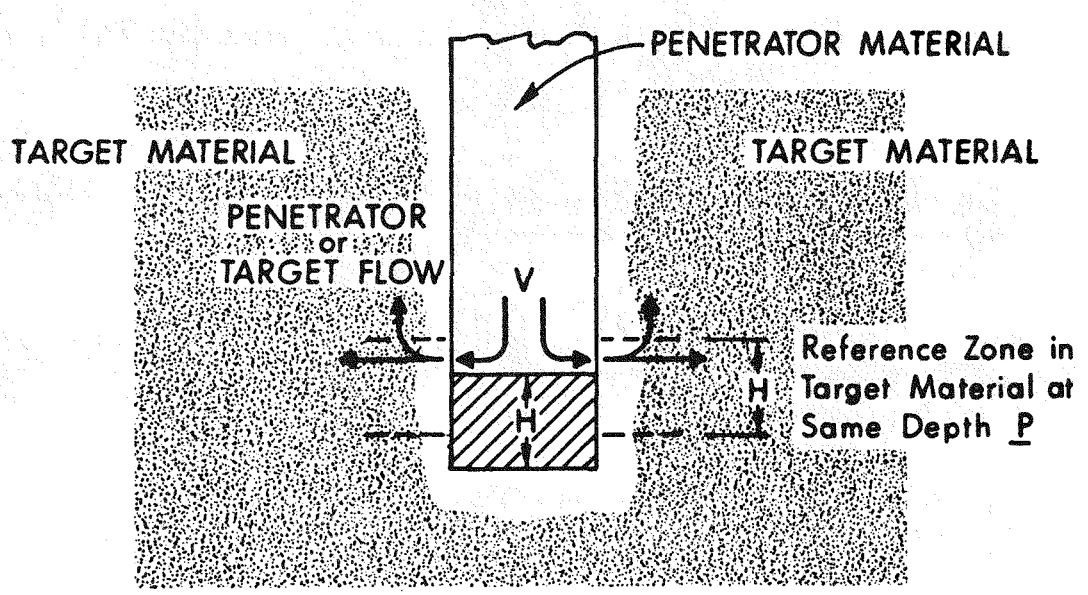

GENERAL TARGET AND PENETRATOR FLOWS FOR REGIME B

Fig. 8 Quasi two-dimensional model with Bernoulli penetration and hole profile from target flow

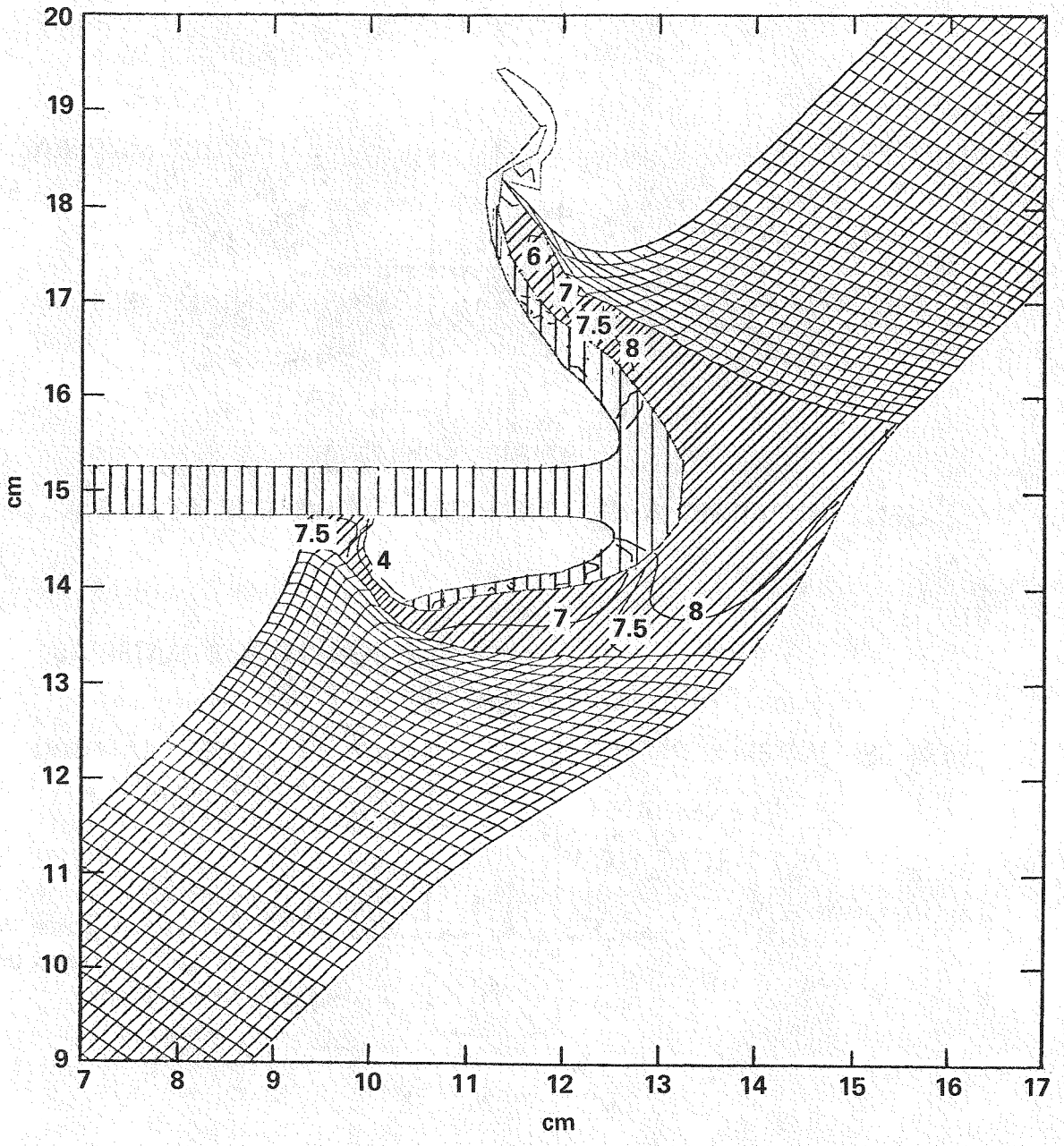

Fig. 9 Two dimensional coupled Lagrangian/Eulerian hydrodynamic analysis

computer times associated with the generalized hydrocode analysis. In this light, the following approach is used.

Liner Collapse and Jet Formation -- A two dimensional hydrodynamic finite element technique will be used to describe the jet configuration. This allows for a fully generalized design of the shaped charge and elimination of all empirical parameters associated with predicting the resulting jet configuration.

Target Penetration -- The one dimensional Bernoulli theory for target penetration will be used as long as the assumptions necessary for the application of the theory are applicable.

Hole Profile -- Due to its simplicity, the basic jet energy/hole volume relationship will be used for predicting hole profile .

III. ANALYTICAL APPROACH

STRUCTURE OF COMPUTER MODEL

The structure of the computer model developed consists of a series of four subprograms linked in a serial mode. The first, second, and fourth subprogram were developed by others and applied to the problem, while the third subprogram was specifically developed for this study by the author. The overall structure of the computer model is presented in Fig. 10. The analytical approach will be described by presenting the function of each subprogram followed by a detailed description of the code written for this study.

MESH GENERATOR SUBPROGRAM

The mesh generator subprogram MAZE[37] is the first code used. MAZE is an iteractive or batch mode mesh generator whose function is to describe the geometry of the problem by assemblying four-node quadralateral elements into a finite element mesh. The geometry of the shaped charge is input into MAZE along with the requirements for the mesh. MAZE determines the coordinates of the nodes, specifies the appropriate element connectivity, and establishes slidelines between adjacent materials that can move relative to one another.

A description of the analytical mesh of the shaped charge is shown in Fig. 11. Note that the wave shaper, case, rear cover, peripheral initiating HE, and detonator are not modeled. The

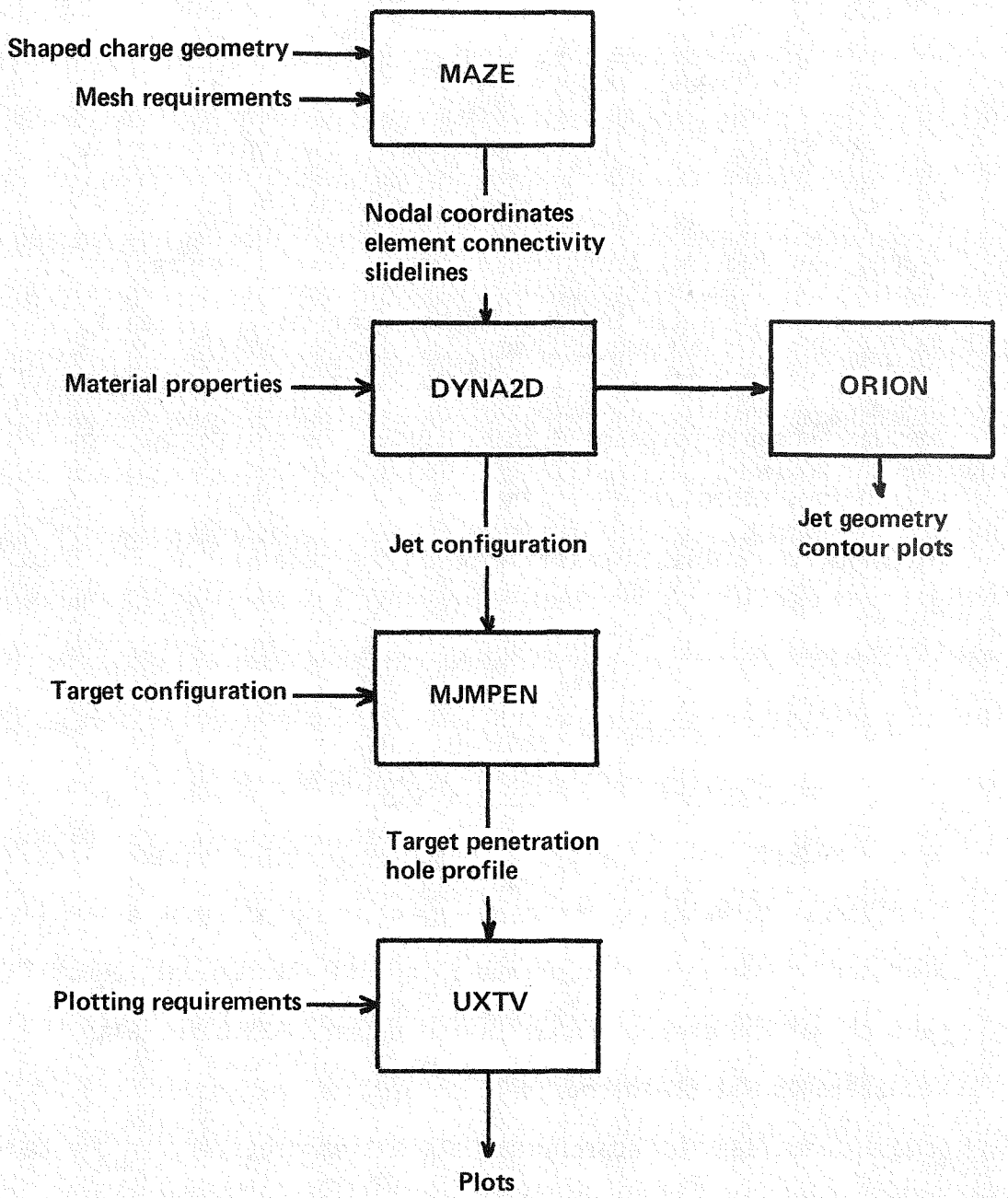

Fig. 10 Structure of computer model

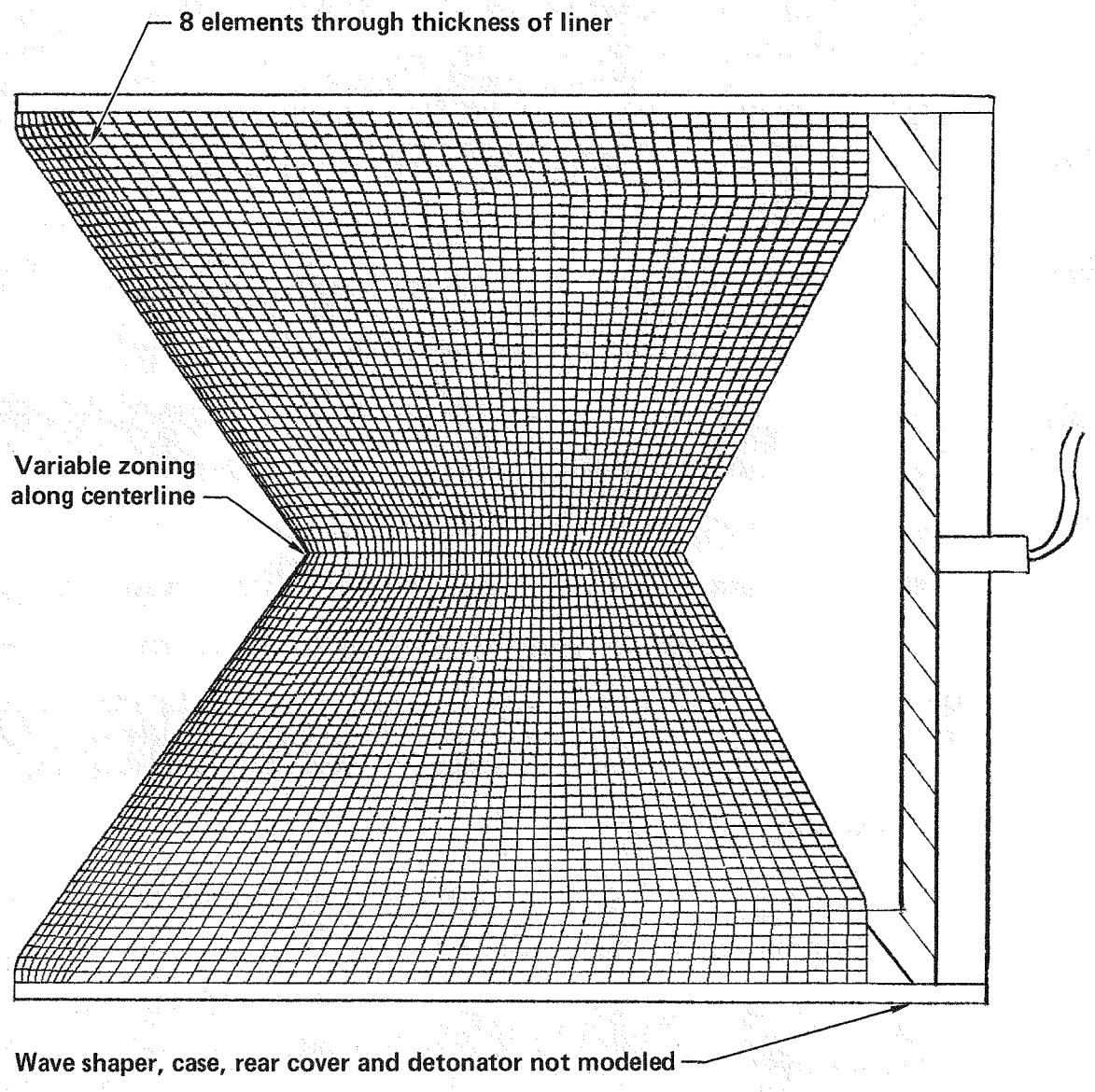

Fig. 11 Analytical mesh of shaped charge generated by MAZE

function of these is to contain and protect the explosive prior to use and to provide a peripheral initiation mechanism and they are not pertinent to the liner collapse and jet formation process. Thicker case confinement may have made it necessary to include the case in the analysis, however, for this problem the case wall was assumed to be thin enough to neglect.

The key factors that make the mesh in Fig. 11 acceptable for describing the shaped charge shown in Fig 3 are:

1) approximately constant aspect ratio zones;
2) nonlinear zoning along the liner axis (required to resolve the high tip velocity associated with this shaped charge);
3) multiple elements through the liner thickness.

The eight elements through the thickness of the liner allow for good resolution of shock wave propagation in the liner. Because the time step in the hydrocode is computed based on the shock transit time through the smallest zone, it is not always prudent to include more zones, but eight zones provide adequate shock wave resolution with an acceptable time step.

LINER COLLAPSE AND JET FORMATION SUBPROGRAM

The hydrodynamic finite-element code DYNA2D[38] used to calculate the explosive detonation, liner collapse, and jet formation process is an explicit, two dimensional, plane strain and axisymmetric, Lagrangian code. It allows gaps and arbitrary two-way sliding between adjacent materials (i.e., the liner and high explosive). Two different types of analytical material models are used to describe the properties of the liner material and high explosive.

The 1100-H aluminum liner material is described with a constitutive model for metals applicable at high strain rates.[39] In hydrodynamic computer codes, the stress-tensor components are split into a hydrostatic equation of state and a modified elastic-perfectly plastic constitutive model. A basic improvement to this model allows for an increase in yield strength with increasing plastic strain (work or strain hardening). The more complex model used to describe the liner material allows for a change in the bulk and deviatoric properties (shear modulus and yield strength) as functions of equivalent plastic strain (ε), pressure (P), and internal energy (temperature, T). This provides for an increase in the yield strength, Y, and shear modulus, G, with pressure and a decrease with temperature. The hydrostatic pressure-volume equation of state, and the constitutive relations for Y and G as functions of ε, P, and T are

$$P = C_0 + C_1\mu + C_2\mu^2 + C_3\mu^3 + (C_4 + C_5\mu + C_6\mu^2)\,Ei \qquad \text{III-1}$$

where

$\mu = \rho/\rho_0 - 1$

ρ/ρ_0 = ratio of current density to initial density (initially one)

Ei = internal energy (initially zero)

and

$$Y = G_0\left[1 + \left(\frac{G'_P}{G_0}\right)\frac{P}{\eta^{1/3}} + \left(\frac{G'_T}{G_0}\right)(T - 300)\right] \qquad \text{III-2}$$

$$G = Y_0[1 + \beta(\varepsilon+\varepsilon i)]^N[1 + (\frac{Y'_P}{Y_0}) \frac{P}{\eta^{1/3}} + (\frac{G'_T}{G_0})(T - 300)] \qquad \text{III-3}$$

subject to the limitation that

$$Y_0[1 + \beta(\varepsilon - \varepsilon i)]^N < Y_{max} \qquad \text{III-4}$$

where, η, is compression, defined as the initial specific volume v_0 divided by the current specific volume v, β, and η are work-hardening parameters, and εi is the initial equivalent plastic strain, normally equal to zero. The subscript 0 refers to the reference state (T = 300 K, P = 0, ε = 0). Primed parameters with the subscripts P and T imply derivatives of that parameter with respect to pressure or temperature at the reference state.

The numerical values of the above defined parameters used in the constitutive equation for 1100-H aluminum are as follows:

C_0 = 0.0	Y_0	=	0.0015 Mbar
C_1 = .7684	G_0	=	.276 Mbar
C_2 = 0.4503	Y_{max}	=	0.0068 Mbar
C_3 = 0.2166	β	=	125.0
C_4 = 2.180	η	=	0.10
C_5 = 0.0	G'_P/G_0	=	65.0
C_6 = 0.0	G'_T/G_0	=	-0.62
	ρ_0	=	2.71 g/cm^3

The expected flow curve for this material is shown in Frame (a) of Fig. 12. When strain hardening is the dominant effect, the curve begins at Y_0 and continues out to a maximum strain hardness of Y_{max}. The solid curve shows the effect of pressure and temperature. During the early stages of deformation when the HE

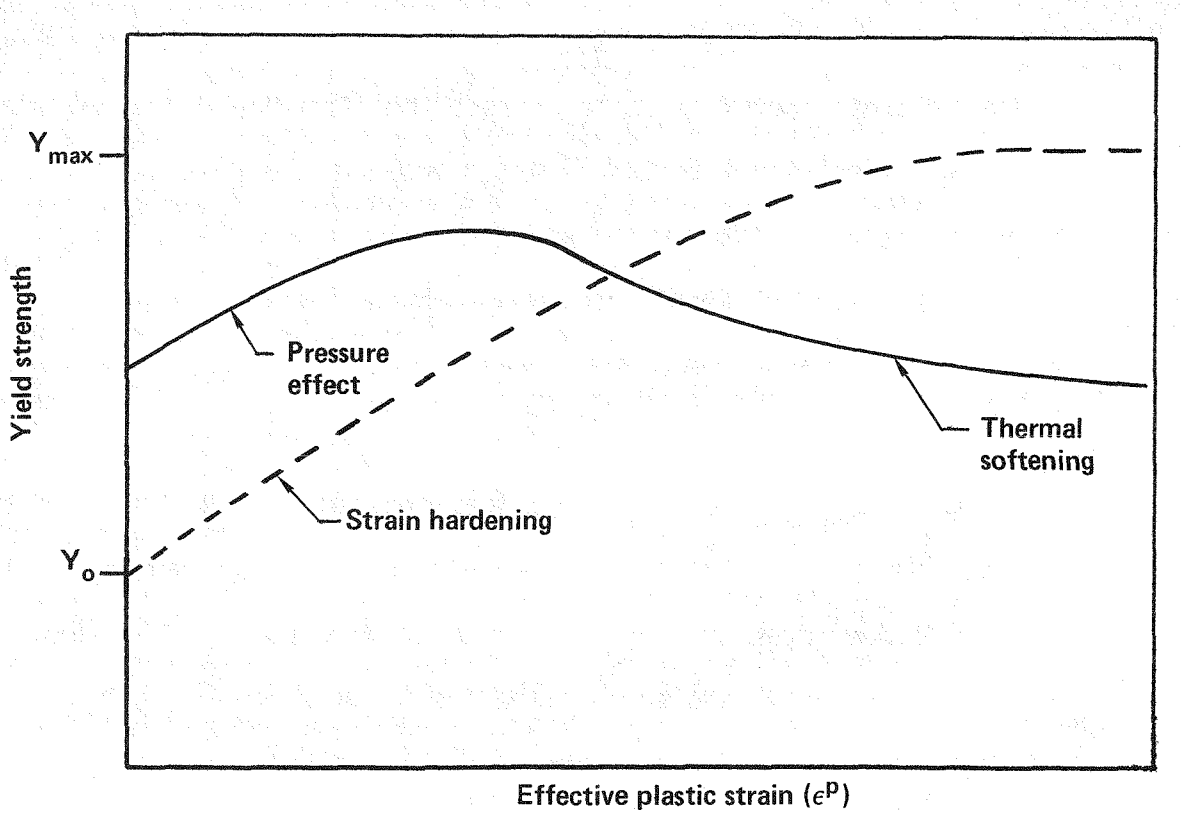

(a) Description of rate-independent high pressure and temperature constititive model of liner material

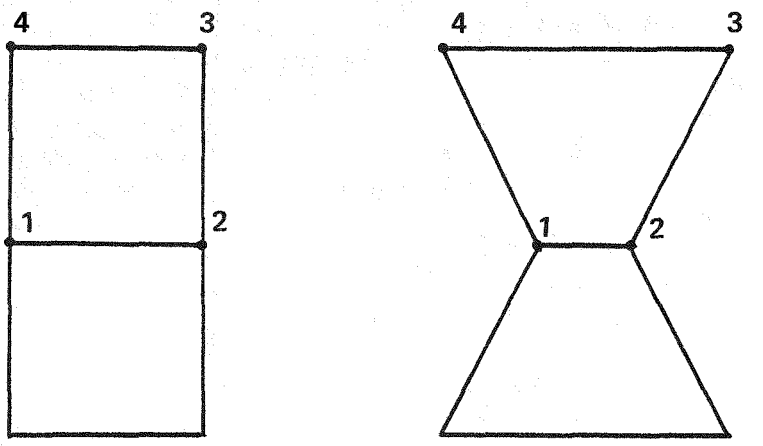

(b) 4 node Lagrangian quadrilateral elements prior to and after hourglass effect

Fig. 12 Liner material constitutive model and description of hourglass effect

pressure is high, the pressure dominates and raises the yield strength. Later in the process, the effect of heating due to a rise in the internal energy tends to degrade the strength of the material.

The explosive material, LX-14, is modeled using the Jones-Wilkers-Lee (JWL), high explosive equation of state.[40] The JWL equation of state defines the pressure, P, as

$$P = A\left(1 - \frac{\omega}{R_1 V}\right)e^{-R_1 V} + B\left(1 - \frac{\omega}{R_2 V}\right)e^{-R_2 V} + \omega \frac{Ei}{V} \qquad \text{III-5}$$

where A, B, R_1, R_2, and ω are empirical constants, V is the relative volume, and Ei is the internal energy. Also needed are the Chapman-Jouguet pressure, P_{cj}, and detonation velocity (D). The empirical constants used to describe the LX-14 are:

ρ = 1.84 g/cm^3

A = 8.524

B = 0.1802

R_1 = 4.6

R_2 = 1.3

ω = 0.38

P_{cj} = 0.370 Mbar

D = 0.88 cm/μsec

Ei = 0.102

By specifying the location and time of initiation, and the detonation velocity, the code calculates the appropriate detonation time of all other elements. When an element is detonated, the pressure is raised to the P_{cj} pressure with the initial relative volume, V, equal to one and internal energy Ei equal to the specified value. From this point on, the pressure decays as the

volume of each element increases according to the pressure-volume equation of state. In this way, the HE applies a pressure to the liner causing it to accelerate. By double integration of the acceleration, a displacement is calculated which allows for more expansion of the HE elements (and lower HE pressure). Basically, this is how the iterative finite element method progresses. However, one more important aspect of the hydrocode must first be considered.

During the course of a calculation, nonphysical "hourglass patterns" can develop in a Lagrange mesh of quadrilateral zones as shown in Fig. 12(b). The reason is that the finite element equations involve only differences in velocities and coordinates of diagonally opposite zone corners.[41] For example, the strain rate in the x direction is given by

$$\dot{\varepsilon}_{xx} = \frac{1}{2A}\left[(\dot{x}_2 - \dot{x}_4)(Y_3 - Y_1)(\dot{x}_3 - \dot{x}_1)(Y_2 - Y_4)\right] \qquad \text{III-6}$$

Thus, grid distortions in which differences in diagonally opposite velocities and coordinates remain constant, cause no strain increase in a zone, and therefore, are not resisted by the zone as they would be in a real quadrilateral piece of material. To eliminate this computational artifact, damping forces which oppose the hourglass effect are added to the other forces on the four zone corners. Since forces are added to all four corners, the total hourglass force exerts no net force on the zone, and momentum is conserved. The method used to calculate the hourglass force is critical as it controls how far a problem will run.

Once DYNA2D has been run for a particular problem, ORION[42] is used to extract the jet configuration from the binary data files that DYNA2D created. ORION will generate plot files showing the geometry of the jet along with various contour plots (velocity, density, pressure, etc.) as the user desires. ORION is not one of the four subprograms necessary to solve the problem but is required for correlation of finite-element calculations and the flash x-ray experiments.

TARGET PENETRATION AND HOLE PROFILE SUBPROGRAM

MJMPEN is the computer code written for the study. It takes the jet configuration from DYNA2D along with the target configuration that is input to MJMPEN and calculates the jet penetration and hole profile in the target. A listing of the program and description of its usage can be found in Ref. 43. Discussion of the more important aspects of the code is provided in section IV.

GRAPHICS OUTPUT SUBPROGRAM

UXTV[44] is used to get hard copies of the plots generated by ORION and MJMPEN. High quality film or VuGraph plots can be obtained overnight, or quick paper plots can be obtained within minutes by specifying the appropriate plotting requirements.

IV. DETAILED DESCRIPTION OF TARGET PENETRATION AND HOLE PROFILE SUBPROGRAM

PROGRAM FLOWCHART

Presented in this section is a detailed description of MJMPEN. As previously discussed, MJMPEN uses the jet description from DYNA2D, along with the target description and computes the total jet penetration and hole profile in the target. A flowchart of MJMPEN is presented in Fig. 13. The following describes the information being specified or calculated in the code.

Input:	Input jet and target variables
Initialize Parameters:	Initialize the various parameters used in the problem.
V_{min}:	Calculation of the critical velocity below which no effective penetration is obtained by the jet material.
Nodal Mass and Velocity:	Calculation of the nodal mass and velocity are required to describe the jet in the MJMPEN program. With this information the jet configuration time history and kinetic energy can be calculated.
Virtual Origin:	The virtual origin is a convenient tool in the study of shaped charge jet penetration. It is assumed that all the jet mass particles are coming from one point in space and

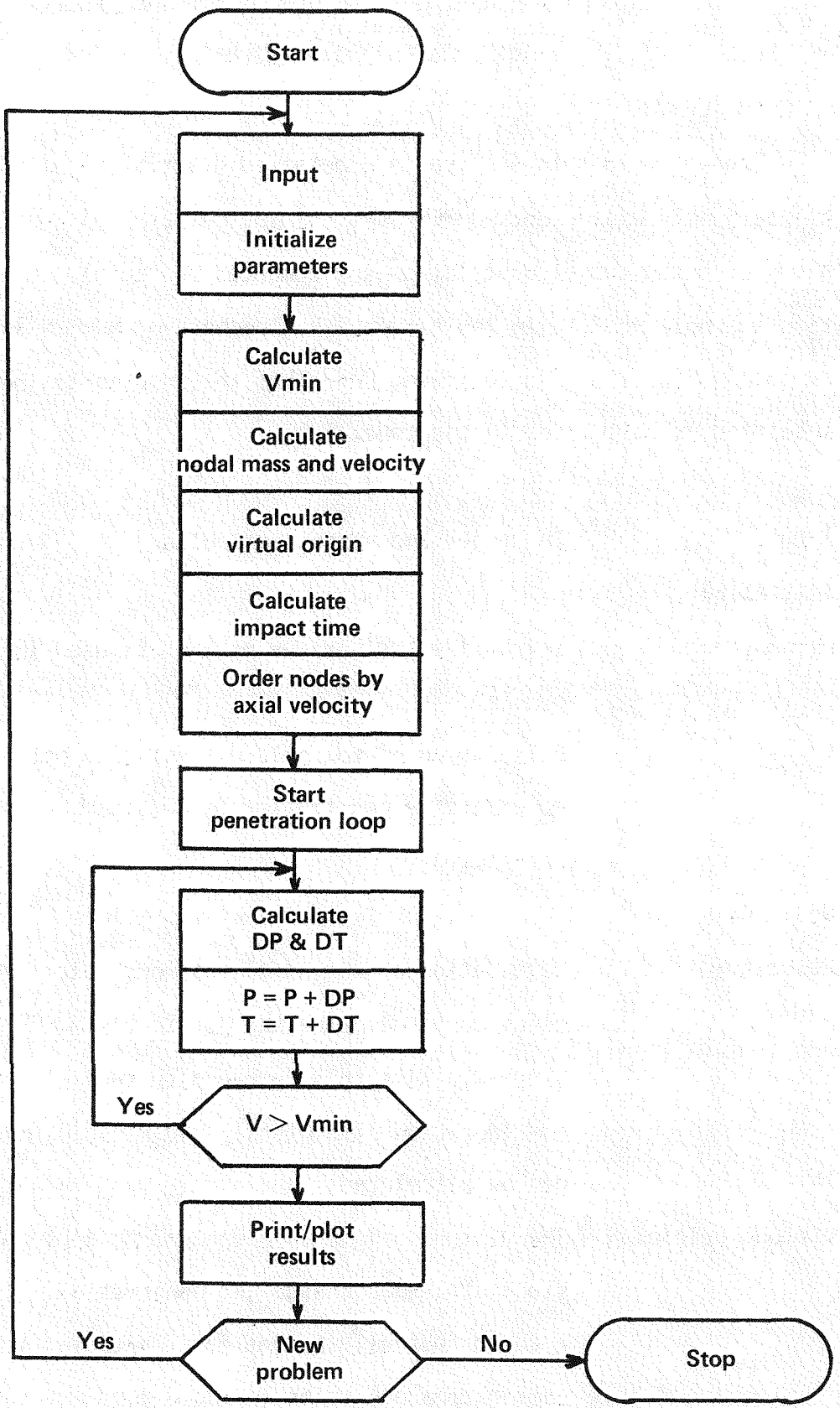

Fig. 13 Flow chart of MJMPEN

time, the virtual origin, each with a different velocity. Since the jet mass particles don't actually originate from the same point in space and time, a leased squared error analysis is used to find the virtual origin.

Impact Time: The impact time, TI, is the time of first jet impact with the target. This is basically the time the virtual origin is formed, $T\phi$, plus the time it takes for the fastest jet element to travel from the virtual origin to the target.

Order Nodes by Axial Velocity: Ordering of the nodes by axial velocity is done to keep track of the sequence in which the nodes impact the target.

Penetration Loop: All calculations up to this point have been to initialize arrays and calculate variables required to do the penetration calculation. This is the start of the penetration calculation loop.

DP and DT: DP and DT are the incremental penetration and time step of each jet element as it penetrates the target. A portion of the jet, DJ, is eroded away while creating the incremental penetraton, DP, during the time increment, DT.

PEN and T: PEN and T are the current depth of penetration and associated time, respectively. In the

penetration loop, PEN = PEN + DP, and T = T + DT where the initial value of PEN and T are zero and TI, respectively.

$V > V_{min}$: After each jet element penetrates the target, a check is made to see if the velocity of the next jet element is greater than V_{min}. If so, the calculation continues; if not, the problem is terminated.

Print/Plot Results: The results are sent to two data files at the end of the penetration process. The first file, OMJM, contains the tabular data of the penetration results. The second file UA80, is a UX80 type file that can be plotted with UXTV. This file contains the penetration/time curve and the hole profile curve.

New Problem: A new problem can be run using the same jet and target parameters. The standoff distance, the distance from the face of the shaped charge to the target, can be changed.

Stop: This indicates the problem is finished. By this point all files have been closed and the problem is completed.

The above description of MJMPEN describes the overall approach used in determining the penetration in the target. The following describes in detail several of the critical calculations made in MJMPEN.

DETERMINATION OF MINIMUM JET VELOCITY FOR PENETRATION

V_{min} is the critical velocity below which no effective target penetration is obtained by the jet material. DiPersio, Simon, and Merendino[28] found the variation of V_{min} with standoff was much more significant than with target material, however, their experiments were into metallic targets at standoffs from 3 to 25 charge diameters. For applications where the desired target hole diameter is equal to the charge diameter, it has been shown that in concrete targets the optimum standoff is approximately 1 charge diameter.[45] Thus, it is not clear whether their data will extrapolate due to the vast variation in jet and target materials (copper into steel) as well as the shorter standoffs. Experimental shots of aluminum jets into concrete at various standoff distances are required to answer this question. Results of the experiments are summarized in Section V.

VIRTUAL ORIGIN METHOD OF JET DESCRIPTION

The virtual origin is the location in space and time where all jet particles originate, each with a different velocity. The concept of a virtual origin was first mentioned by Allison and Bryan in 1957.[46] Allison and Vitali[47] later incorporated the virtual origin into a formal penetration theory in 1963. In the

development of the virtual origin description of the jet, flash x-rays of several fragmented (due to jet stretching) copper jets were examined. The velocities of the jet fragments were monitored at different times and shown to be constant. Using the velocity, the jet fragments were projected back to an initial point near the apex of the shaped charge liner. Since all of the jet fragments were projected back to approximately the same point, the location was termed the virtual origin.

The concept of a virtual origin as described above involved only its position in space. It wasn't until 1981 that Chou, Hirsch, and Walters[48] showed that in order to fully understand and model the kinematics of target penetration using the virtual origin concept it is necessary to extend the virtual origin to a point in the time-space plane. Since the liner collapse and jet formation process occurs so quickly in comparison to the total penetration time, the description of the virtual origin as a point in the time-space plane is a logical extension. This can be accomplished easily when a Lagrangian description of a fully formed jet is available as shown in Fig. 14. The figure shows a shaped charge prior to detonation and a fully formed jet at 40 μsec after detonation. In a Lagrangian system, the position and velocity of each node is known and a plot like the top half of the figure can be generated. This figure shows conceptually how the virtual origin is calculated.

At 40 μsec the position of each node of the jet is known. The slope of the line passing through this point is the inverse of the velocity of the node. A similar line can be generated for each

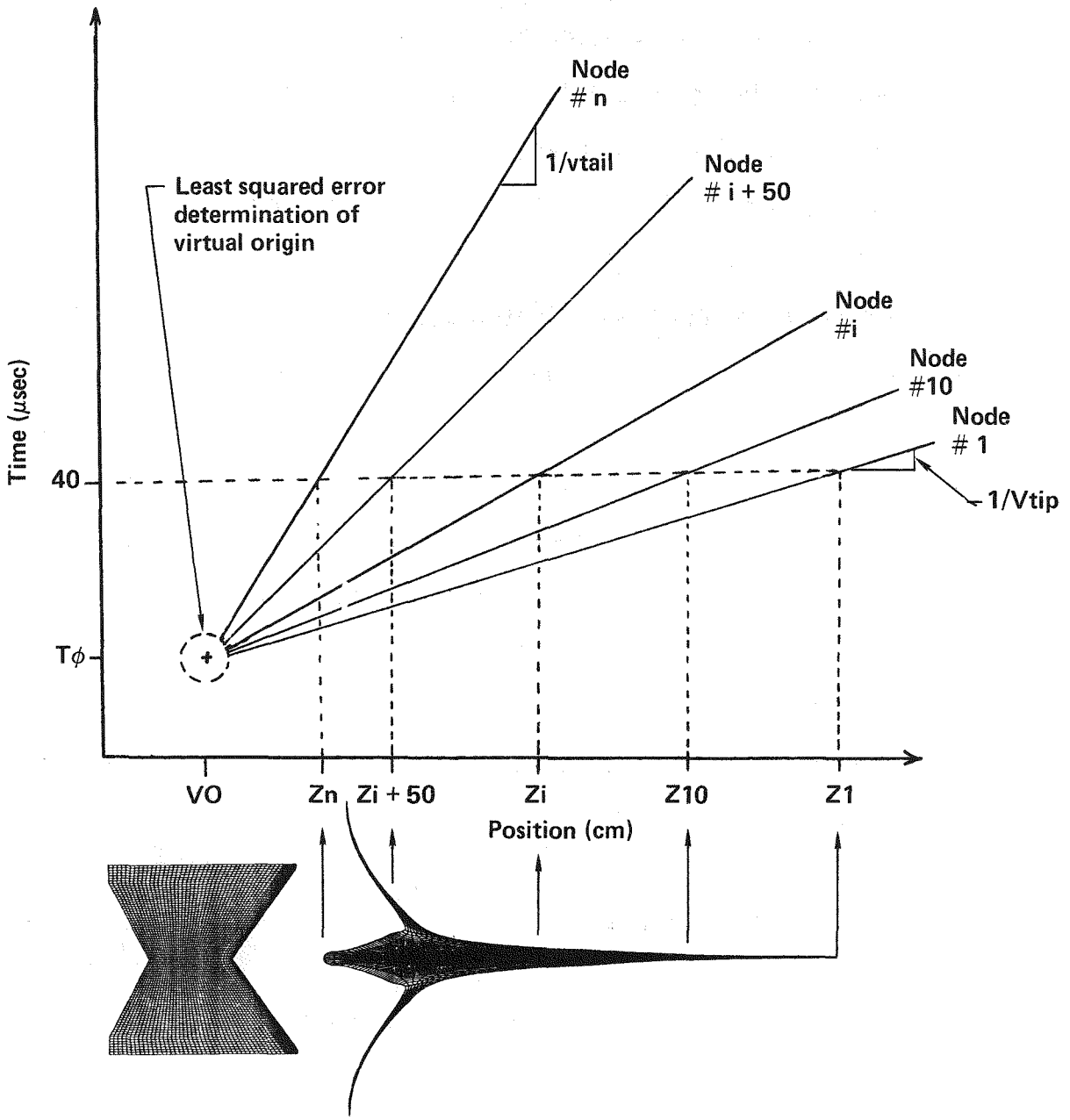

Fig. 14 Least squared error determination of virtual origin

node. The virtual origin is found by extrapolating all of the lines back to a point where they meet in the time-space plane. In actuality, however, they don't all arrive back at the same point. Thus, a least squared error determination of the "best" point is required. The following describes the analytical method used in the code to determine this "best" point in the time-space plane. The spacial position of the virtual origin is defined as VO and the time position as $T\phi$. By defining the position and velocity of each node as Zi and Vi, respectively, the following equation for the nodal position as a function of time can be generated,

$$Zi = VO + Vi(t - T\phi) \qquad \text{IV-1}$$

where Zi is the position at time t. For this example, Zi, Vi, and t are known from the hydrocode calculation. For a fixed t, the following error, ERi, can be introduced because all of the nodal velocity lines don't extrapolate back to the same point.

$$ERi = VO + Vi(t - T\phi) - Zi \qquad \text{IV-2}$$

Now find the best VO and $T\phi$ such that the summation of the square of the error is minimized.

$$\sum_{i=1}^{n} ERi^2 = \text{minimum} \qquad \text{IV-3}$$

This is accomplished by defining a new function, g, such that

$$g(VO, T\phi) = \sum ERi^2 \qquad \text{IV-4}$$

Taking the partial of g with respect to VO and $T\phi$ and setting the equations equal to zero yields the following two equations.

$$\frac{\partial G}{\partial VO} = 2 \sum_{i=1}^{n} [(VO - Zi) + Vi(t - T\phi)] = 0 \qquad \text{IV-5}$$

$$\frac{\partial G}{\partial TO} = -2 \sum_{i=1}^{n} [(VO - Zi) + Vi(t - T\phi)]\, Vi = 0 \qquad \text{IV-6}$$

rearranging the equations results in

$$n \cdot VO - \sum Zi + t \sum Vi - T\phi \sum Vi \qquad \text{IV-7}$$

$$-\sum ViVO + \sum ZiVi - t \sum Vi^2 + T\phi \sum Vi^2 = 0 \qquad \text{IV-8}$$

which produces the following two equations in two unknowns

$$n \cdot VO + (-\sum Vi)\, T\phi = \sum (Zi - tVi) \qquad \text{IV-9}$$

$$(-\sum Vi)\, VO + (\sum Vi^2)\, T\phi = \sum (Vi^2 t - Zi\, Vi) \qquad \text{IV-10}$$

By introducing 6 variables, A_1 through A_6, these equations can be redefined as

$$A_1 \cdot VO + A_2 \cdot T\phi = A_3 \qquad \text{IV-11}$$

$$A_4 \cdot VO + A_5 \cdot T\phi = A_6 \qquad \text{IV-12}$$

where

$$A_1 = n$$

$$A_2 = -\sum Vi$$

$$A_3 = \sum (Zi - tVi)$$

$$A_4 = -\sum Vi$$

$$A_5 = \sum Vi^2$$

$$A_6 = \sum (Vi^2 t - Zi\, Vi)$$

Equations IV-11 and IV-12 can now be solved for VO and $T\phi$

$$VO = (A_3/A_1 - A_6/A_4)/(A_2/A_1 - A_5/A_4) \qquad \text{IV-13}$$

$$T\phi = (A_3/A_2 - A_6/A_5)/(A_1/A_2 - A_4/A_5) \qquad \text{IV-14}$$

INCREMENTAL PENETRATION AND HOLE PROFILE MODEL

The methodology used in calculating the incremental penetration and hole volume is presented in Fig. 15. At time $t = T\phi$, the

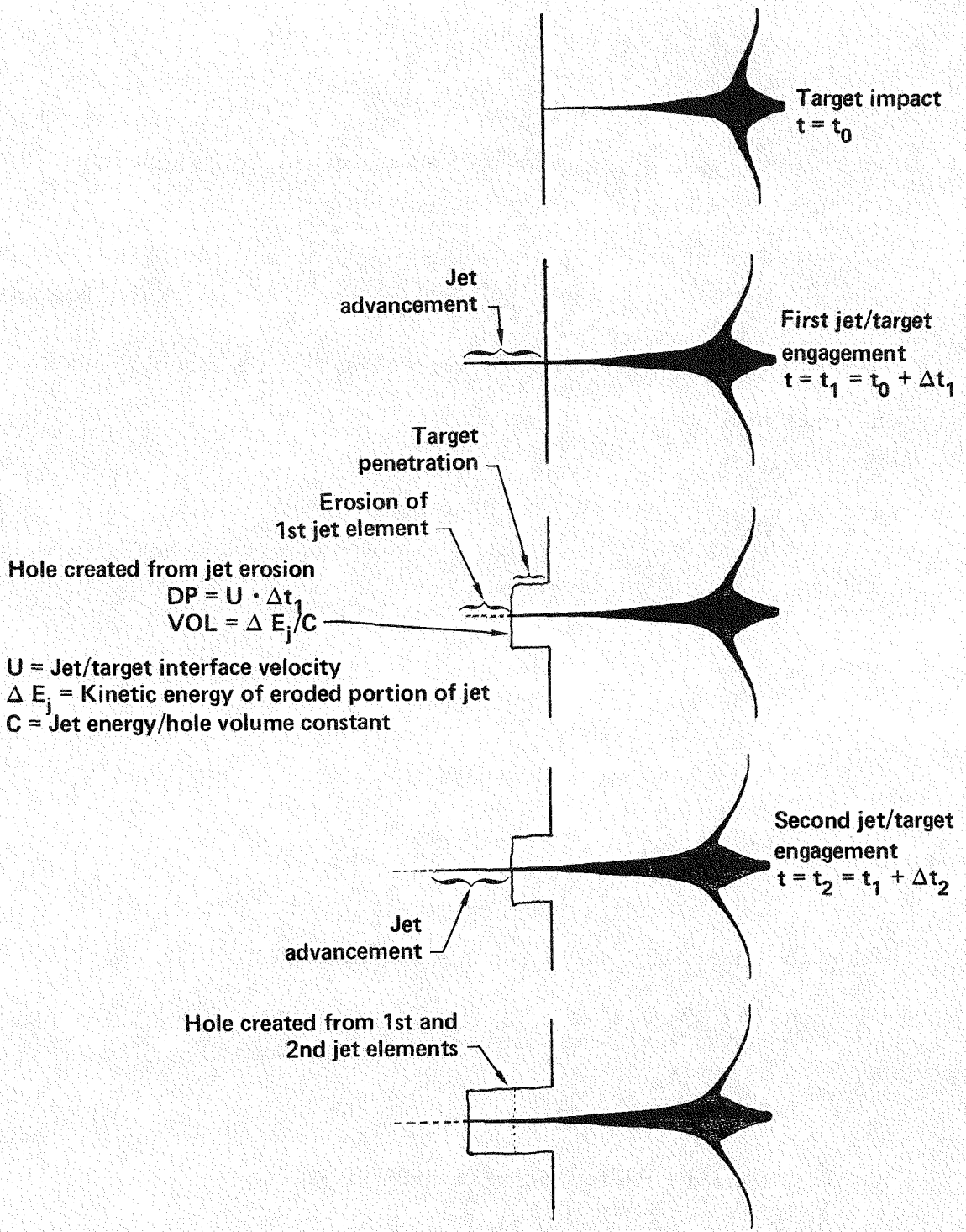

Fig. 15 Piecewise penetration and hole volume methodology

first jet particle will reach the front surface of the target. At this point the portion of the jet to be considered for the first jet/target engagement is specified as an input value. Once the target penetration of this portion of the jet is determined, the hole diameter is calculated based upon a proportionality between the energy of the portion of the jet that is eroded and the volume of the hole in the target. This is shown graphically in Frame 3 of Fig. 15. During time Δt, the jet advancement shown will take place. However, not all of the jet advanceament shown below the surface in the second frame engages the target, because a hole is created by the first half of the jet advancement. Thus Frame 3 shows the situation at the end of time $t = t_\phi + \Delta t$. At this time, a second jet/target engagement is undertaken as shown in the Frames 4 and 5. This basically describes the methodology used in determining the penetration in the target. The following describes how the delta penetration, DP, and delta time, DT, are calculated.

From the Bernoulli hydrodynamic theory the pressure at the jet/target interface can be defined as P_s

$$P_s = \frac{1}{2} \rho_j (V - U)^2 + \sigma_j = \frac{1}{2} \rho_t U^2 + \sigma_t \qquad \text{IV-15}$$

where

P_s = stagnation pressure at interface

ρ_j = jet material density

ρ_t = target material density

V = jet velocity at interface

U = target velocity at interface

σ_j = characteristic strength of jet

σ_t = characteristic strength of target

As discussed previously, two basic assumptions are necessary to apply the Bernoulli theory;

1) the jet and target behave as incompressible fluids during the penetration process;

2) flow is assumed to be steady state when viewed from a frame of reference moving with the penetration velocity, U, so that for the streamline along the axis of symmetry, the stagnation pressure at the jet/target interface is P_s.

The applicability of this method when used with these assumptions has been shown by numerous others as referenced in the theory section.

Rearranging Eq. IV-15 and then solving for U, the target velocity at the interface, yields the penetration rate, dP/dt. This is the velocity of the bottom of the hole in the target.

$$(\rho_t - \rho_j)U^2 + 2\rho_j VU + (\sigma_t - \sigma_j - \rho_j V^2) = 0 \qquad \text{IV-16}$$

$$U = \frac{dP}{dt} = \frac{-2\rho_j V \pm \sqrt{4\rho_j{}^2 V^2 - 4(\rho_t - \rho_j)(\sigma_t - \sigma_j - \rho_j V^2)}}{2(\rho_t - \rho_j)} \qquad \text{IV-17}$$

Simplifying, the following equation for the penetration rate, dP/dt, is derived

$$\frac{dP}{dt} = \frac{\rho_j V + (\rho_j{}^2 V_j{}^2 - (\rho_t - \rho_j)(\sigma_t - \sigma_j - \rho_j V^2))^{1/2}}{(\rho_t - \rho_j)} \qquad \text{IV-18}$$

Once dP/dt is known, the time, dt, that it takes this jet element to penetrate the target must be determined. To do this an examination of the jet element that is penetrating the target is required.

The method used for determining DP and DT for a single jet element is shown in Fig. 16. Frame (a) shows the jet as it would be at target impact. A portion of the jet with length DJLI (defined in the input section of the code) is considered for penetration. Frame (b) shows that a number of nodes may be located in this portion of the jet. The kinetic energy, momentum, mass, tip velocity, and tail velocity for this jet element is calculated as shown using the nodes that reside within this portion of the jet. The jet element is then reconfigured as shown in Frame (c) with its kinetic energy and mass conserved and average velocity based on a momentum balance. At the end of the penetration process for this element, the total depth of penetration in the target will have increased by DP. The back end of the jet element will have moved DJLI + DP at a velocity V_{tail} during the time DT. Thus

$$V_{tail} \cdot DT = DJLI + DP \qquad \text{IV-19}$$

and knowing dP/dt from Eq. IV-18 the following is true

$$(dP/dt) \cdot DT = DP \qquad \text{IV-20}$$

solving for DT and DP the following equations are derived

$$DT = DJLI/(V_{tail} - dP/dt) \qquad \text{IV-21}$$

$$DP = (dP/dt) \cdot DT \qquad \text{IV-22}$$

The hole volume is determined from the jet energy/hole volume relationship;

$$Vol = SKE/CTRGT \qquad \text{IV-23}$$

where

Vol = volume of hole created by jet element

SKE = kinetic energy of jet element

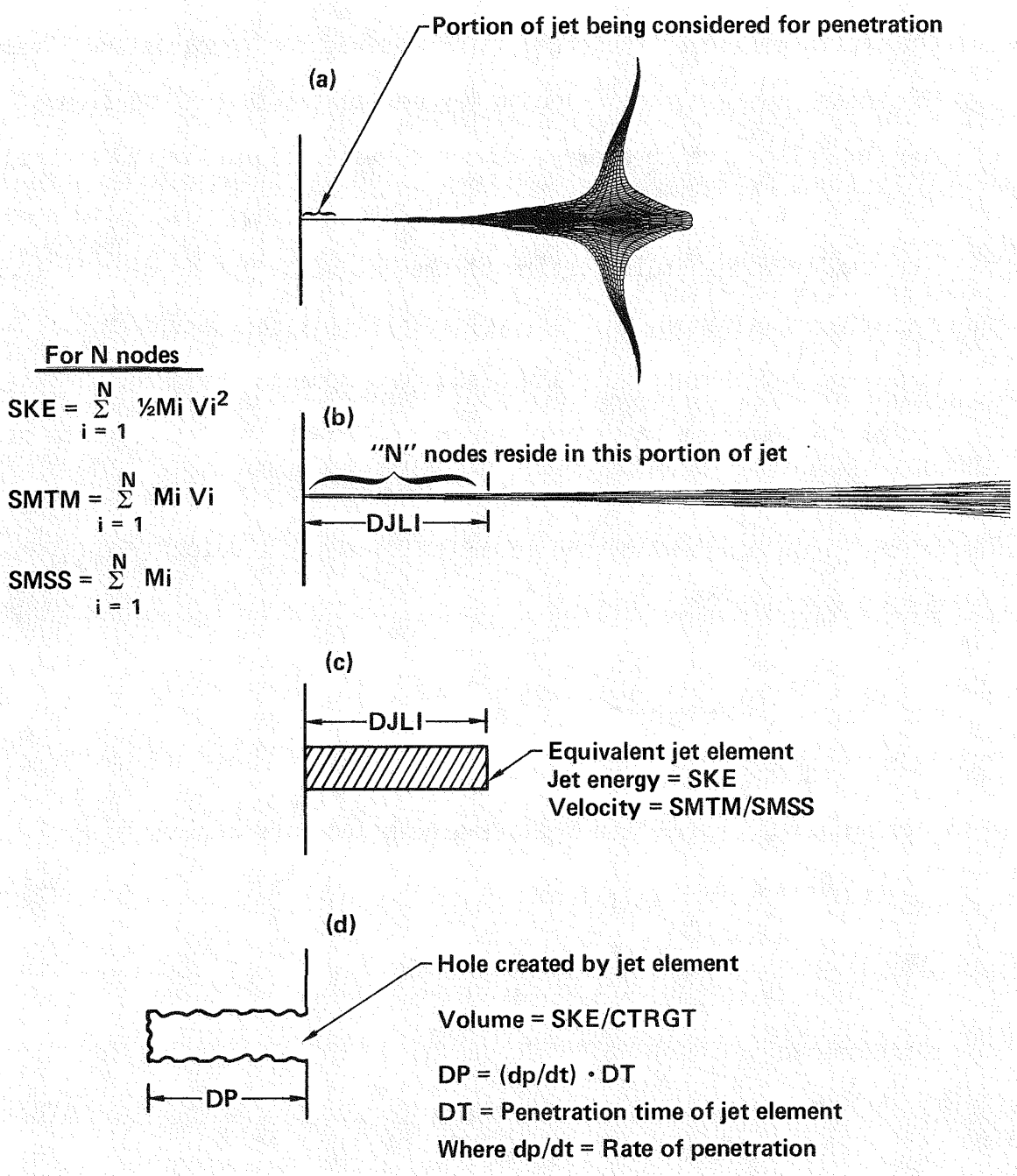

Fig. 16 Determination of DP & DT for single jet element

CTRGT = jet energy/hole volume constant of target.

The hole radius associated with the incremental penetration, DP, is defined by the following equation

$$\text{Radius} = \sqrt{\text{Vol}/\pi \cdot \text{DP}} \qquad \text{IV-24}$$

V. CORRELATION OF EXPERIMENTAL RESULTS WITH ANALYTICAL PREDICTIONS

OBJECTIVE OF EXPERIMENTAL APPROACH

The overall objective of the experimental program is to calibrate and validate the computer model being developed. To meet this objective three types of experiments have been developed to provide the necessary information for computer correlation. A flash x-ray experiment is used to verify the hydrocode prediction of the shaped charge jet configuration. A series of penetration/time experiments are used to calibrate and verify the penetration program (MJMPEN) predictions of the penetration process. Finally, penetration/hole profile experiments are required to determine the appropriate jet energy/hole volume constant for the concrete target.

SHAPED CHARGE DESIGN CONFIGURATION

The shaped charge used in this study is described in Fig. 17. Two sizes of this charge are used, a 114 mm size and 127 mm size (the 114mm size is shown). A photograph of the actual hardware used in the experiments is shown in Fig. 18. The shaped charge is detonated with as EX-12 detonator which initiates the detasheet explosive. The detonation wave in the detasheet propagates radially outward until it detonates the the LX-14 explosive. The foam wave shaper prevents the detonation wave from preigniting the LX-14 in the interior region. This wave shaping method changes the angle of the incidence of the detonation wave on the liner providing for an extremely high collapse and jet tip velocity.

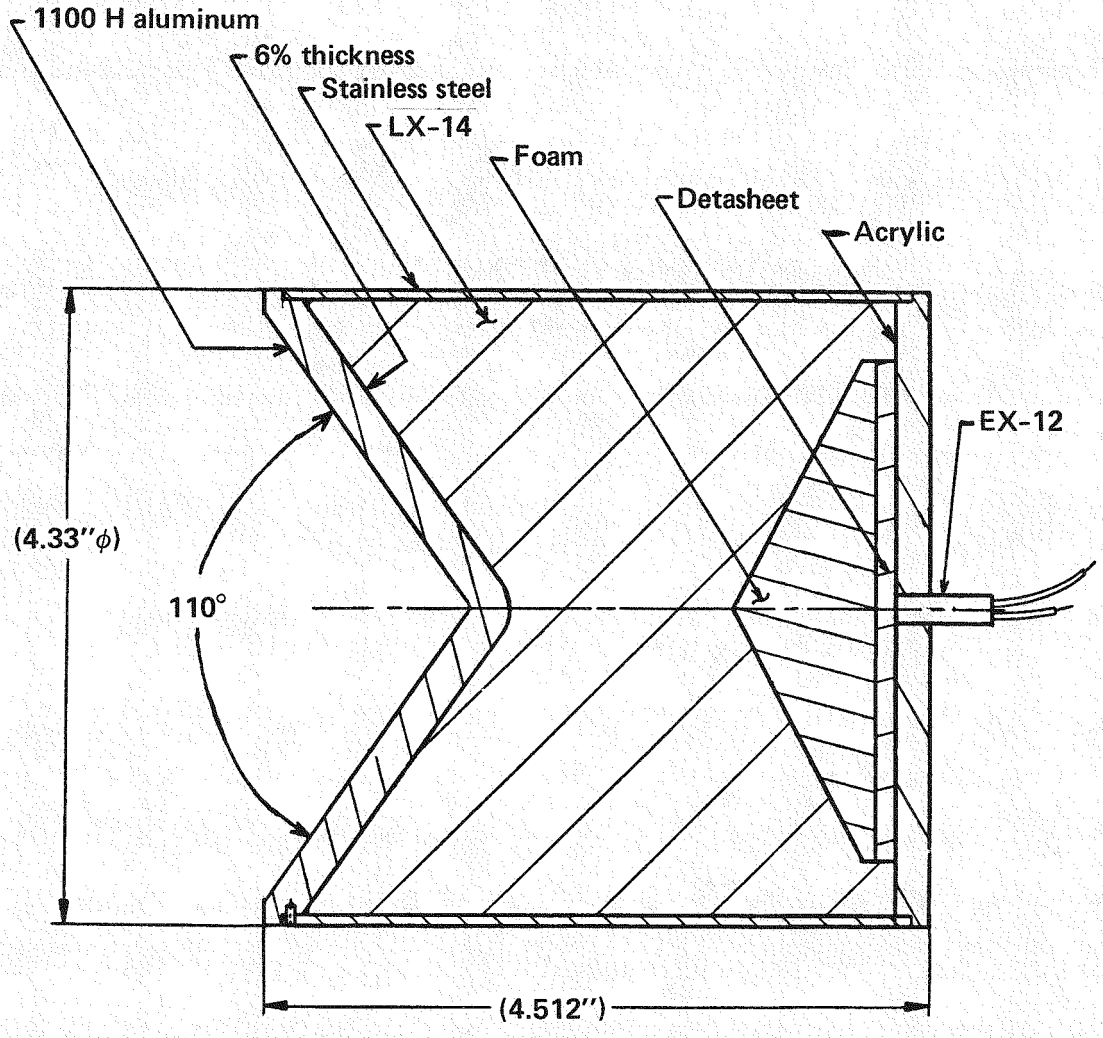

Fig. 17 Shaped charge design configuration for code calibration and verification

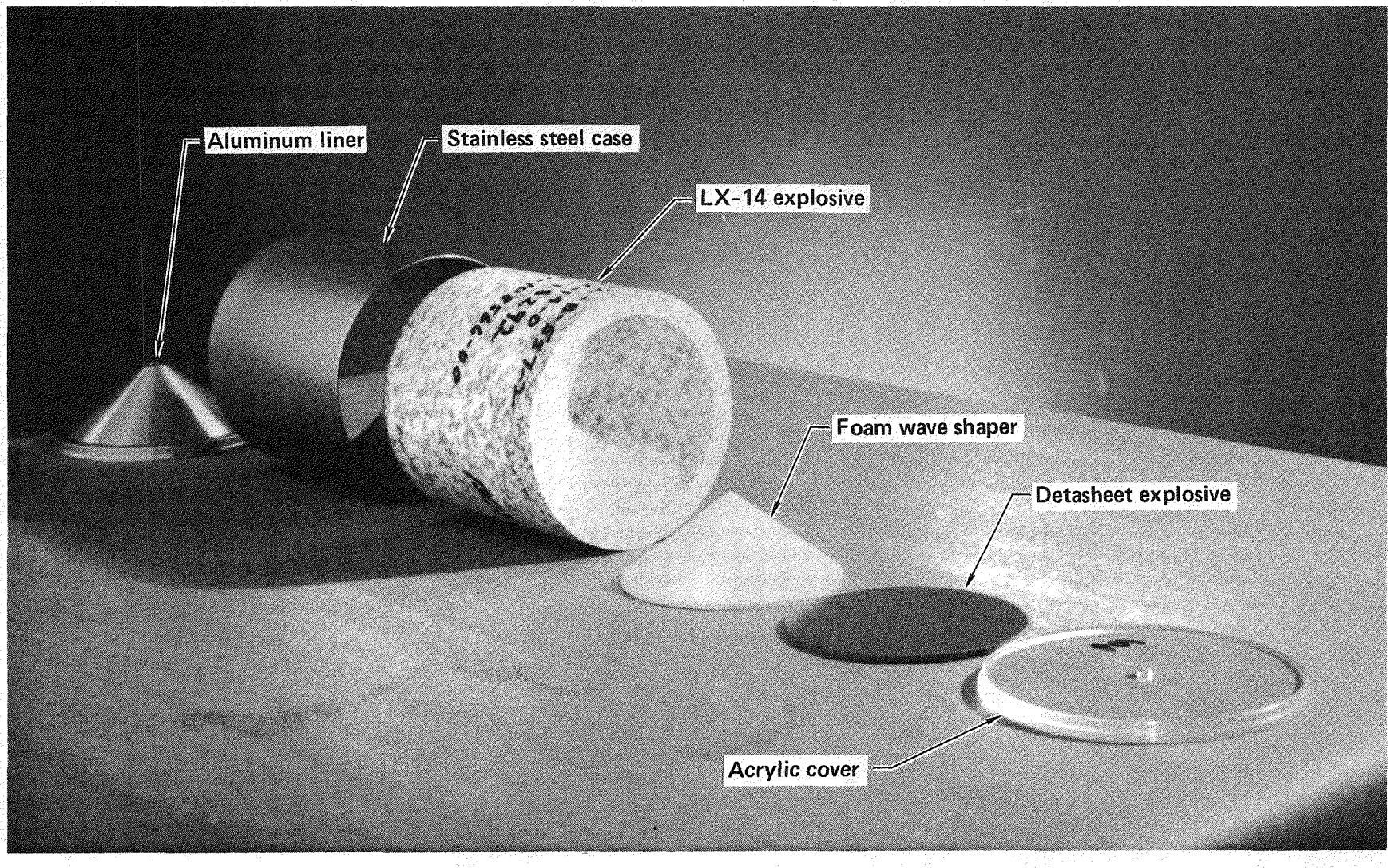

Fig. 18 Photograph of shaped charge hardware

FLASH X-RAY EXPERIMENT OF JET FORMATION

Flash x-ray is a type of radiography that can be used to produce sequential images of dynamic events. Conventional radiography differs from the flash x-ray method in that the object is virtually motionless during the exposure to x-rays due to the short duration (20 nsec) of the x-ray pulse. Basically, the flash x-ray system takes a 20 nsec duration snapshot of an object that is between the x-ray tube and the film casset. A complete description of flash x-ray systems can be found in Ref. 49.

The flash x-ray method used in this study is shown in Figure 19. Figure 19(a) shows a diagram of a typical flash x-ray system. When the trigger is activated the shaped charge is detonated. After a delay, allowing the shaped charge jet to form, the x-ray tube is pulsed producing a 20 nsec duration x-ray pulse. Figure 19(b) shows how the x-ray beam creates a shadow graph of the jet as it passes between the x-ray tube and film casset. The trigger timing and tube head location are critical as the jet tip velocity of the shaped charge is in excess of 1.0 cm/μsec and the window available for capturing a shadowgraph of the jet is small.

The configuration used in the flash x-ray experiment is shown in Fig. 20. Frame (a) is a line drawing of the top view of the system. The five x-ray tubes used in the experiment are triggered at 30, 35, 45, 60, and 90 μsec. The tubehead to shaped charge distance is 5 feet and the shaped charge to film casset distance is 1 foot. Frame (b) shows the actual experimental setup. The shaped charge is placed above a blast shield and fired straight down into the ground. The tubeheads and film cassets are located below the

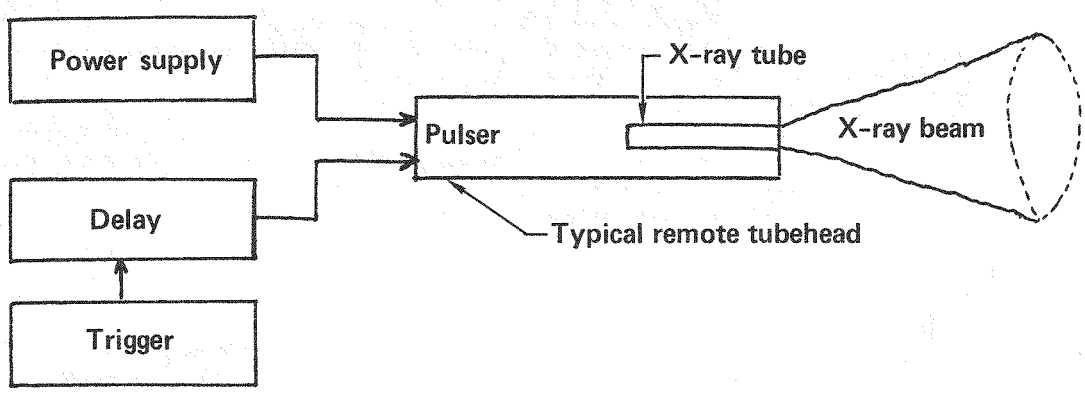

(a) Diagram of x-ray system

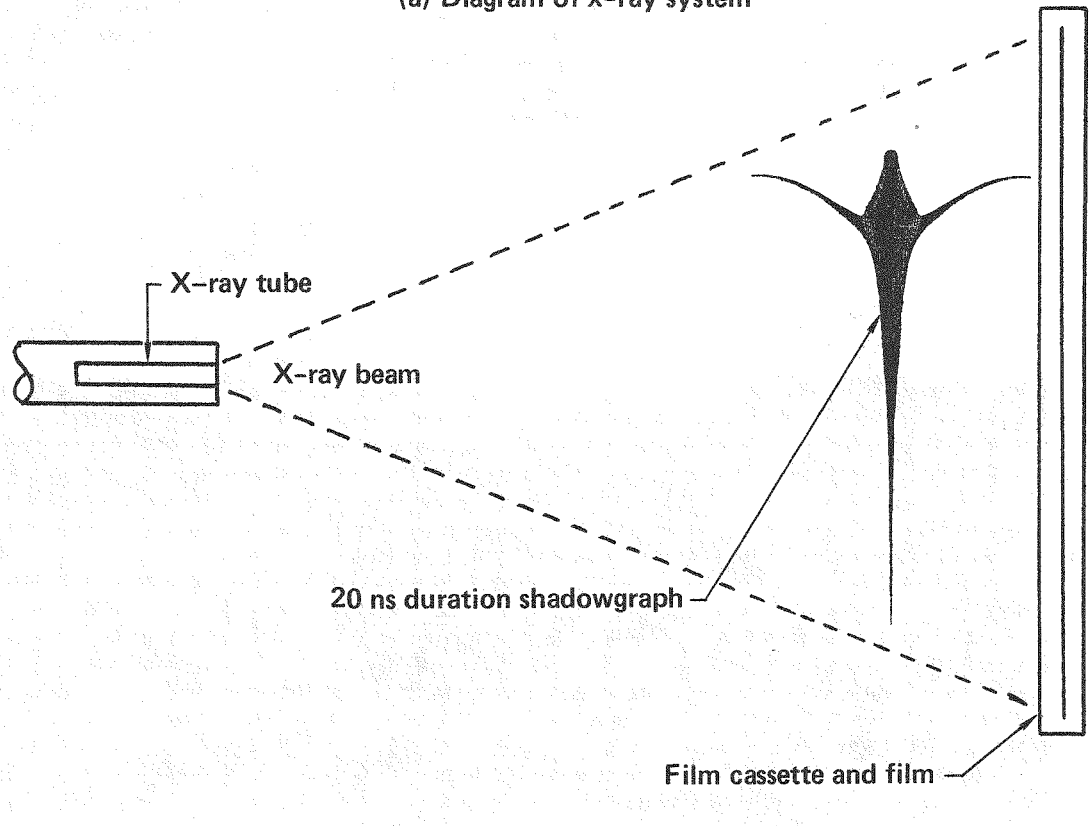

Fig. 19 Flash X-ray experimental method

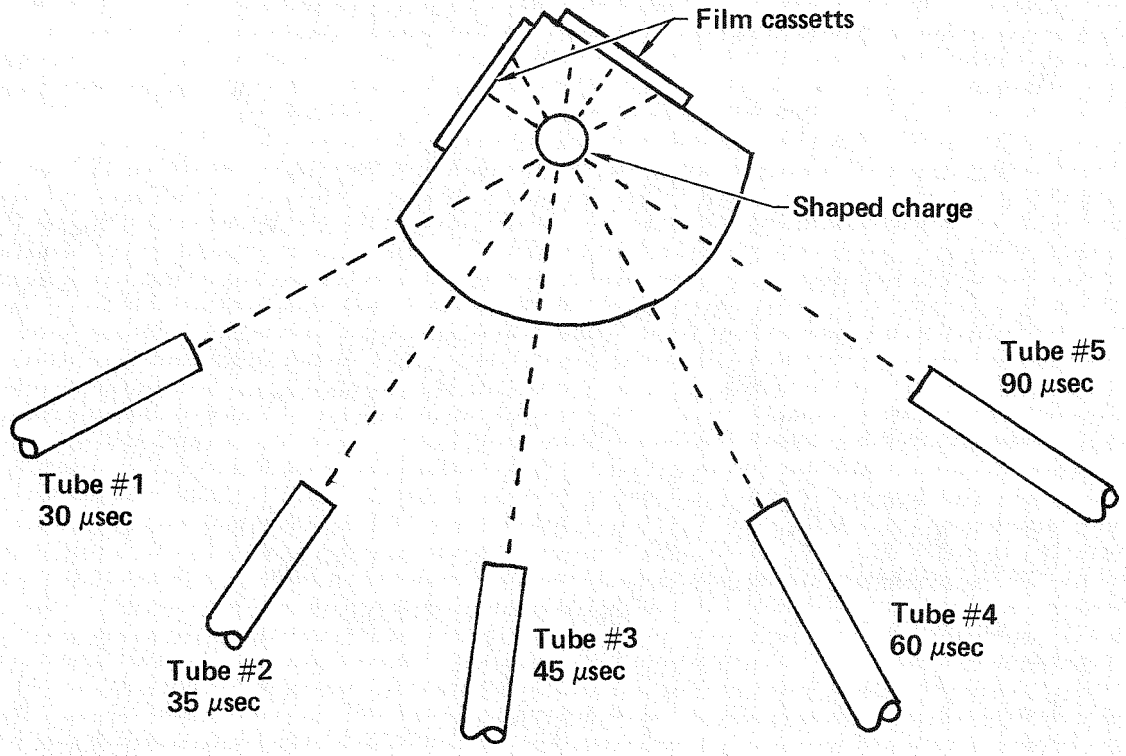

(a) Line drawing of top view

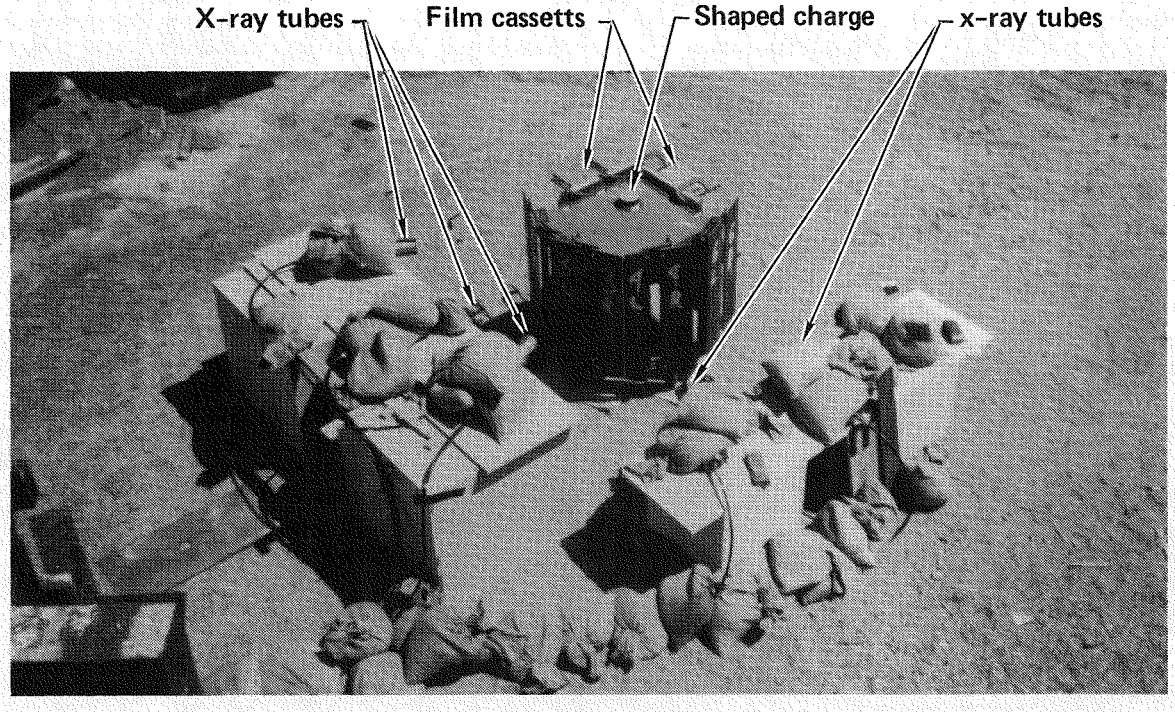

(b) Photograph of actual test setup

Fig. 20 Configuration of flash x-ray experiment with 5 x-ray tubes

blast shield out of the line of sight of the explosive. Because of paralax caused by the line of sight restriction only the standoff region greater than 1 cm is exposed on the casset.

Results of the x-ray test are presented in Figs. 21 and 22. Figure 21 shows the jet configuration at 30, 35, and 45 μsec. Due to the hostile environment, numerous pressure points obscure the print, however, the jet configuration can still be resolved. It should be pointed out that the film cassets were thrown 20 feet during the experiment, with the data being recorded before any casset motion occurred. Due to the low mass of the jet tip and the loss of resolution from copying the original negative, it is not possible to locate the jet tip on this print. The original negatives, however, show the jet tip velocity is in excess of 1.0 cm/μsec which correlates well with the hydrodynamic computer simulations. Figure 22 shows the jet configuration at 60 and 90 μsec. Note the coalescence of mass at the leading edge of the jet. (Again it is not possible to resolve, but the jet tip is well beyond this point.) This lump of mass could possibly be the result of jet interaction with the air or just an artifact of this experiment. If either of the above possibilities were true, however, the analysis would not predict it as the hydrocode assumes the process takes place in a total vacuum and that the liner is perfectly machined and alligned with the HE.

HYDRODYNAMIC ANALYSIS OF JET FORMATION

The analytical prediction of the jet configuration at 30, 35, and 45 μsec is shown in Fig. 23 The fact that the x-ray timing

Note: dashed lines added for clarity

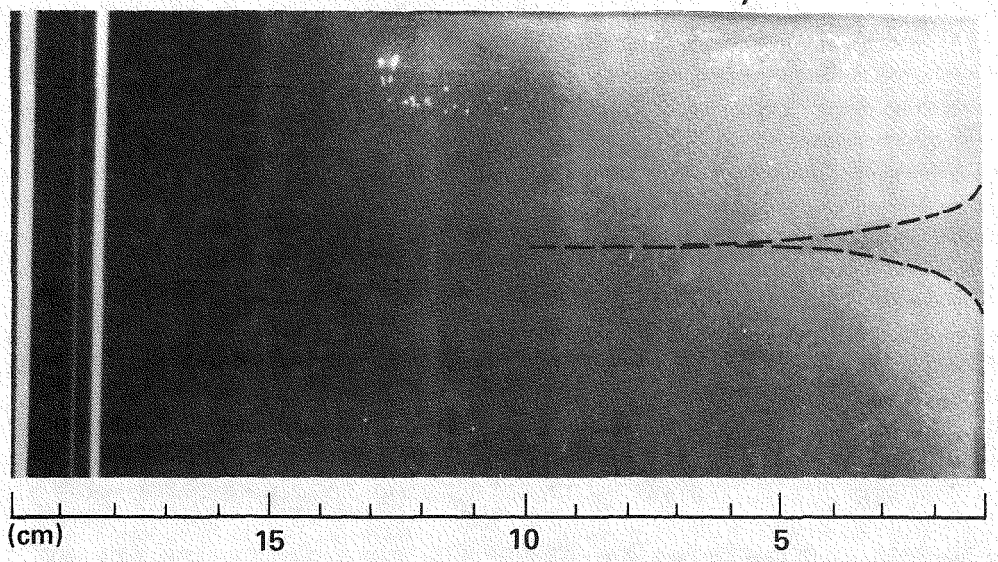

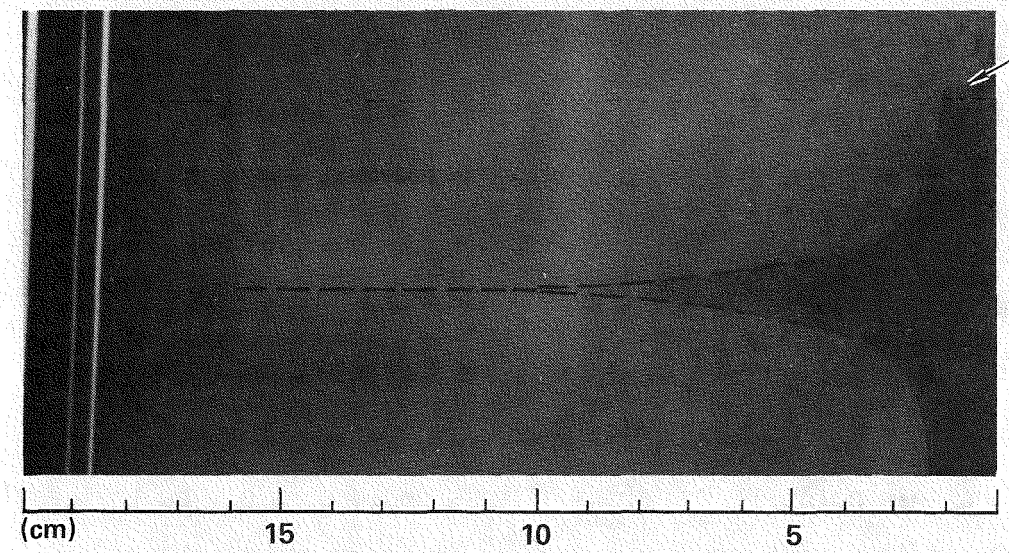

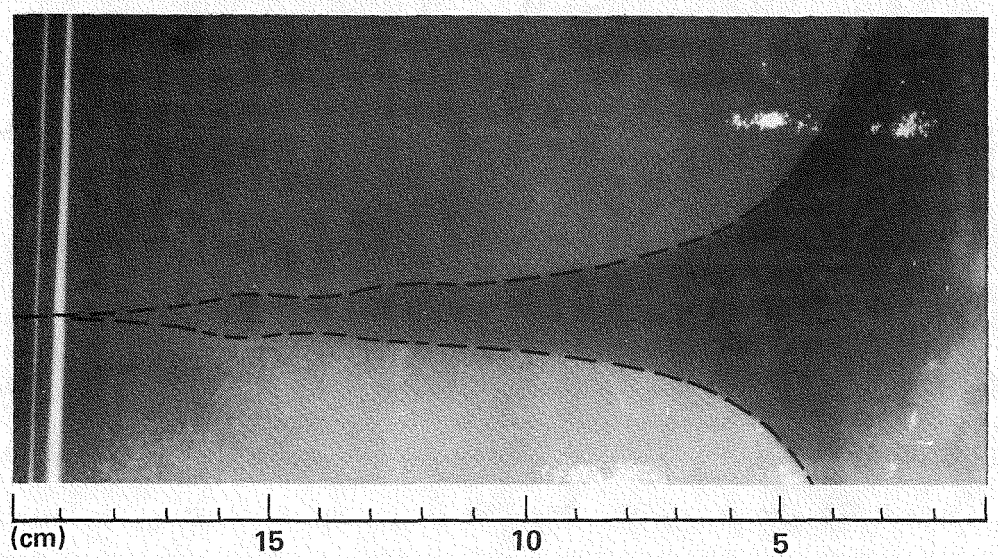

Fig. 21 Flash x-ray of jet at 30, 35, and 45 μsecs

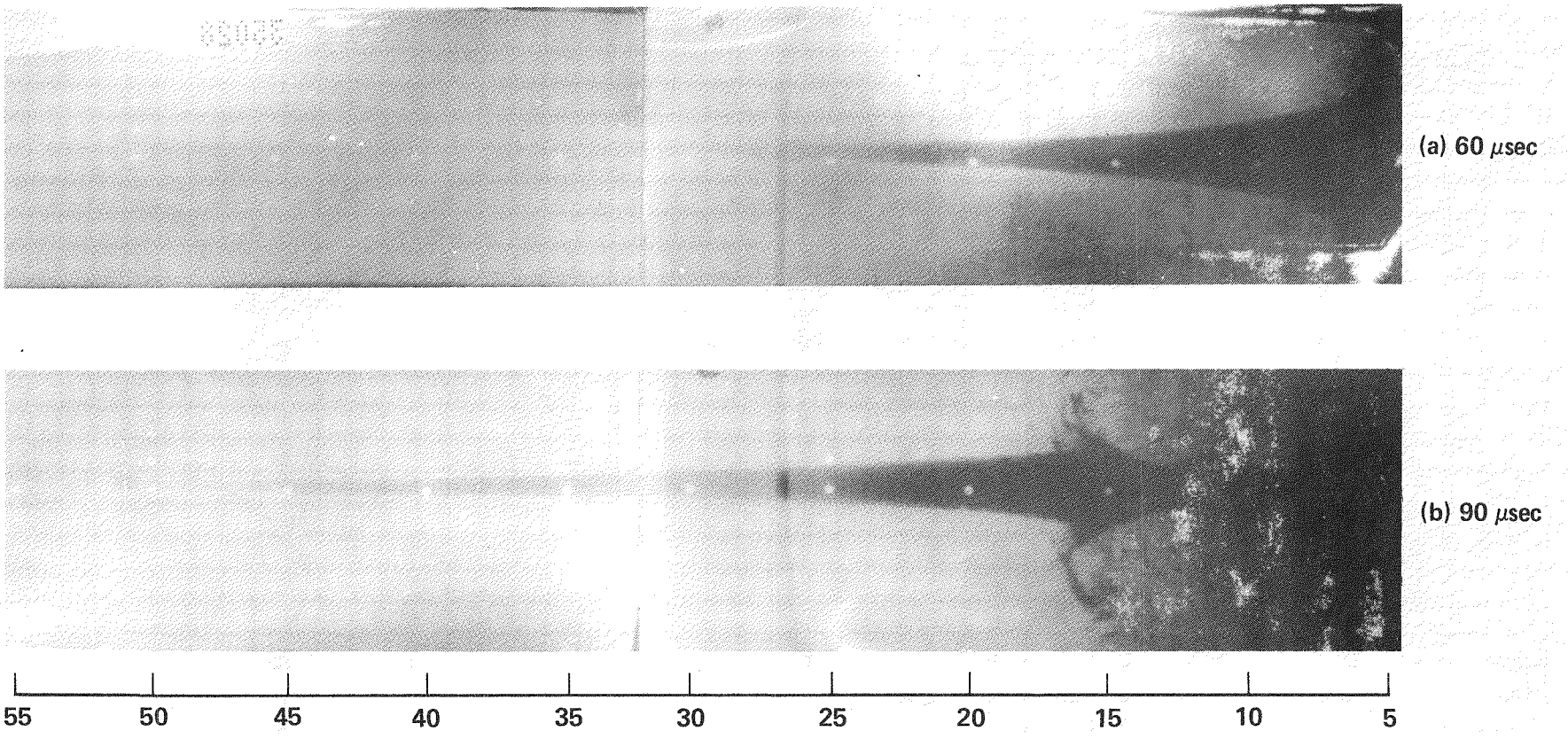

Fig. 22 Flash x-ray of jet at 60 and 90 μsec

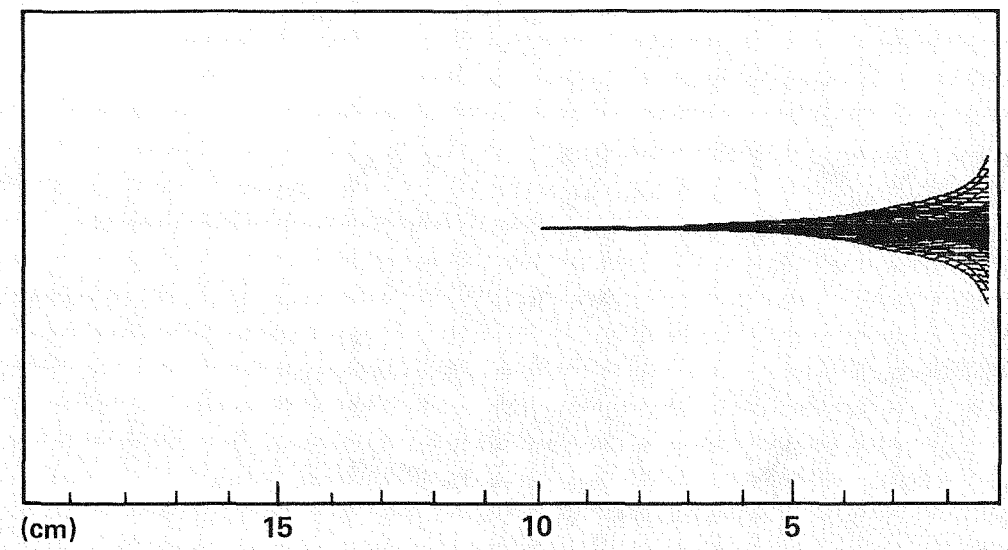

(a) 30 μsec

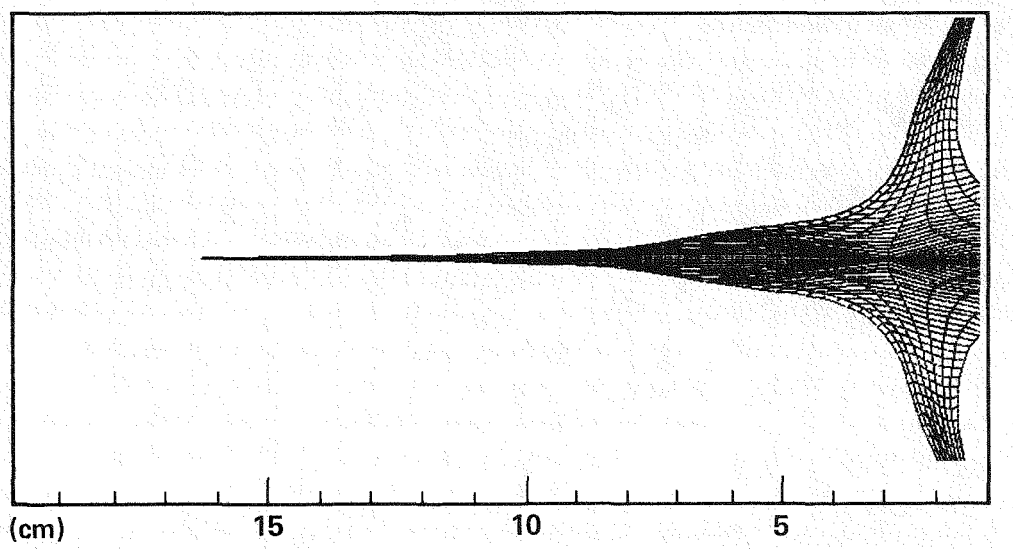

(b) 35 μsec

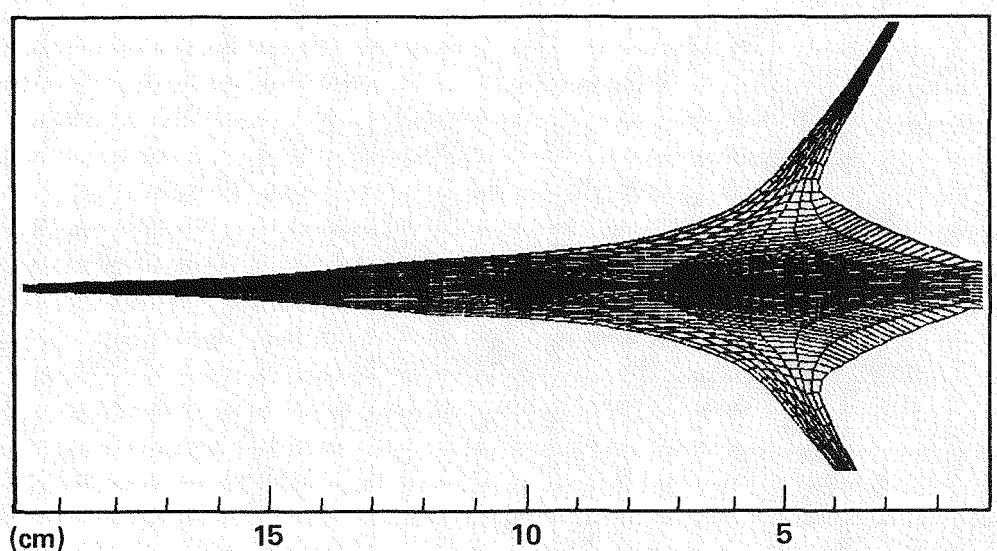

(c) 45 μsec

Fig. 23 Analytical prediction of jet configuration at 30, 35, 45 μsec

provides excellent shadow graphs of the jet is a preliminary indication that the code accurately predicts the explosive detonation, liner collapse, and jet formation process because the code is used to determine the x-ray pulse timing and tubehead location.

Referring back to Frame (b) of Fig. 21, spallation of the jet in the wing region can be observed. Because a Lagrangian code is being used for the analysis, it is difficult to model material separation due to spall. However, the density contour plot shown in Fig. 24 reveals that the code predicts an eminent spall in this region. Normally, one would plot something other than density (possibly cumulative damage or plastic strain) to investigate spall. But since the jet material has undergone such extensive deformation, the density plot reveals the spall location most graphically.

The analytical correlation to the flash x-ray experiment has shown that the hydrocode DYNA2D with the appropriate material models and hourglass damping can be used to numerically model the extremely complex explosive detonation, liner collapse, and jet formation process of a shaped charge. It is not prudent to pursue the absolute accuracy of the hydrocode calculation any further as the experimental error possibilities cannot be assessed in this single shot experiment. At $10,000 per experiment as compared to approximately $100 per analysis it would be most efficient to accept any minor errors (if they exist) and account for any variations due to the hydrocode analysis in the overall model that is being developed.

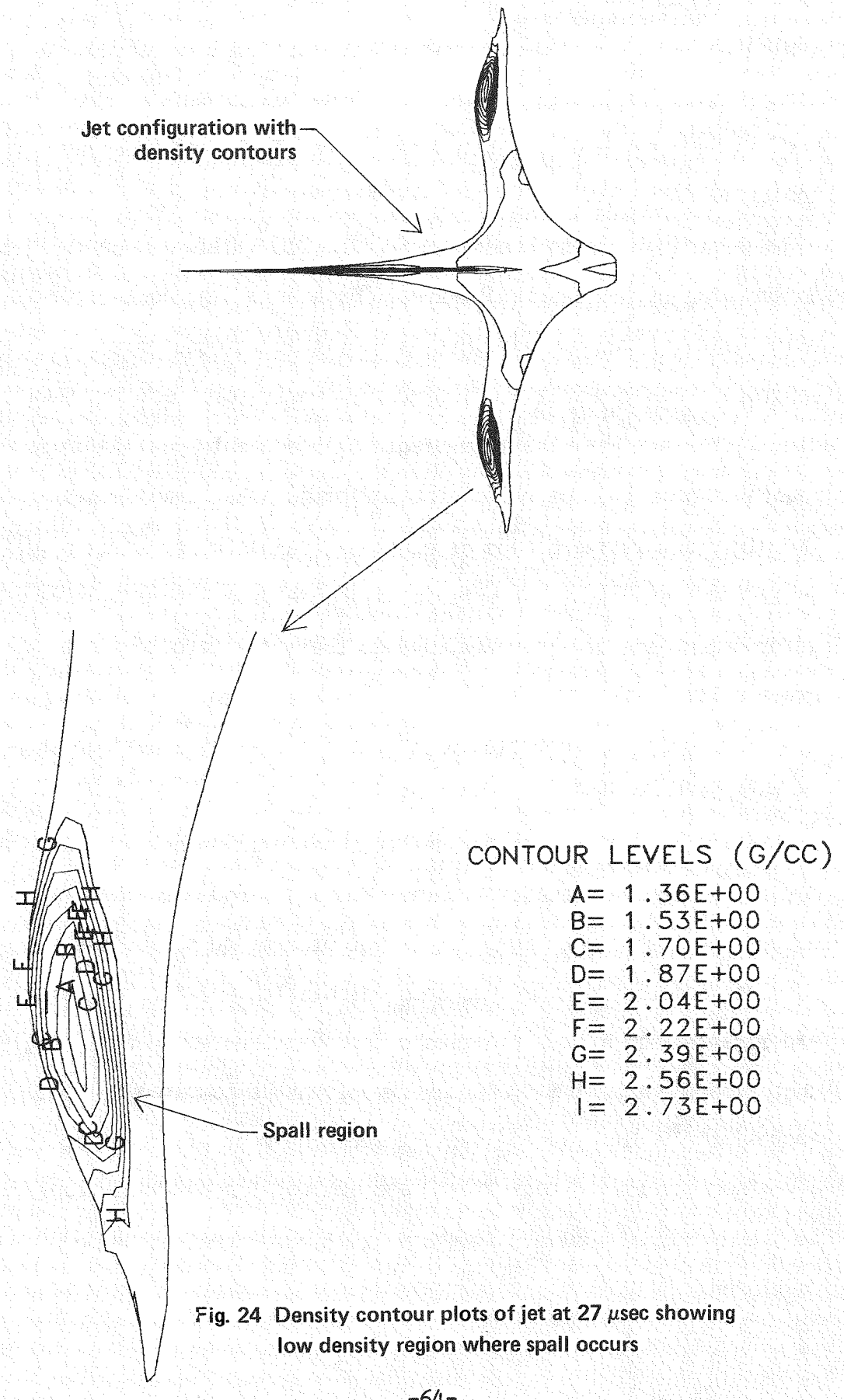

Fig. 24 Density contour plots of jet at 27 μsec showing low density region where spall occurs

PENETRATION TIME HISTORY EXPERIMENTS

The objective of the penetration/time experiments is to determine the penetration rate, dP/dt, for correlation with computer predictions as well as the determination of V_{min} for this target at short standoffs. A line drawing of the experimental configuration is shown in Frame (a) of Fig. 25. At the time of fire, the bunker capacitive discharge unit (CDU) discharges an electrical pulse simultaneously to the shaped charge detonator, recording scope, and time interval meters (TIM). As the explosive detonation process causes the liner to collapse and the jet to form, the recording devices keep track of the elapsed time. As the jet tip impacts the target the front switch breaks triggering a pulse on the scope and stopping the TIM. The TIM is used as a backup. Frame (b) of Fig. 25 shows a typical scope trace for two switches. Since only two switches could be connected to each scope, 8 scopes are required to monitor all 15 switches.

Hardware used in the experiment is shown in Fig. 26. Frame (a) of the photograph shows the contact switch (normally open) mounted on a plywood board. The cable is connected to the pin switch power supply resulting in an open circuit. As the jet contacts the switch it closes the circuit sending a pulse to the scope. Frame (b) shows a fully loaded switch box prior to filling with concrete. The switches are spaced at 10 cm intervals. A controlled mixture of concrete is backfilled into the box containing the switches, allowing a minimum of 30 days for curing. The pre- and post-shot configuration of the switch box is shown in Fig. 27. Frame (a) shows the shaped charge lying horizontal and spaced at one caliber

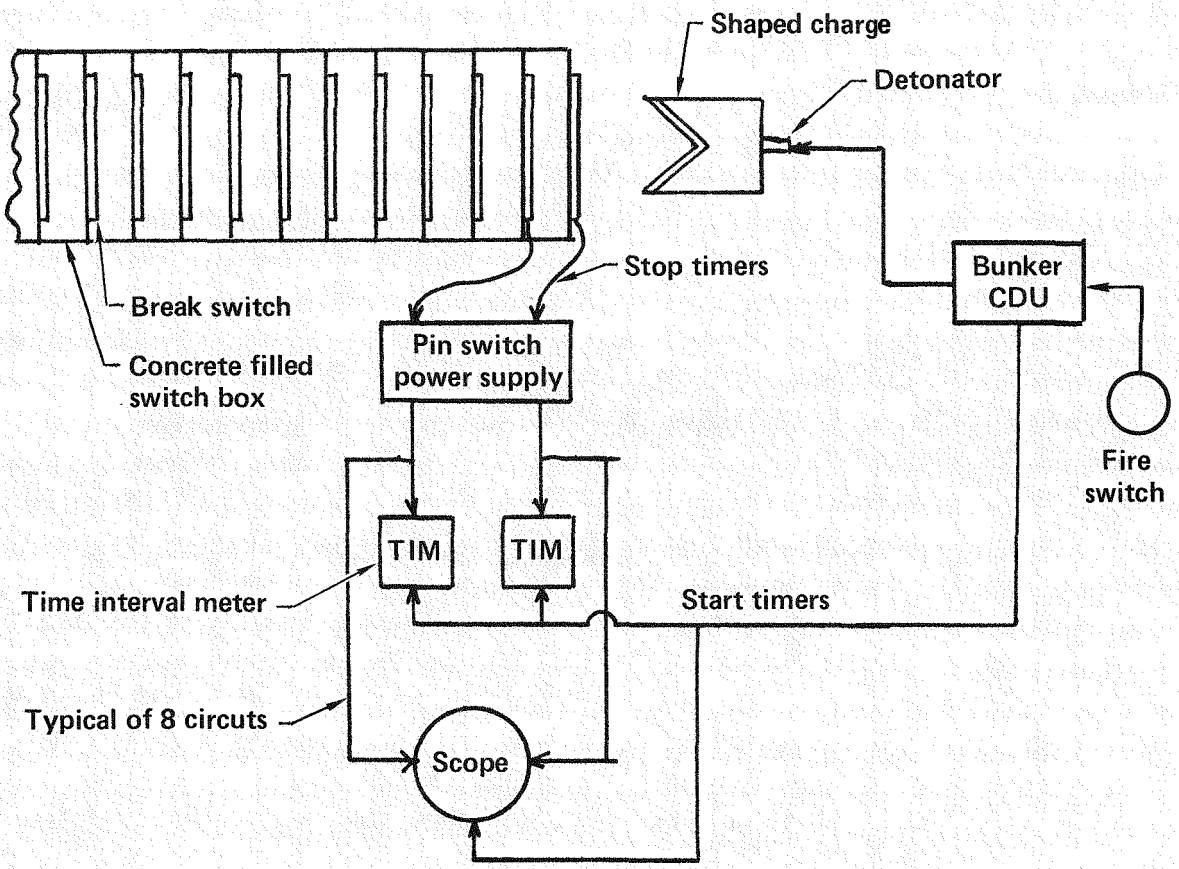

(a) Line drawing of experimental configuration

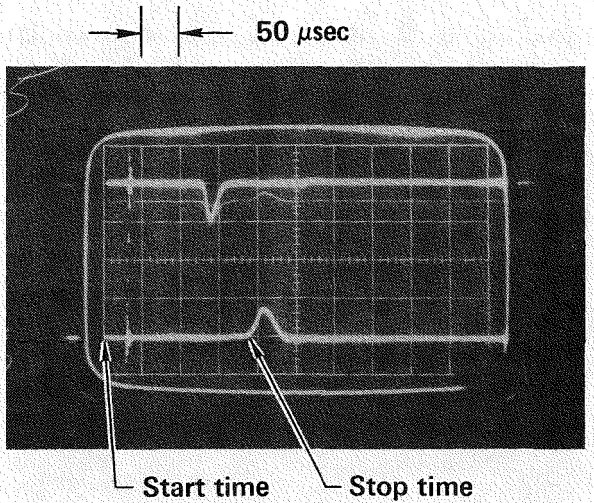

(b) Typical scope trace of elapsed time for two switches

Fig. 25 Configuration and typical results of penetration/time experiment

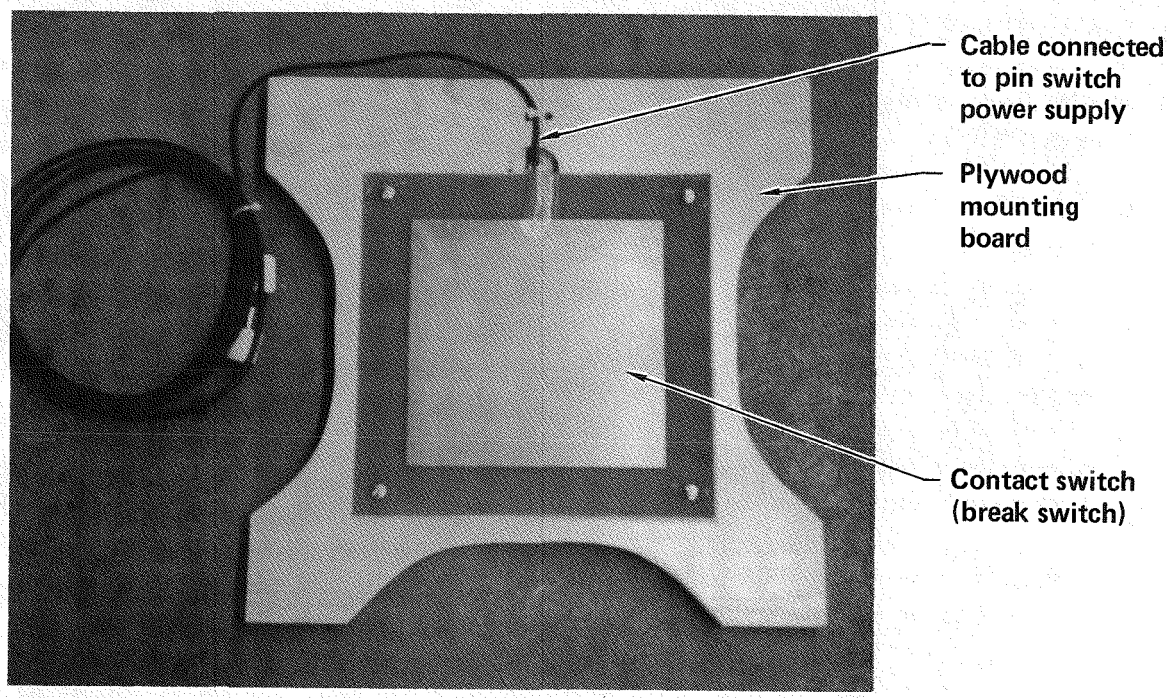

(a) Contact switch

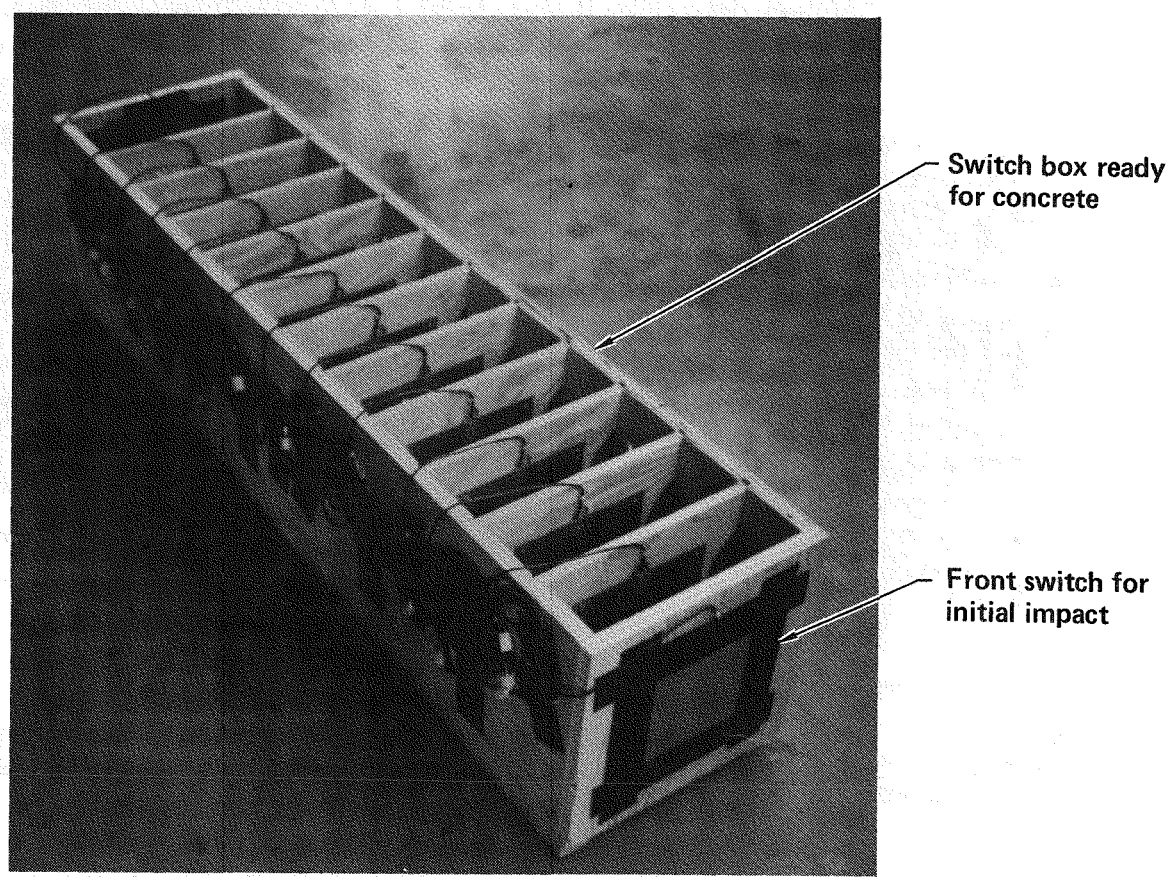

(b) Switch box

Fig. 26 Hardware for penetration/time experiment

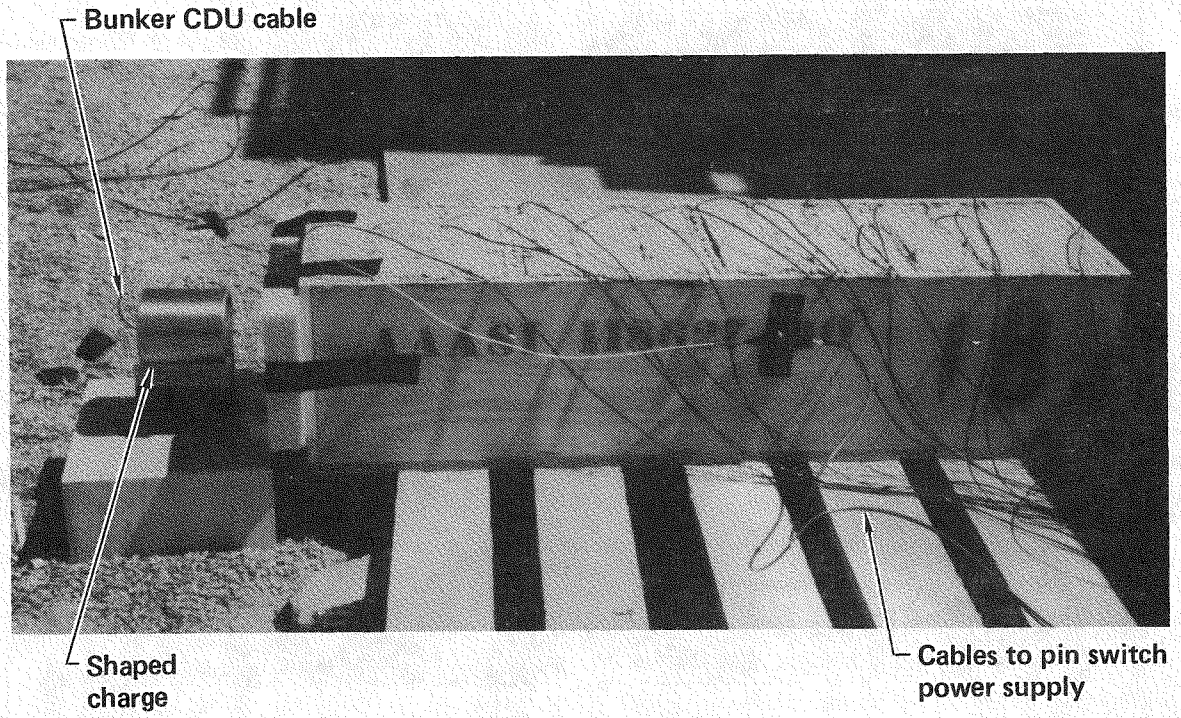

(a) Pre-shot configuration

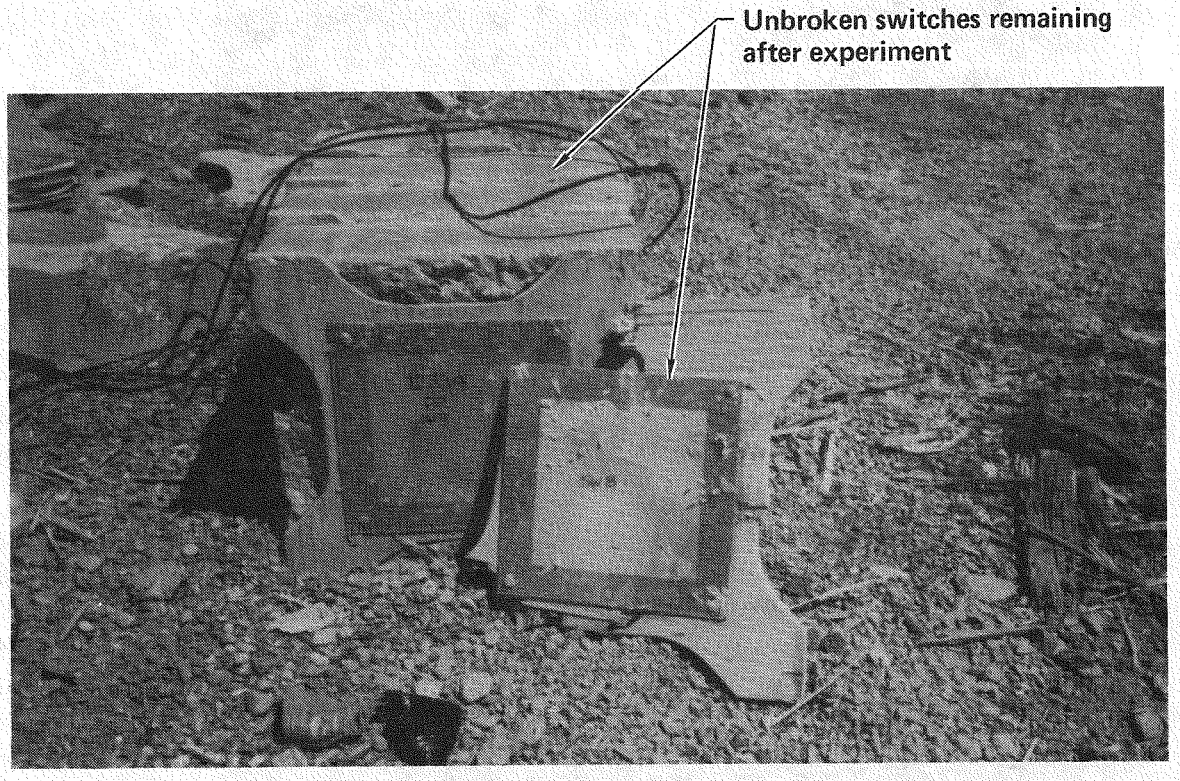

(b) Post-shot configuration

Fig. 27 Pre-shot and post-shot experimental configuration

standoff from the target. The post shot configuration showing the switches remaining after the experiment is presented in Frame (b).

The minimum jet penetration velocity, V_{min}, can be determined from this experiment by determining the velocity of the portion of the jet that closes each switch. From the hydrocode analysis, the location in space and time of the virtual origin is known. From the previous discussion of the virtual origin it can be assumed that each jet particle eminates from this point at a fixed velocity. It is now possible to determine the velocity of the element that closes each switch because it is known how far the jet element is displaced by the location of the switch and how long it takes to get there from the timing scope. The displacement over time ratio yields a jet velocity for closure of each switch. Thus a curve showing jet velocity versus penetration can be generated.

The curve of jet velocity versus scaled depth of penetration for the one charge caliber standoff experiment is shown in Fig. 28. The dashed portion of the curve indicates an extrapolation of how the jet continues to penetrate, however, it should be noted that the jet does not reach the next switch located beyond the total penetration line that is drawn. By knowing the total penetration in the target, the minimum jet velocity for target penetration can be ascertained.

A curve of scaled penetration versus scaled standoff (in charge diameters) is presented in Fig. 29. The curve shown is a least squares straight line curve fit to experimental data in concrete. Thus, at a standoff of one, the scaled penetration is approximately 4.9. Referring to Fig. 28 it can be seen that with a scaled

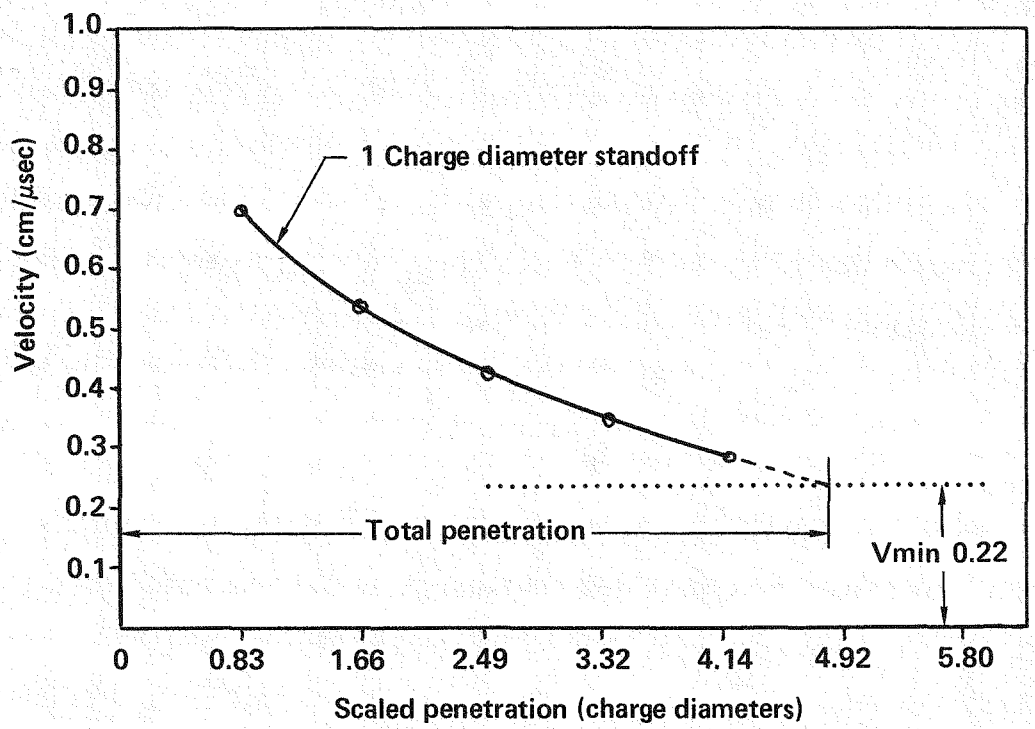

Fig. 28 Jet velocity versus scaled penetration

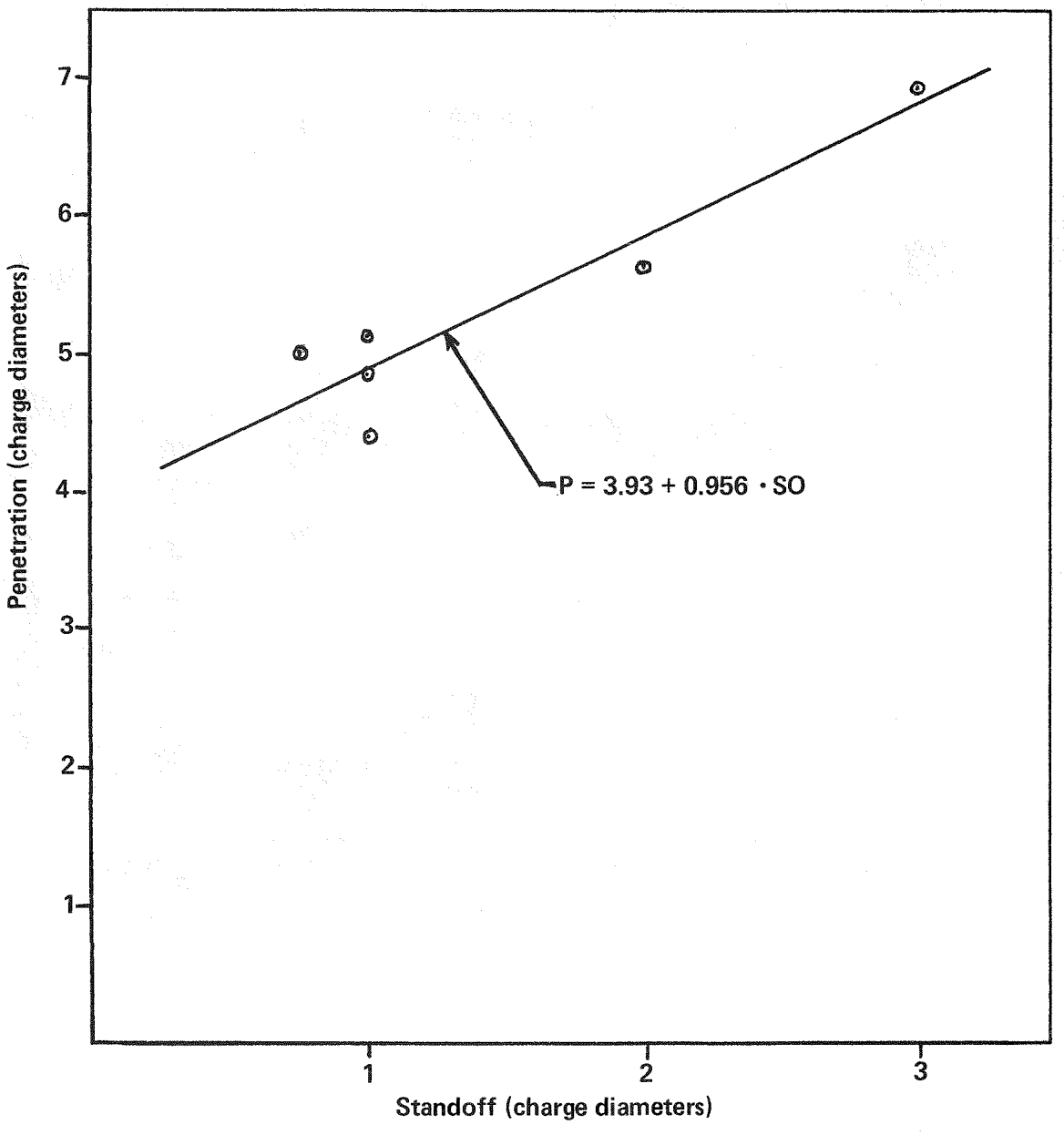

Fig. 29 Scaled penetration versus scaled standoff

penetration of 4.9, V_{min} is approximately 0.22 cm/μsec for one charge caliber standoff. Before describing the results at different standoffs, the concept of a minimum velocity for penetration will be discussed in more detail.

EXPERIMENTAL DETERMINATION OF MINIMUM VELOCITY FOR PENETRATION

The critical velocity below which no effective penetraton is obtained by the jet material is called V_{min}. The value of V_{min} was originally thought to be only a function of the target material. DiPersio, Simon, and Merendino[28] determined the total penetration of the jet into different target materials at a constant standoff (2 charge diameters) and found that V_{min} varied from 0.20 cm/μsec in mild steel to about 0.24 cm/μsec for a BHN 320 armor target. Further investigation showed that the variation of V_{min} with standoff was much more significant than with target material as shown in Table V-1.

Table V-I. V_{min} versus Standoff

Standoff (Charge Diameters)	V_{min} (cm/μsec)
3	0.30
6	.36
10	.42
15	.46
20	.50
25	0.53

The results show the last effective jet element that contributes to penetration does not have the same velocity at all standoffs. Rather, the "cutoff" velocity increases quite substantially as the standoff increases.

Results of the experiments presented in this study correlate with the Ballistic Research Laboratory (BRL) data of DiPersio, Simon, and Merendino. Frame (a) of Fig. 30 shows the jet velocity versus penetration curves at 0.5, 1, and 2 charge diameter standoffs. The total penetration at these three standoffs provide a determination of V_{min} at very short standoffs into concrete. Frame (b) of the figure shows how this data compares with the BRL data. The significance of this data is that it shows that V_{min} may not be at all sensitive to target material. The BRL set of data is for copper jets in steel targets and the new set of data is for aluminum jets in concrete targets. A curious fact about this is that the jet-to-target density ratio for each set of experimental data is just a little over 1 and it may be that the curve presented is only valid for the ratio equal to approximately one. At the present time there is no experimental data available to show how V_{min} versus standoff curve is affected by the jet to target density ratio in other regimes.

EXPERIMENTAL/ANALYTICAL DETERMINATION OF PENETRATION EFFICIENCY

The next step in the development of the analytical model is the correlation of analytical predictions of the penetration time history to experimental results. Experiments discussed previously provide for a penetration time history as well as the velocity

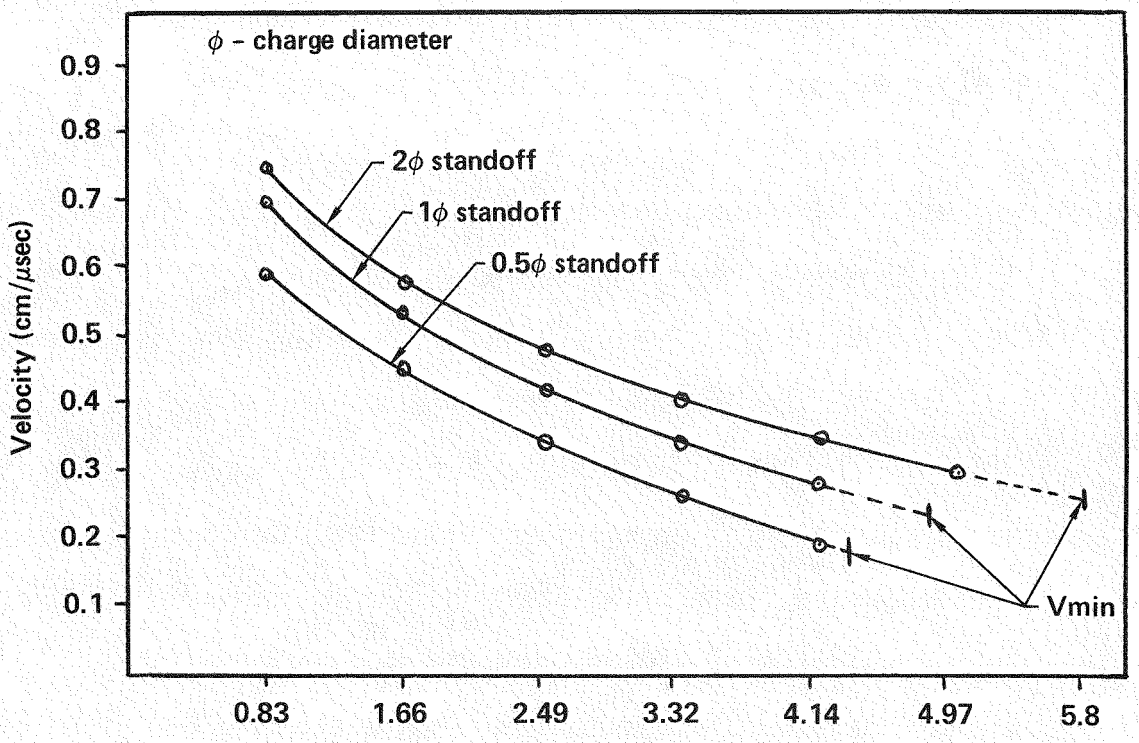

(a) Jet velocity vs scaled penetration

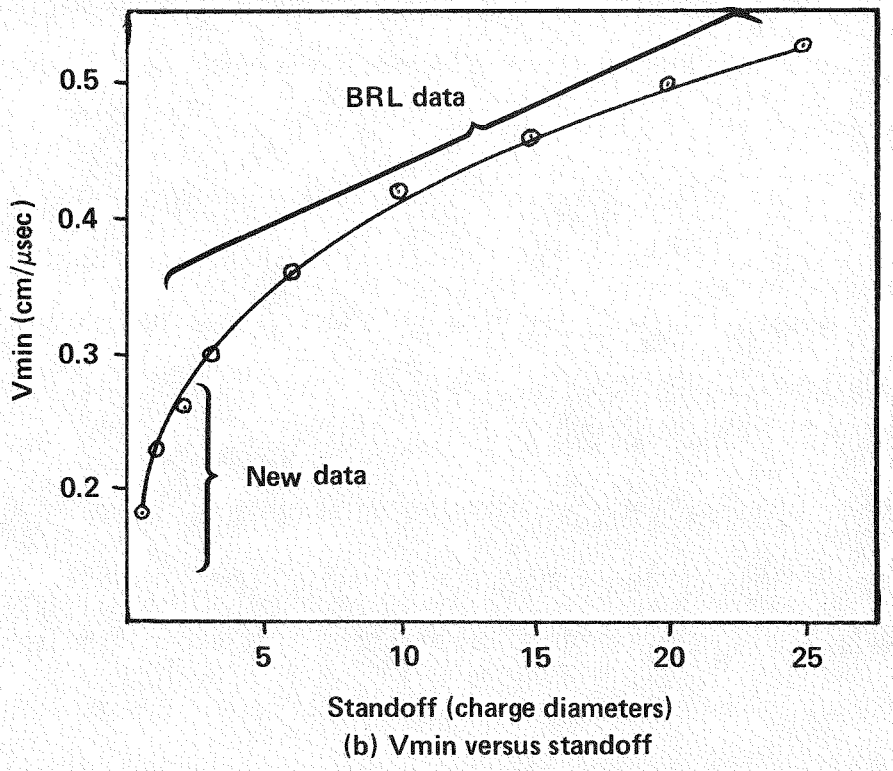

(b) Vmin versus standoff

Fig. 30 Determination of Vmin as a function of standoff

versus penetration data. A comparison of the experimental and analytical penetration time history for the two caliber standoff experiment is shown in Frame (a) of Fig. 31. This figure shows the computer model is over predicting the experimental target penetration. At a time of 230 μsec the analysis has overpredicted the penetration by 20% while the total penetration is overpredicted by approximately 100% (Fig. 31). Frame (b) shows the comparison of total penetration as a function of standoff. This figure shows that at short standoffs the code is fairly accurate and at larger standoffs tends to have increasingly larger deviations. This is probably due to some inefficiencies in the penetration process that become more predominant at deeper depths of penetration. Simon, DiPersio, and Merendino[50] have pointed out that jet-target interactions in the form of washback, plugging, and pile-up may slow down the "idealized" (no losses) penetration process.

To account for losses that occur during penetration, an efficiency factor, proportional to the depth of penetration, is introduced. The efficiency, η, is calculated based on the current depth of penetration, PEN, the standoff, SO, and an empirical constant, DEPTH

$$\eta = \frac{\text{DEPTH}}{(\text{DEPTH} + \text{PEN})} \qquad \text{V-1}$$

where

$$\text{DEPTH} = 3.228 + 20/\text{SO} - 30/\text{SO}^2 + 22/\text{SO}^3 \qquad \text{V-2}$$

PEN = Scaled penetration (charge diameters) V-3

SO = Scaled standoff distance (charge diameters) V-4

Thus, as the penetration increases the efficiency factor drops. For each increment of penetration, DP, a new increment of penetration,

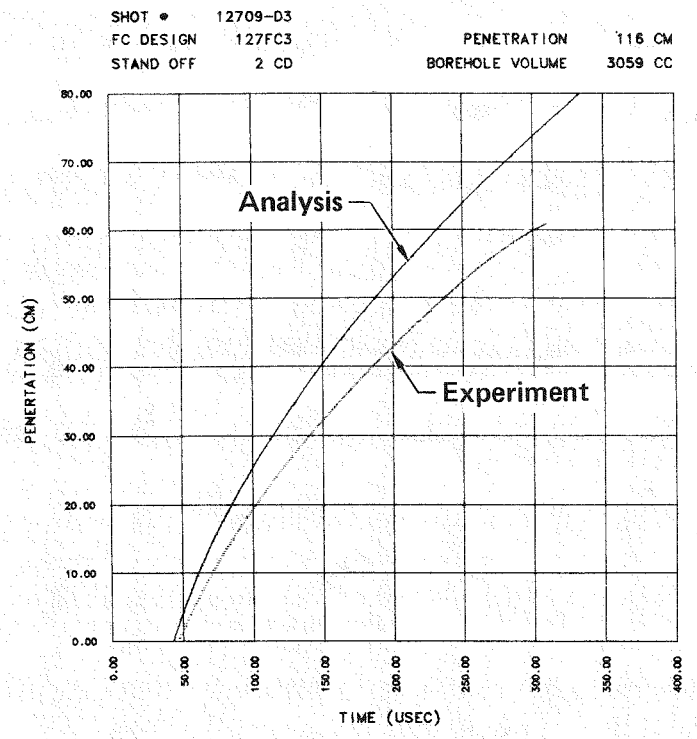

(a) Experimental and analytical penetration time history

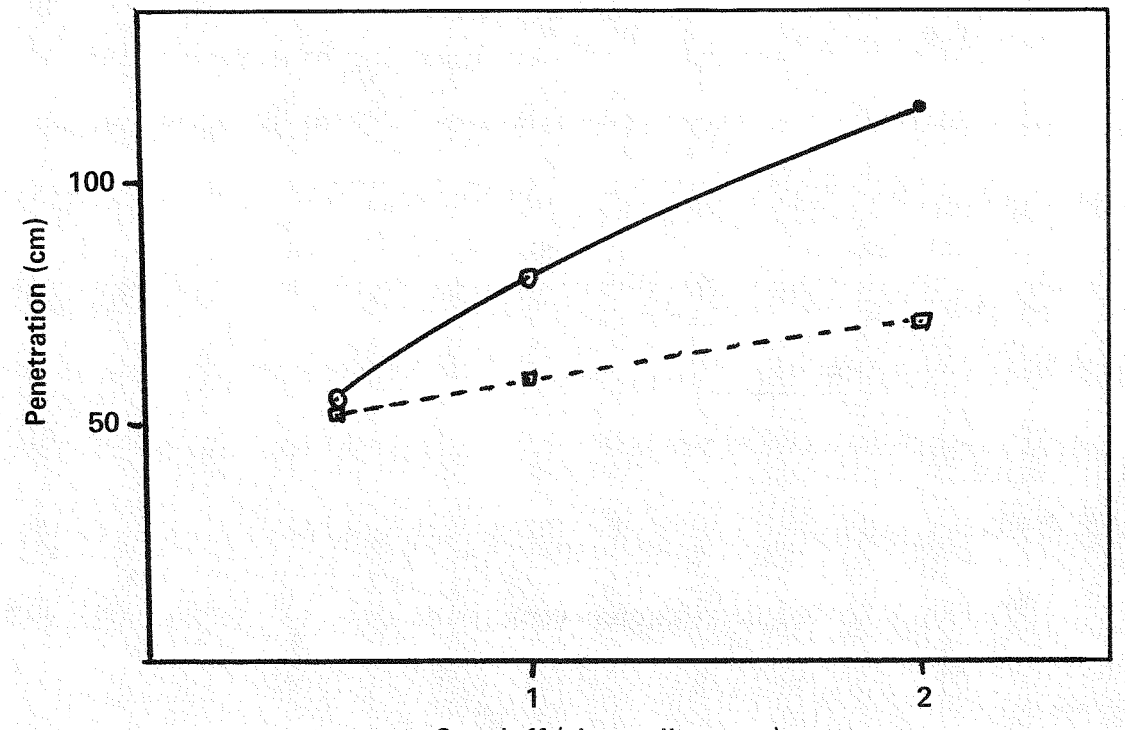

(b) Comparison of total penetration versus standoff

Fig. 31 Comparison of analytical predictions of penetration with experimental results

NEWDP, is calculated such that;

$$NEWDP = DP * \eta \qquad V\text{-}5$$

A curve of jet penetration efficiency versus target penetration is shown in Fig. 32. At zero penetration, the efficiency is one and as the depth of penetration increases, the efficiency drops off. The empirical efficiency parameter is generated by correlating the experimental penetration-time results with analytical predictions presented in the next section.

PENETRATION/TIME HISTORY ANALYSIS

The experimental/analytical correlations of penetration versus time at various standoffs is presented in Fig. 33. Frames (a), (b), and (c) are for the 127 mm shaped charge design at three standoff distances. The empirical constant, η, was generated based on these three experiments. Due to the limited supply of experimental data, the effect of experimental error cannot be assessed. However, the experimental data appears to be self consistant. Frame (d) of Fig. 33 shows the correlation for the 114 mm shaped charge at one charge diameter standoff. This comparison is not as good as the first three where η was calibrated, however, it is within the bounds of the allowable experimental error. Note that in all cases the analytical prediction of total penetration is greater than the experimental value. This is due to the fact that the experimental curve stops at the last switch that is broken. It is assumed that penetration continues past this switch but not as far as the next switch. To determine total penetration a target that is not destroyed during the experiment is required .

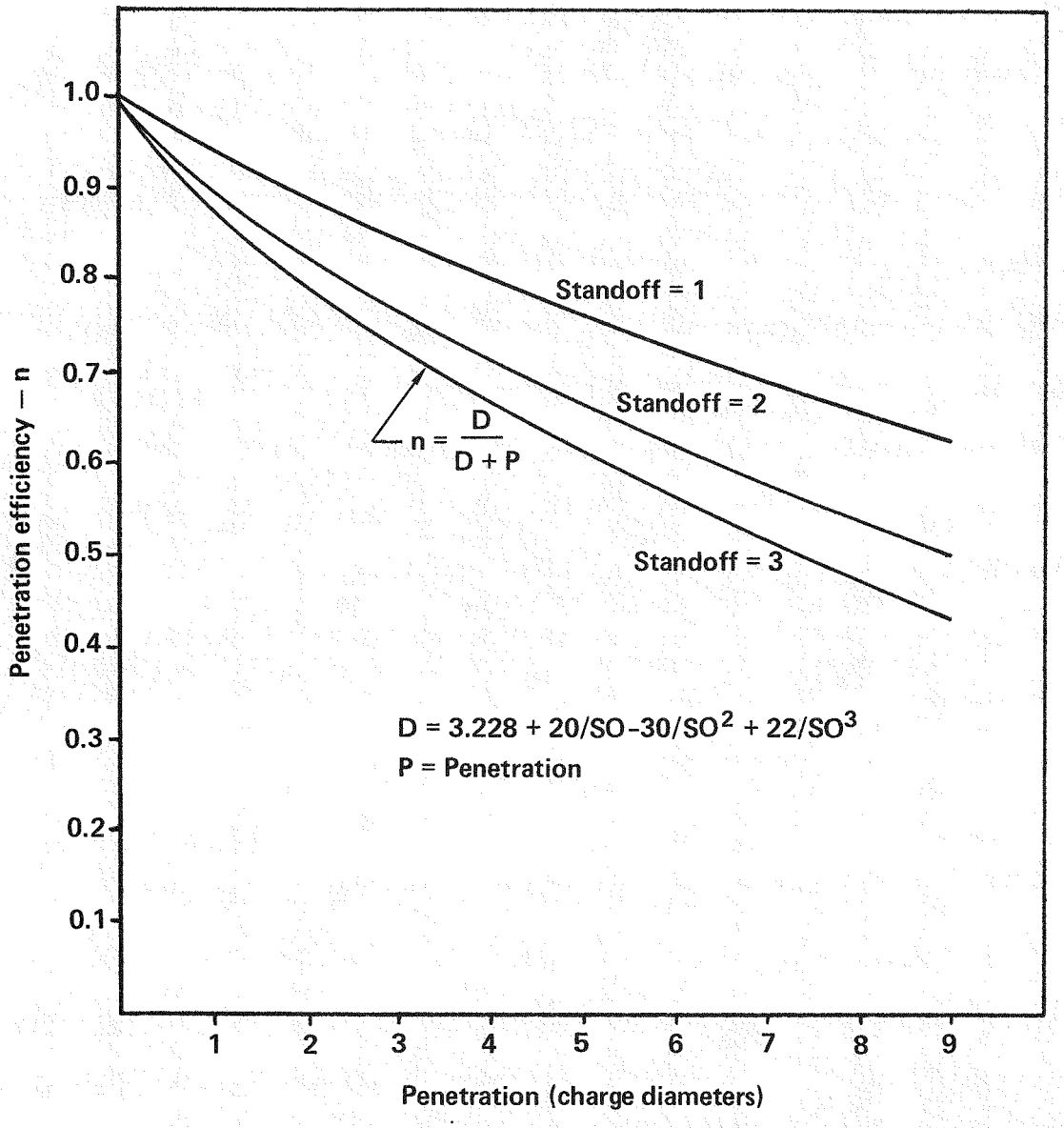

Fig. 32 Jet penetration efficiency versus target penetration

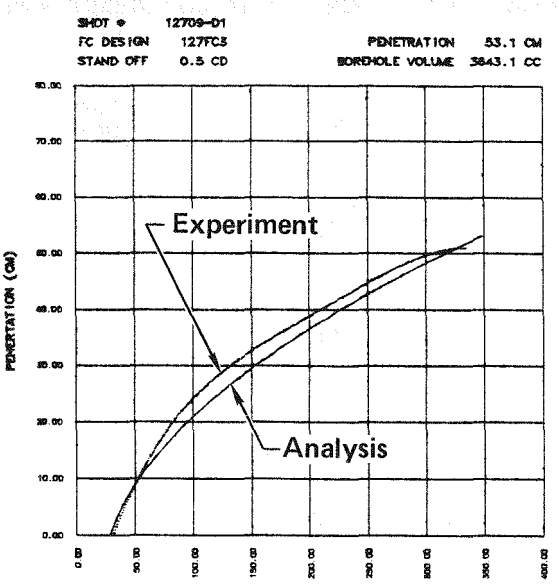

(a) Standoff = 0.5 CD*

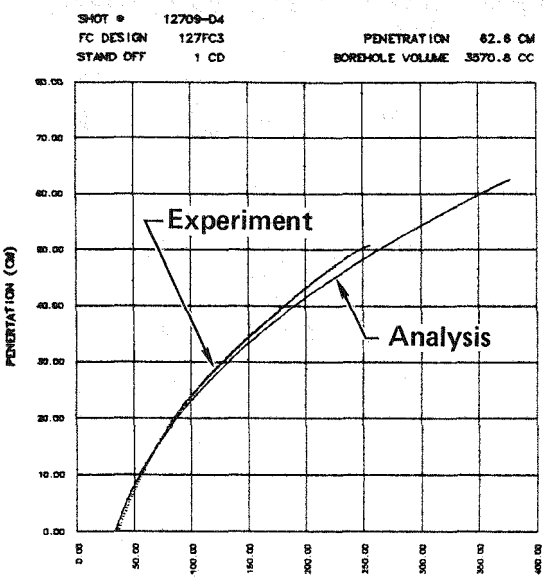

(b) Standoff = 1.0 CD

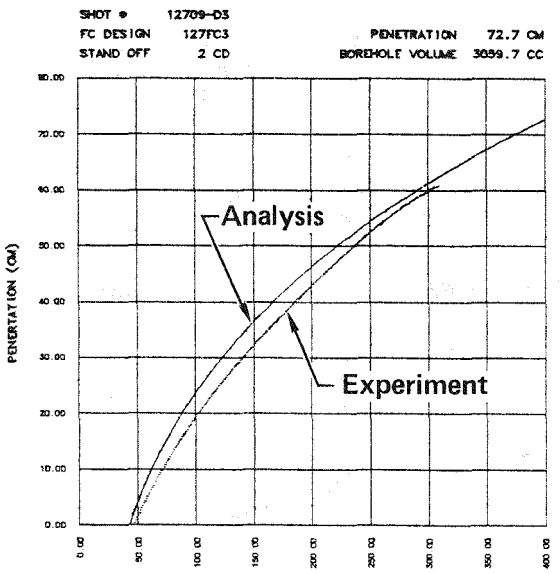

(c) Standoff = 2.0 CD

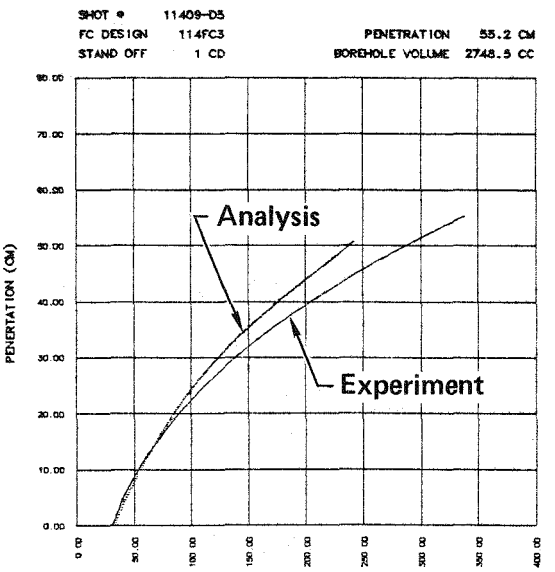

(d) Standoff = 1.0 CD

*CD: Shaped charge cone diameters

Fig. 33 Experimental/analytical correlation of penetration at various standoffs

TOTAL PENETRATION AND HOLE PROFILE EXPERIMENTS

Penetration/hole profile experiments are required to determine the total depth of penetration and hole profile in the target. The configuration used in these experiments is shown in Fig. 34. In these experiments the target consists of three 10 x 10 x 1 ft thick 3000 psi unreinforced concrete blocks that are grouted together. The shaped charge is alligned normal to the target at a standoff distance that varies from 0.75 to 3 charge diameters as shown in Frame (a). Three layers of materials act as a target surface momentum trap to minimize the front surface spall typical of concrete target experiments.

As the jet impacts and penetrates the target, a pressure greater than 1 Mbar exist in the interaction region. A spherical pressure wave propagates radially outward from this reqion and reflects from the front surface of the target as a tensile stress causing a large surface crater to exist due to target spall. With the current analytical method being developed, the target spall effects are not being modeled. Thus, target spall tends to obscure the experimental data that is desired. To minimize the spall, the three layers of materials act as a momentum trap. As the compressive pressure wave reaches the front surface of the target it propagates into the materials becoming "traped" in them as they essentially jump away from the target. Frame (b) of Fig. 34 shows a photograph of the actual target at the test location. Both two- and three-foot thick targets are shown in this figure.

The hole in the target is vacuumed out at the completion of each experiment. The total depth of penetration is first measured

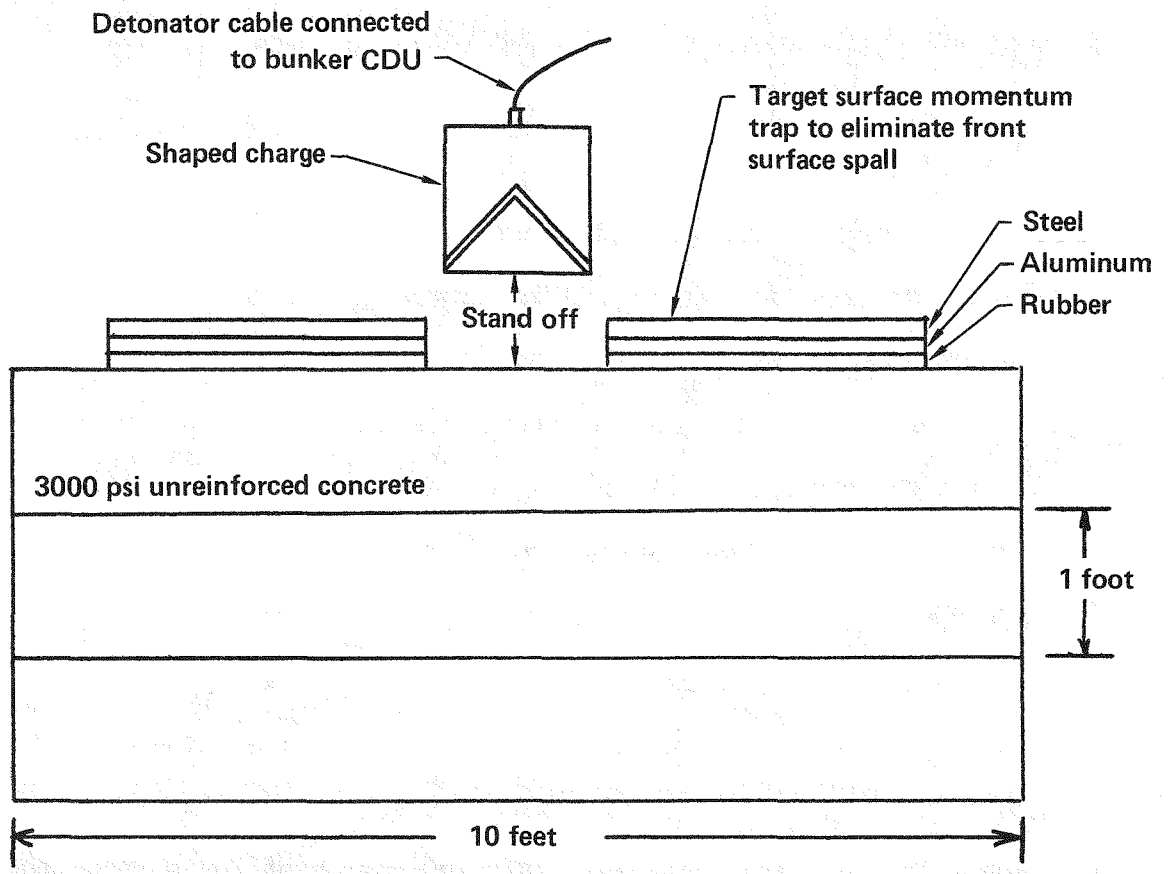

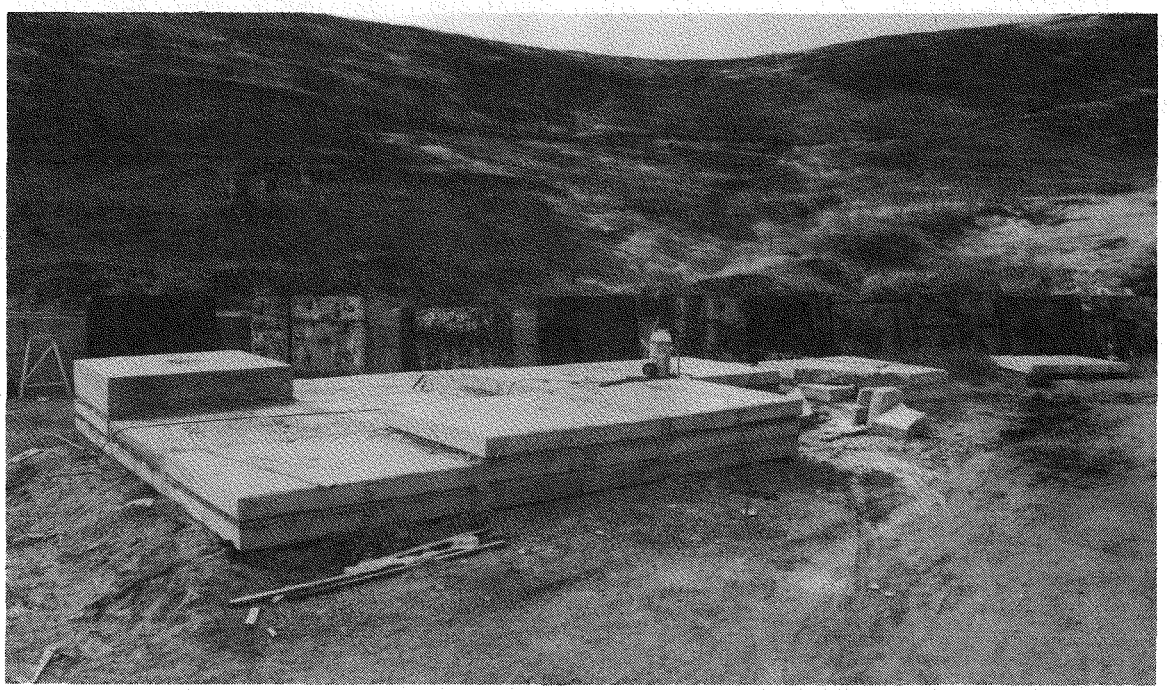

Fig. 34 Configuration of penetration/hole profile experiments

and recorded. The hole is then sequentially backfilled with sand to determine the hole profile. A known volume of sand is added and the depth to the top of the sand is measured. In this way, the incremental volume associated with an incremental depth is used to calculate the hole radius as a function of depth. Using this method the hole profiles presented in Fig. 35 are generated. These frames show the experimental hole profiles for four standoffs; 0.75, 1, 2, and 3 charge diameters. The dashed lines at the top of each hole indicate the probable hole profile without front surface spall.

TOTAL PENETRATION AND HOLE PROFILE ANALYSIS

The previous comparison of experimental and analytical results give the depth of penetration as a function of time but do not include any prediction of hole radius versus depth. In order to accomplish this, a method for predicting hole profile is required. The most basic model producing acceptable results is the jet energy/target hole volume model. The only parameter necessary to utilize this model is an empirical constant, c, where

$$\text{Hole volume} = \text{Jet energy}/c \qquad \text{V-6}$$

The author could not find published data of the target constant for concrete, however, conversations with C. S. Godfrey[51] of Lawrence Livermore National Laboratory (LLNL) indicated that the value for concrete is approximately 0.003 g/cm-μsec^2. For these experiments a value of 0.0036 g/cm-μsec^2 gives good correlation in the range of standoffs studied for this concrete. The analytical prediction of penetration and hole profile is presented in Fig. 36. Note that as the standoff is increased the penetration increases but

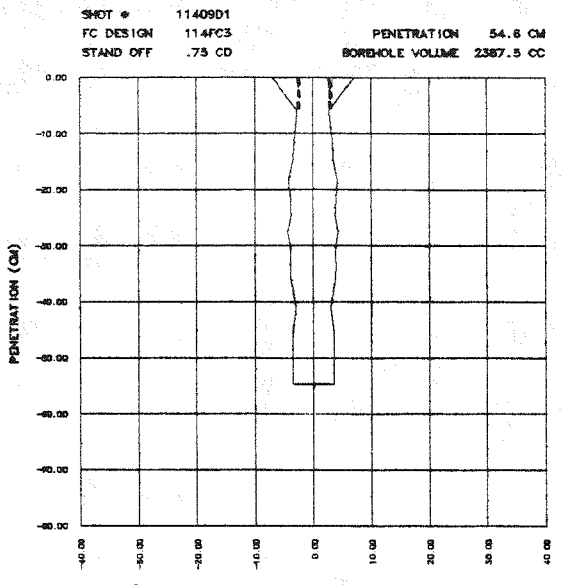

(a) Standoff = 0.75 CD

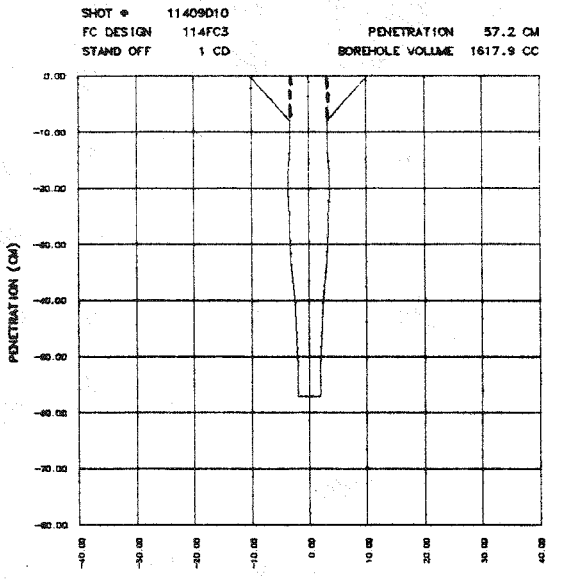

(b) Standoff = 1.0 CD

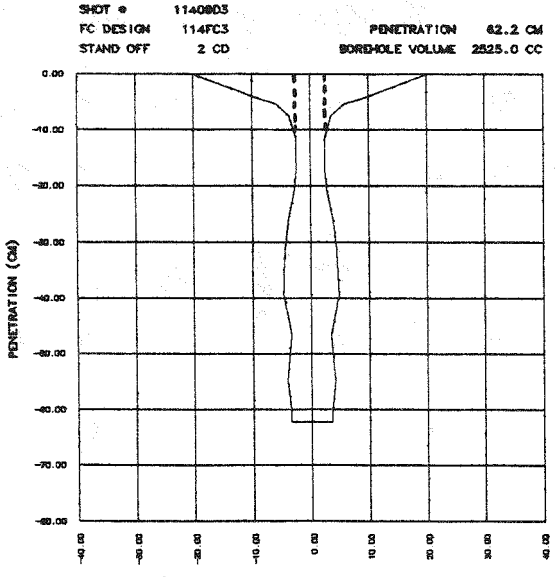

(c) Standoff = 2.0 CD

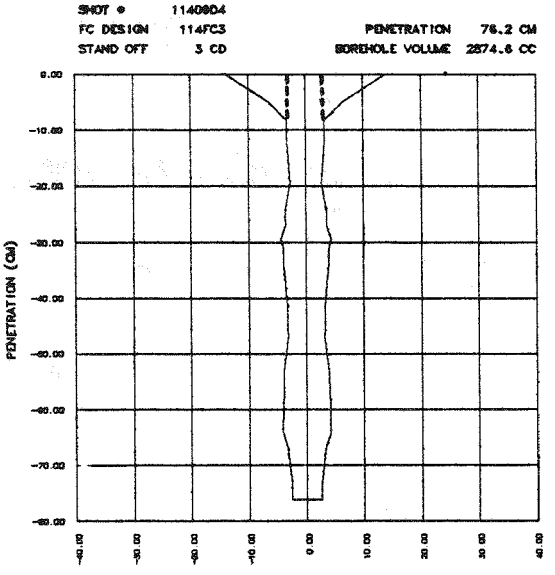

(d) Standoff = 3.0 CD

Fig. 35 Results of penetration and hole profile experiments at various standoffs

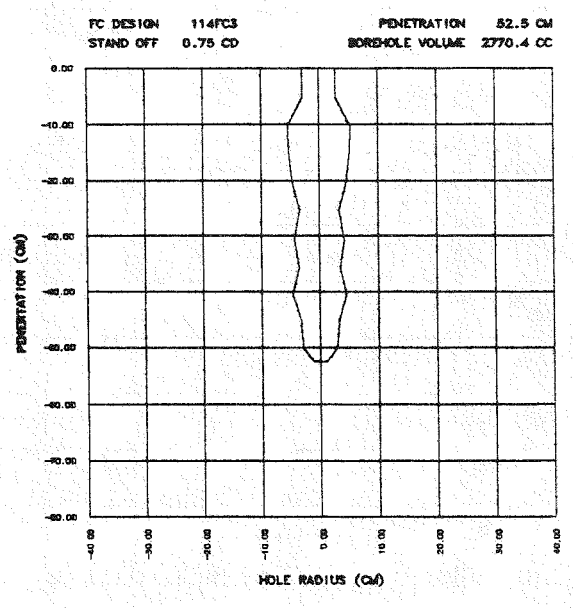

(a) Standoff = 0.75 CD

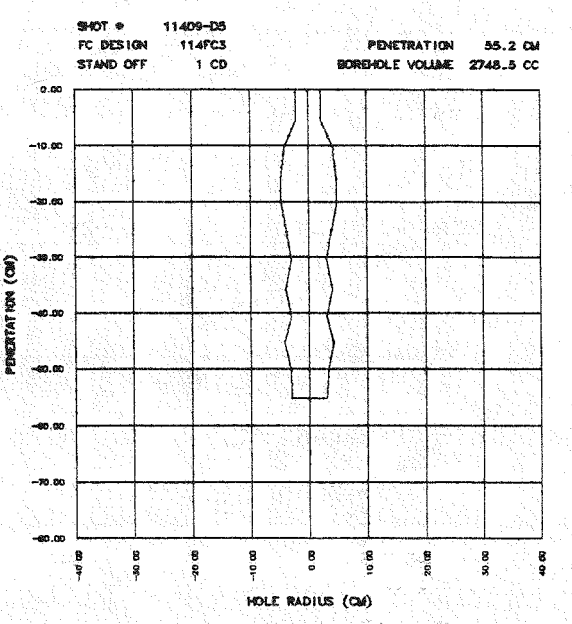

(b) Standoff = 1.0 CD

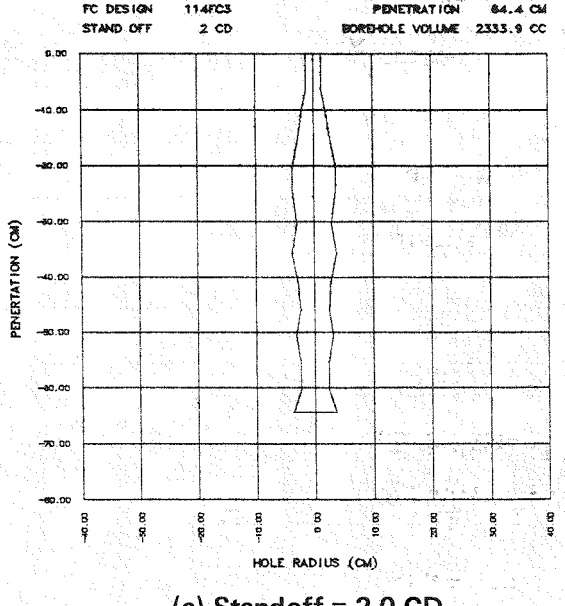

(c) Standoff = 2.0 CD

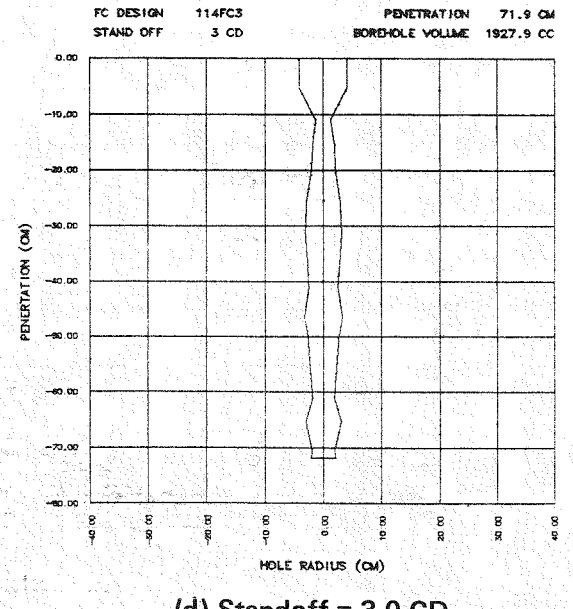

(d) Standoff = 3.0 CD

Fig. 36 Analytical prediction of penetration and hole profile at various standoffs

the borehole diameter and total borehole volume decrease. The borehole diameter decrease is expected because at longer standoffs the jet stretches more, delivering less energy to the target per unit of penetration.

Assume a 1 cm portion of the jet is being considered in a one charge caliber standoff experiment. If this portion of the jet is 1 cm long when it arrives at the target, it will produce a hole in the target proportional to its length with volume proportional to its kinetic energy. For a two charge caliber experiment, this portion of the jet will arrive at the target later in time and will be longer than 1 cm due to the jet velocity gradient. Thus, its increment of penetration will be more than for the one charge caliber experiment but the hole volume from each will be the same because the kinetic energy is the same. To account for the deeper penetration and equal hole volume, the hole diameter must decrease.

When comparing the analytical predictions of borehole volume as a function of standoff, it can be seen that volume decreases with an increase in standoff. The total borehole volume decrease is due to the increase in V_{min} with standoff. As V_{min} is increased, less of the jet material (and ultimately less kinetic energy) is available for jet/target interaction because all jet elements at velocities less than V_{min} are not allowed to interact with the target.

SUMMARY

A summary of the experimental and analytical penetration and hole profile results is presented in Fig. 37. Frame (a) shows that

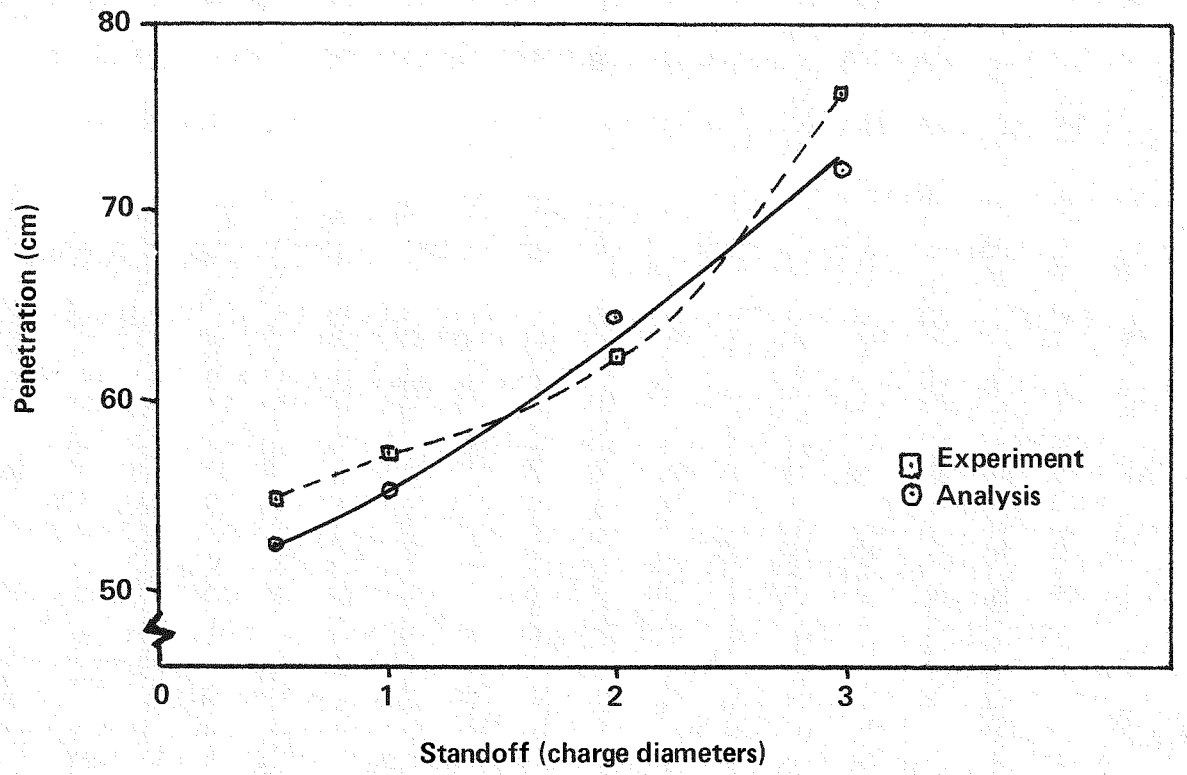

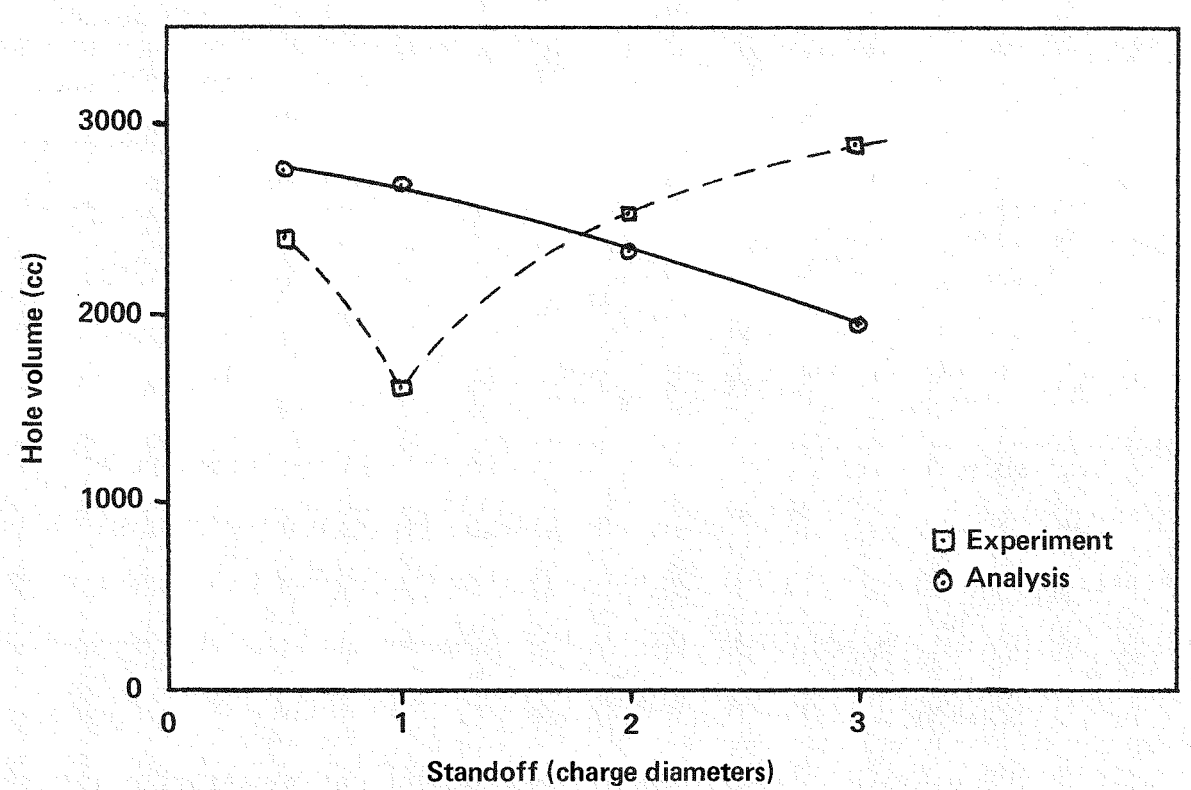

Fig. 37 Summary of experimental/analytical correlation for penetration and hole volume

the penetration depth as a function of standoff is accurately being predicted. Frame (b) shows that the experimental scatter for the hole volume is too large to distinguish whether a trend exists. However, the predictions are well within the bandwidth of the experimental data. DiPersio, Simon, and Merendino have shown that hole profiles for nonprecision shaped charges cannot be accurately predicted by theory because jet waver causes very noncircular and nonreproducible holes in metallic targets. Since this is not a "precision" shaped charge it is possible that nonreproducible target holes are the result of shot-to-shot variations in the jet.

A computer model has been developed and verified with experimental results for one shaped charge design over a small range of standoff distances. To study the applicability of this computer model, the following section investigates the effect of liner angle and liner thickness on the penetration and hole profile.

VI. APPLICATION OF COMPUTER MODEL

LINER ANGLE STUDY -- 8% THICK LINER

The configuration of the shaped charge used in the 8% thick liner angle study is shown in Fig. 38. Liner angles tested using this configuration are 75, 90, 105, and 120 degrees. Liner material for the design is 6061-T6 aluminum and the explosive type is C-4. The head height (distance from liner cone apex to detonator) is held constant and the length of the charge is varied as the liner angle is changed. Experimental results for the four designs are presented in Fig. 39. The critical effects of the liner angle variations can be summarized as follows.

1. Depth of penetration decreases with increasing liner angle.
2. Transition depth (intersection of surface crater with jet borehole) increases with increasing liner angle. Because of the increase transition depth and decrease in penetration with increasing liner angle, the 120 degree experiment results in a large surface crater and no borehole.
3. Borehole volume cannot be correlated to liner angle variations for the experimental data available.

Analytical predictions of the shaped charge jet configurations at 30 μsec for the four designs are presented in Fig. 40. From this figure it can be seen that by increasing the liner angle, the jet length is reduced due to a smaller velocity gradient in the jet A further reduction in tip velocity over the design used in the code calibration study is also realized due to the point initiation scheme. A comparison of a peripheral initiated to point

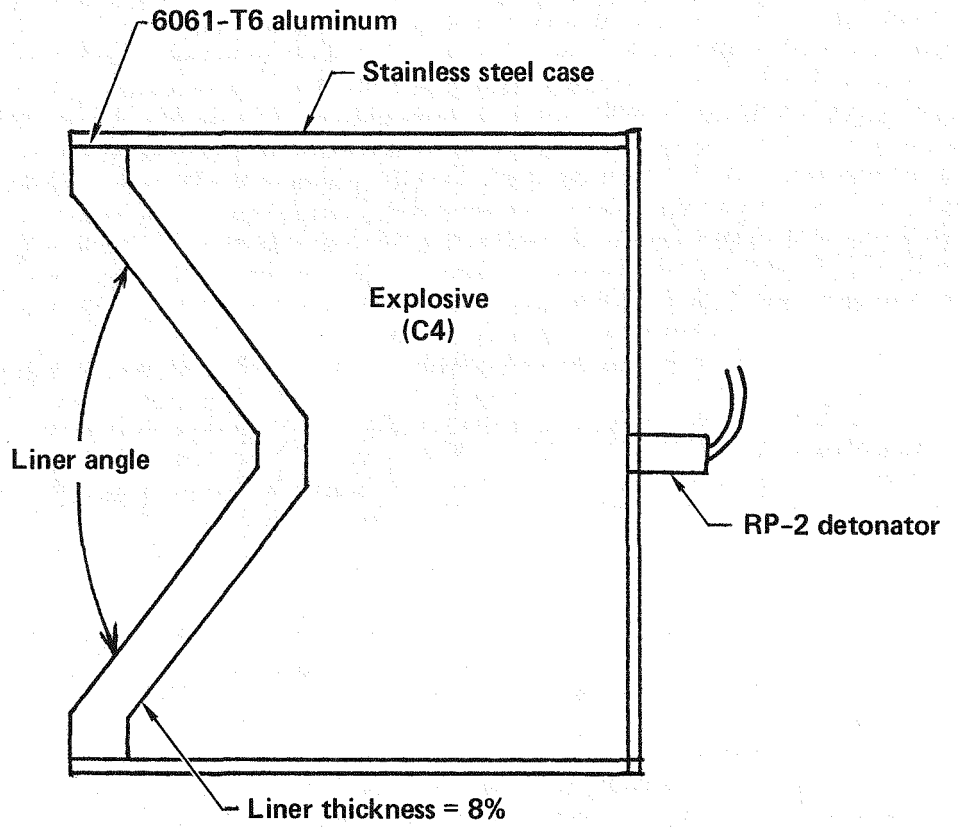

Fig. 38 Configuration of point initiated shaped charge used in 8% liner angle study

Shaped charge	①	②	③	④
Concrete				
Liner angle	75°	90°	105°	120°
Max. depth (cm)	44.5	40.0	31.8	21.6
Trans. depth (cm)	8.9	10.2	15.9	21.6
Borehole diam (cm)	4.1	3.8	6.4	–
Borehole volume (cm^3)	766	641	742	–

Fig. 39 Experimental results for 8% liner angle study

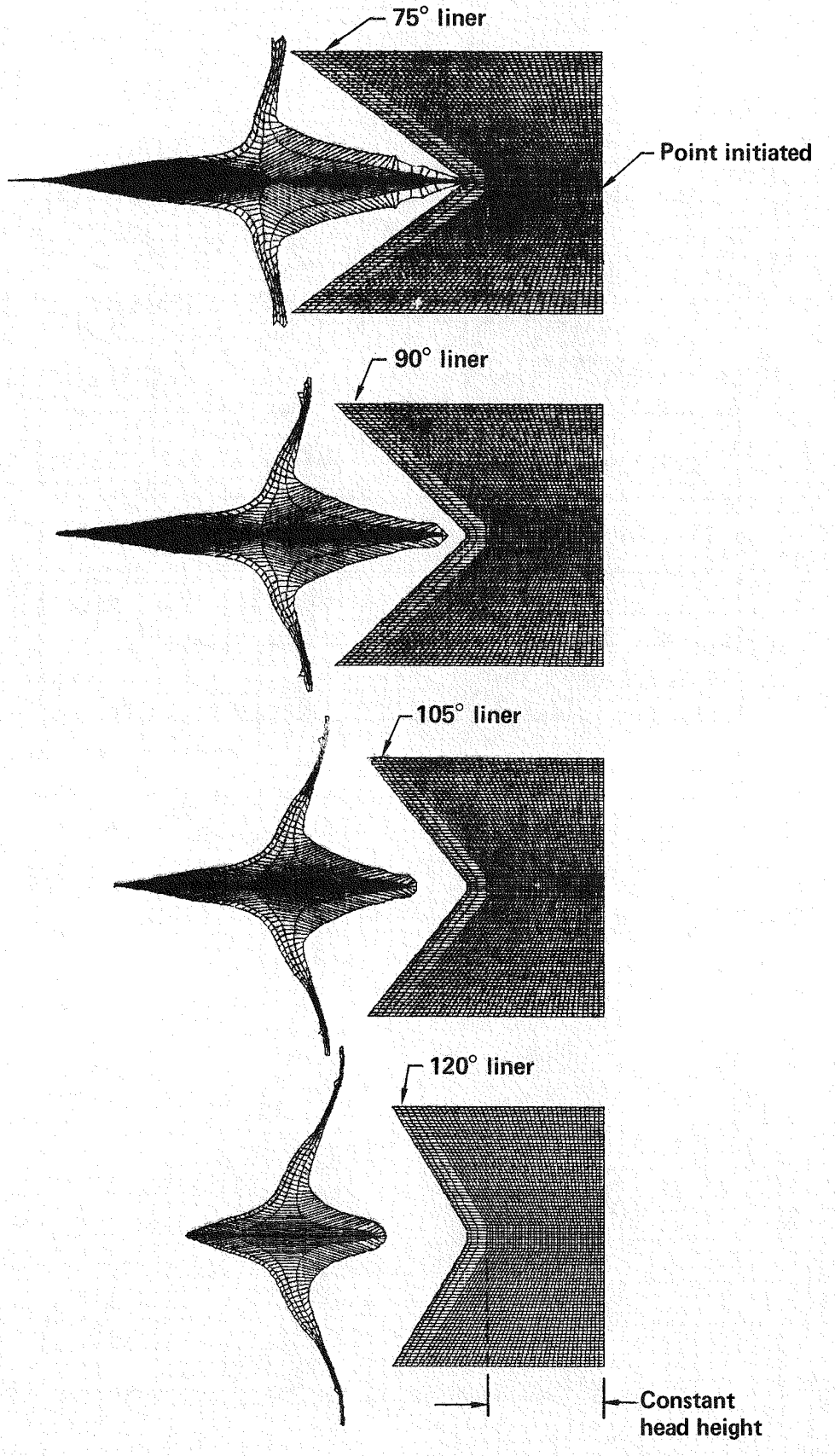

Fig. 40 Analytical configuration of shaped charges and jets at 30 μsec

initiated jet is shown in Fig. 41. The peripheral initiated shape charge jet has a tip velocity of 1.2 cm/μsec while the point initiated jet tip velocity is only 0.5 cm/μsec. An attempt to predict the jet penetration of the point initiated charge using the V_{min} as determined for the peripheral initiated charge results in substantial under prediction of the actual penetration. This indicates that the V_{min} for a slow moving jet should be less than for a fast moving jet. This is reasonable when it is pointed out that V_{min} is a function of standoff which means it is also a function of jet length at target impact. For a stretching jet (due to the velocity gradient) the overall length is controlled by the standoff distance and tip-tail velocity difference.

Since the original experiments all used the same shaped charge, with the same tip velocity and velocity gradient, the effect of tip velocity and velocity gradient has not been assessed. To account for the change in V_{min} for low tip velocity shaped charges, a reduction in V_{min} is introduced. The method for determining the reduction in V_{min} is to correlate the 105 degree 4% liner analysis to the experiment by varying the originally calculated V_{min} and then check the correlation for the other three liner angle designs by equally scaling them. The experimental/analytical comparisons of penetration and hole volume using this method are presented in Fig. 42. Frame (a) shows that the simple modification to V_{min} produces good correlation for the other three liner angles. Frame (b) shows that analytical predictions of hole profile, and ultimately hole volume, are low by approximately 25%. Potential reasons for the low predictions are:

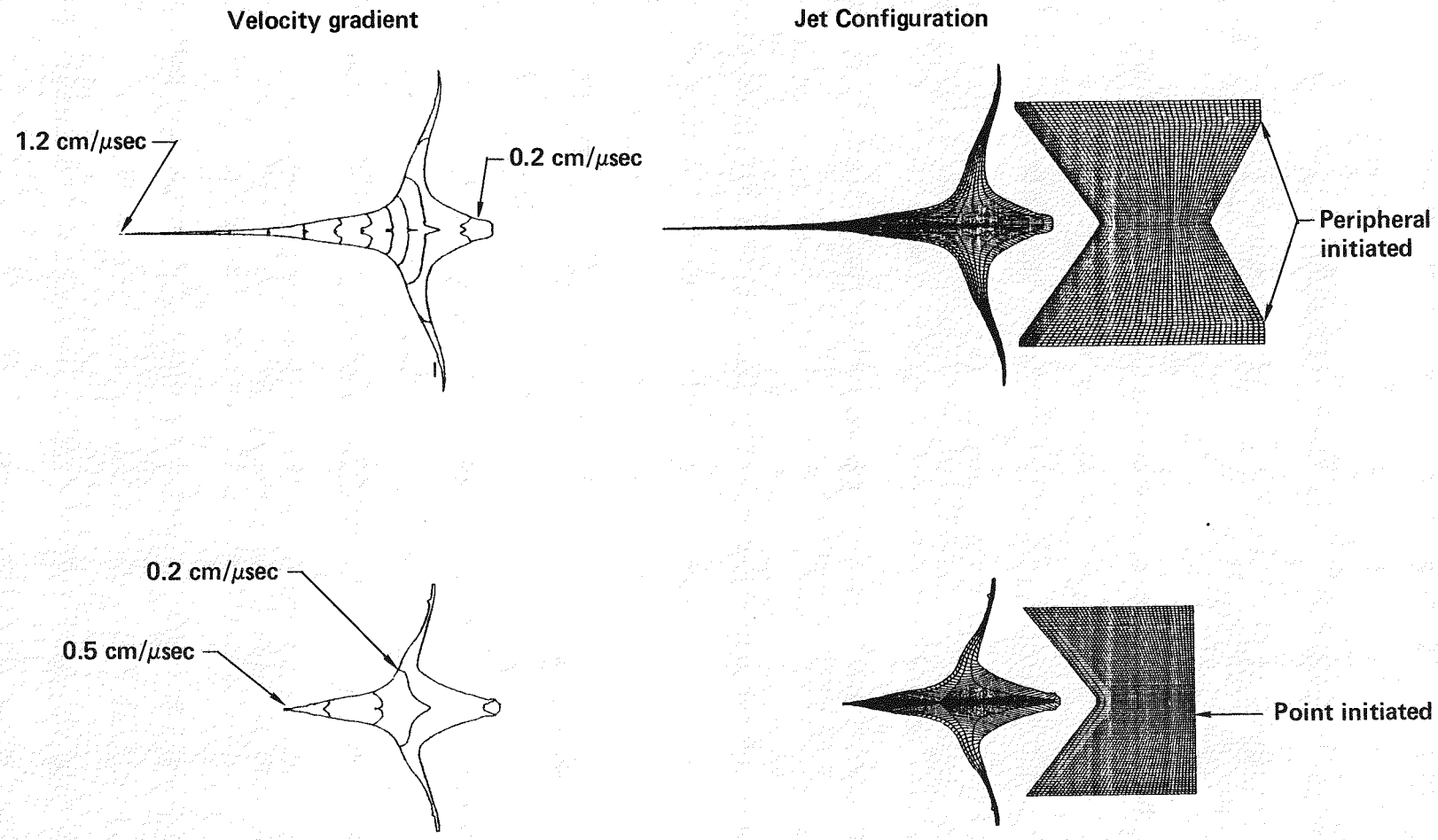

Fig. 41 Comparison of peripheral and point initiated jets at 30 μsec

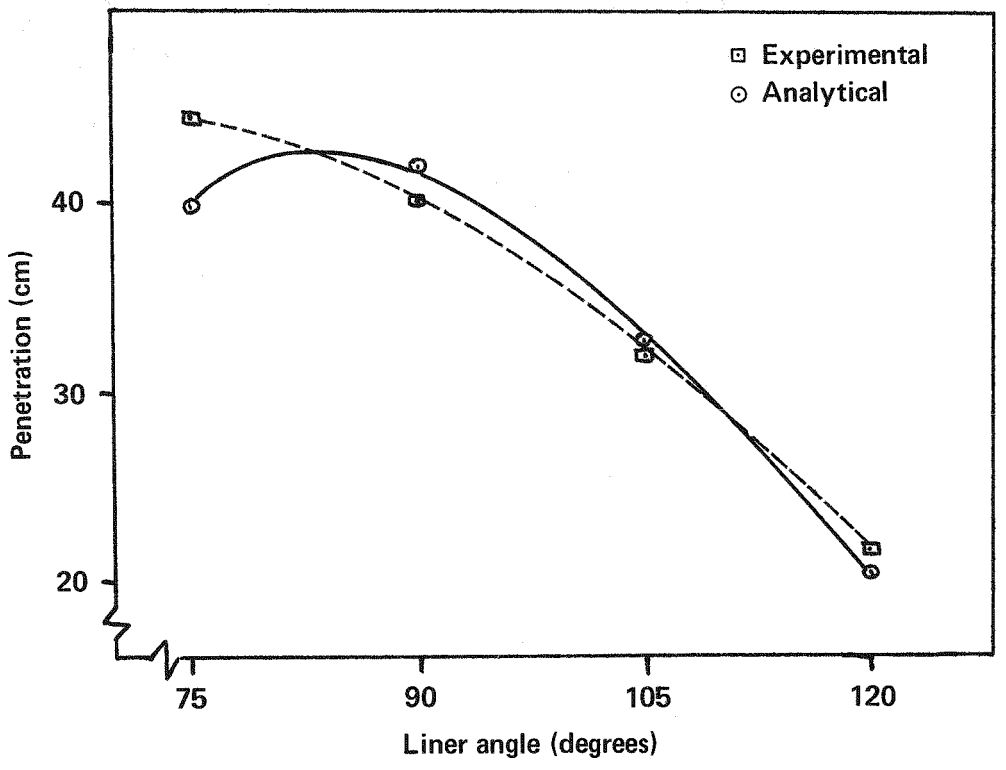

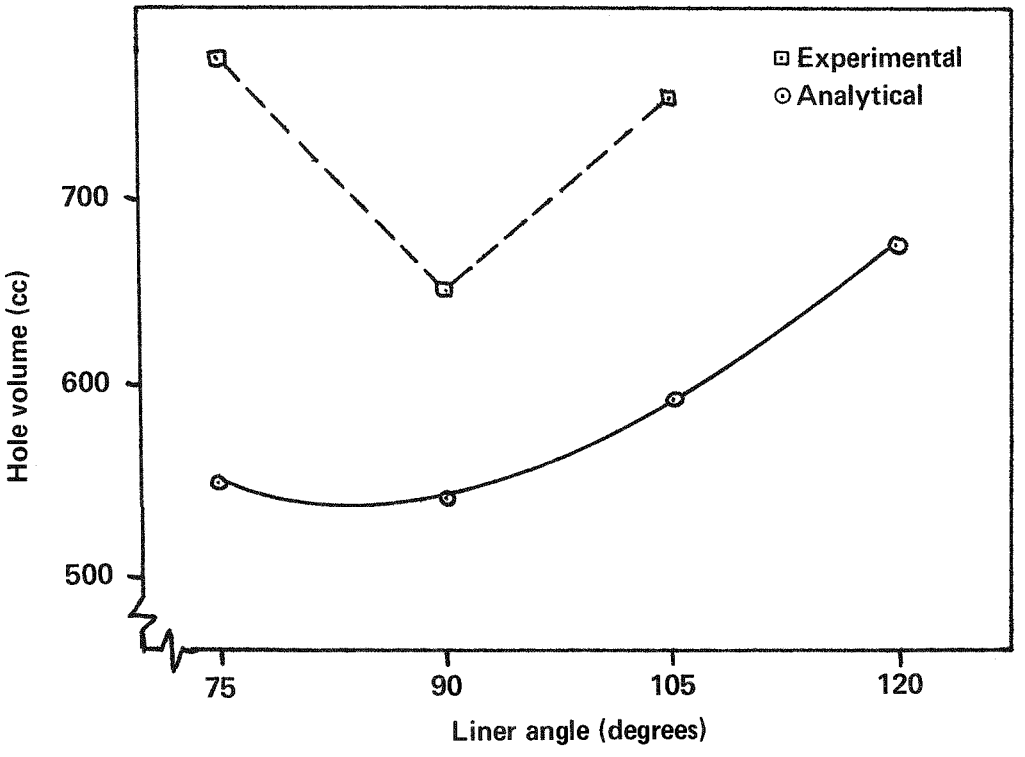

Fig. 42 Experimental/analytical comparison of penetration and hole volume for liner angle study

1) lack of experimental data (due to one shot statistics);

2) the jet energy/hole volume constant may be different due to a different target material. This target was made by a different contractor three years prior to the manufacture of the project targets.

The 8% thick liner angle study shows the code accurately predicts the penetration process when a modification to V_{min} for point initiated charges is accounted for. The experimental data shows that a trend exists in penetration when the liner angle is varied and that the analytical method accurately predicts the trend. With respect to hole volume, a definite trend in the experimental data is not observed. It appears, however, that the code underpredicts the hole volume for this target.

LINER ANGLE AND LINER THICKNESS STUDY

To further investigate the applicability of the code, a study of the effect of liner angle and liner thickness variations is presented. The configuration of the shaped charge is shown in Fig. 43. This is a point initiated design with octol explosive. In this study, the liner thickness is first held constant at 4% while the liner angle is varied from 100 to 120 degrees. The liner angle is then held constant at 105 degrees while the liner thickness is varied from 2% to 8%. Figure 44 summarizes the experimental results for the eight shaped charges. There are two definite trends that can be observed:

1) as the liner angle is increased from 100 to 120 degrees the depth of penetration decreases;

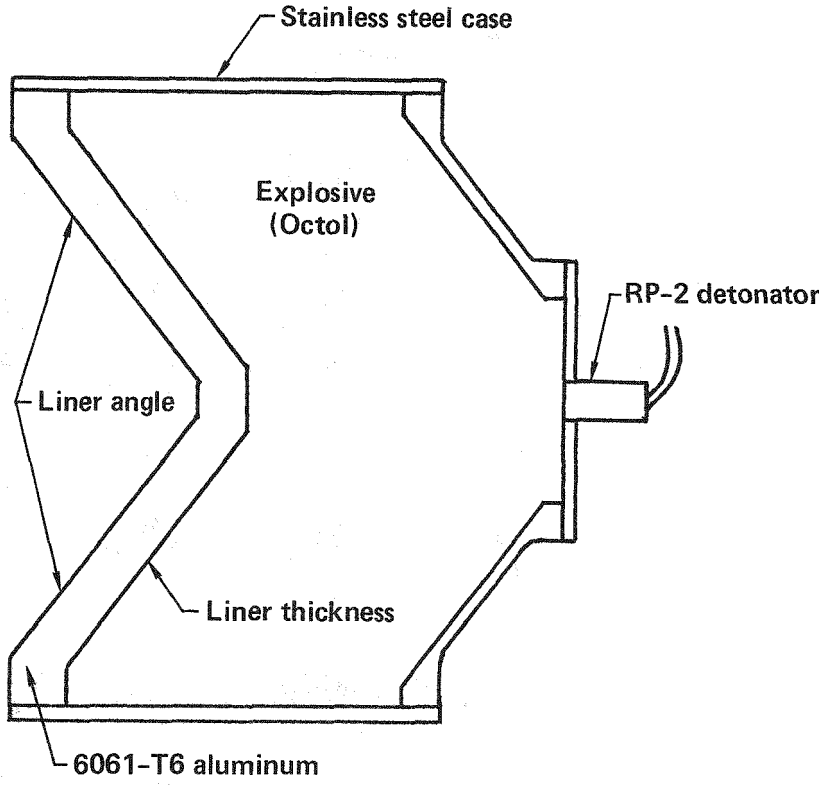

Liner angle = 100, 105, 110, 115, 120 degrees (4%)
Liner thickness = 2%, 4%, 6%, 8% (105 degrees)

Fig. 43 Configuration of point initiated shaped charge used in liner angle and liner thickness study

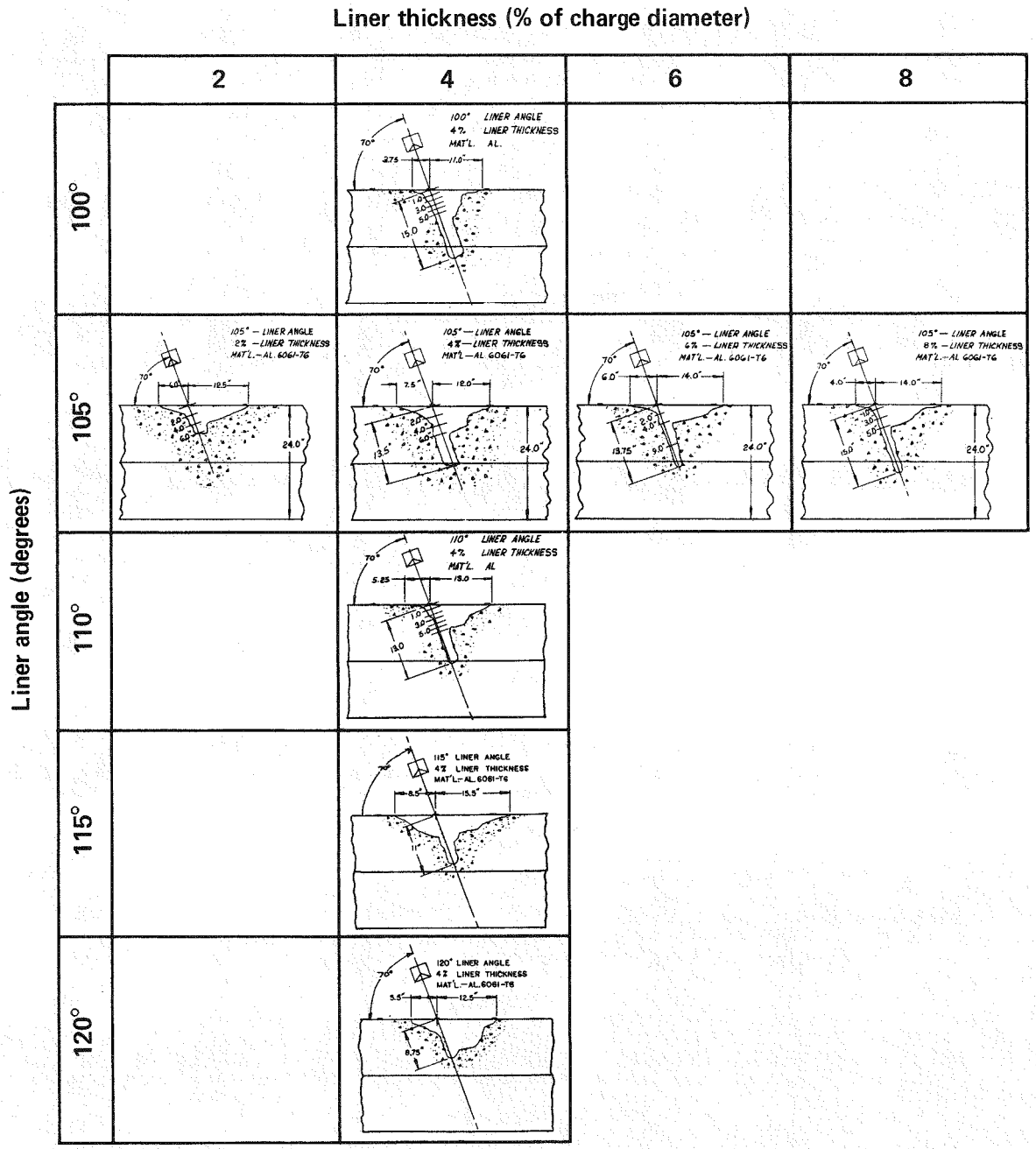

Fig. 44 Experimental results of the liner angle and liner thickness study

2) as the liner thickness is increased from 2% to 8% the depth of penetration increases.

The analytical configurations of the shaped charge jets for the liner angle study are given in Fig. 45. The most important information that can be extracted from this figure is that as the liner angle is increased from 100 to 120 degrees the overall jet length decreases due to a lower tip and higher tail velocity. Since the basic hydrodynamic theory shows the depth of penetration is proportional to jet length, it would be expected that the corresponding penetration would be less for the larger angle charge designs with shorter jet lengths .

The analytical configurations of the shaped charge jets from the liner thickness study are presented in Fig. 46. This figure shows that the 2% jet is shorter and moving faster than the 4, 6, and 8% designs which appear to be similar in length and velocity. The analytical predictions of the hole profiles are shown in Fig. 47. The figure shows the trend observed in the experimental data as the liner angle is varied from 100 to 120 degrees is predicted accurately with the code. However, the experimental trend as the liner thickness is varied is not predicted. A more graphical description of the experimental and analytical correlation is seen in Fig. 48. Frame (a) shows that the trend for lower penetration as liner angle is increased is modeled by the code. However, an overprediction of the penetration of approximately 25% is also observed. A further modification of V_{min} could reduce this deviation although more experimental data are needed before a complete understanding of the parameters controlling V_{min} can be

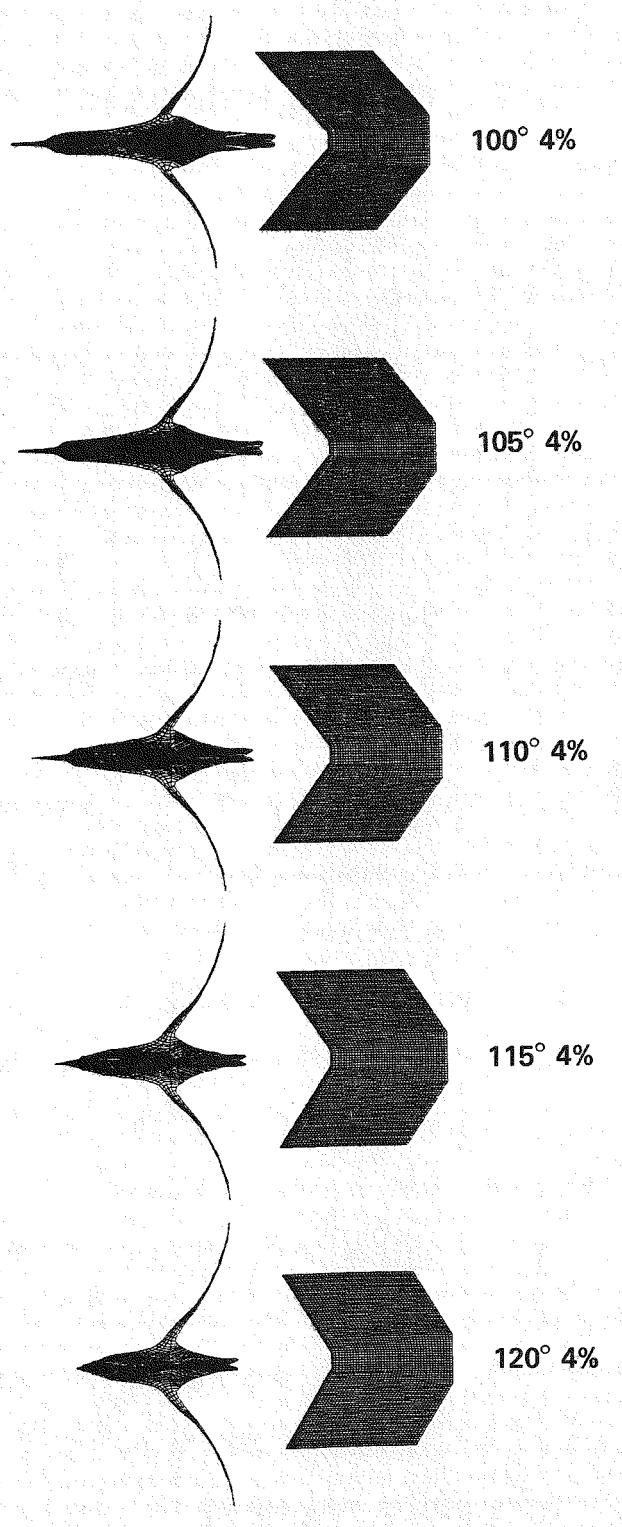

Fig. 45 Analytical configuration of shaped charge jets from liner angle study

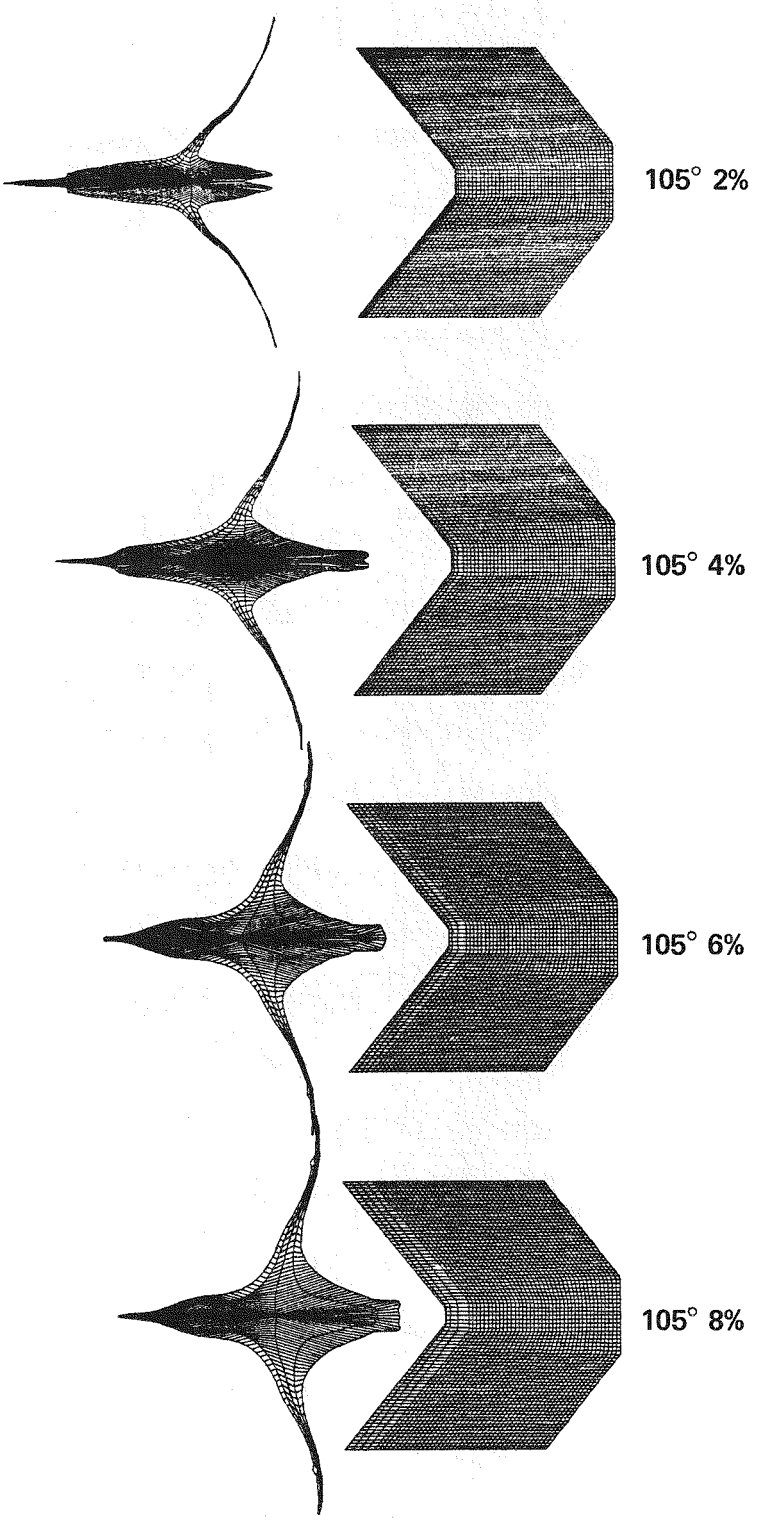

Fig. 46 Analytical configurations of shaped charge jets from the liner thickness study

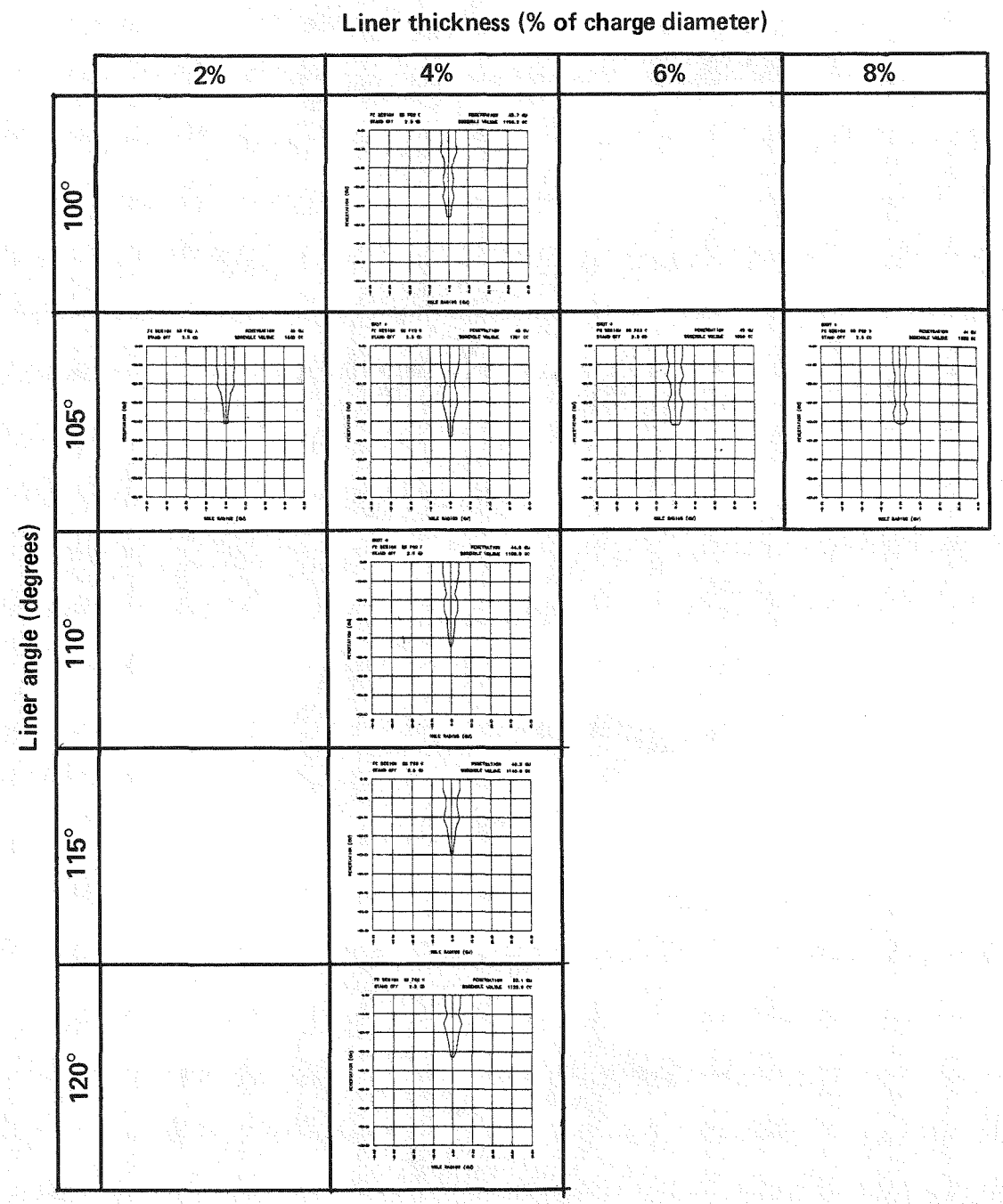

Fig. 47 Analytical prediction of the liner angle and liner thickness study

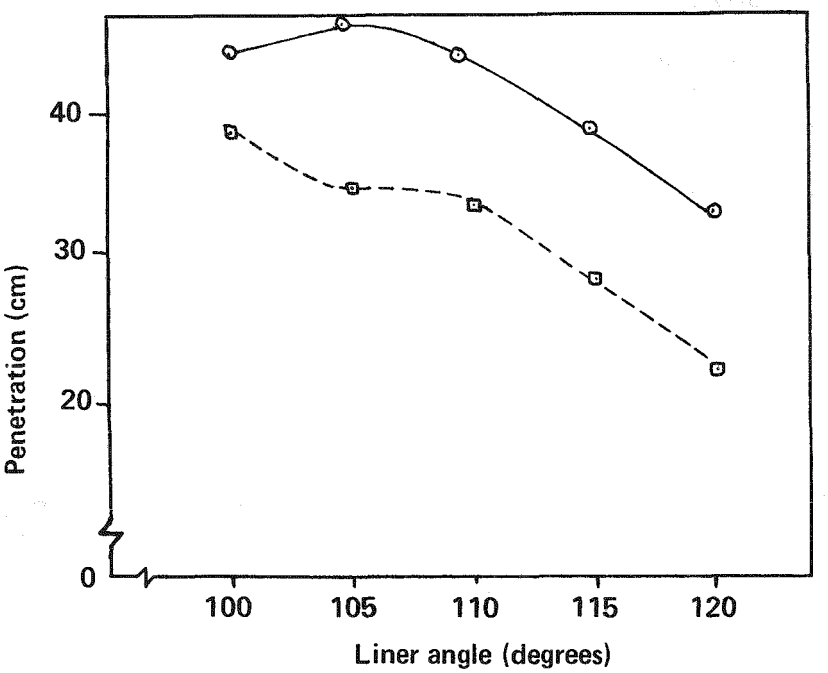

(a) Penetration vs liner angle

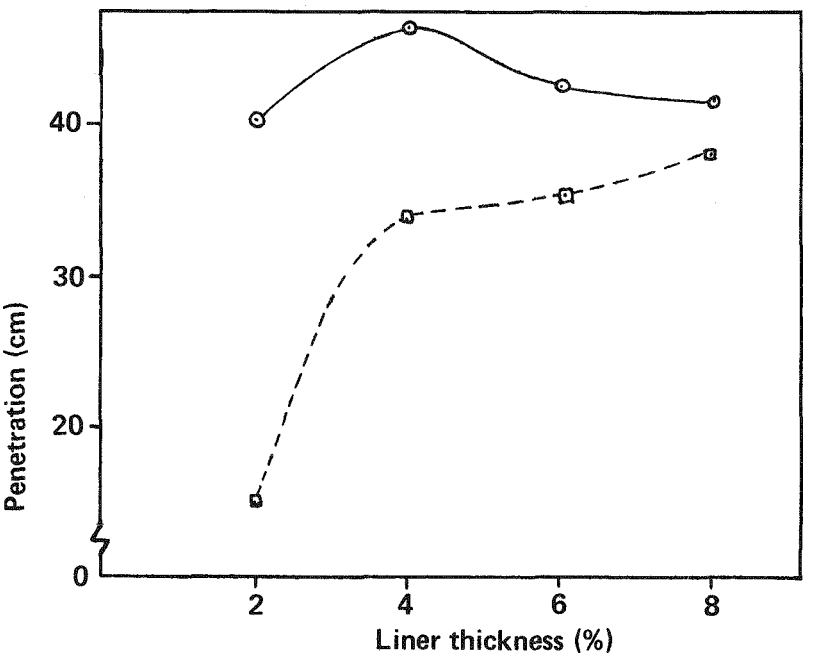

(b) Penetration vs liner thickness

Fig. 48 Comparison of experimental and analytical penetration versus liner thickness and liner angle

obtained. Frame (b) shows the comparison of penetration as the liner thickness is varied. Aside from the 2% experiment, the correlation is acceptable. It is hypothesized that with the 2% experiment the liner is too thin and a material failure may cause nonsymmetries in the jet. Such problems are not accounted for analytically because the code solves an idealized problem. In summary, it is clear that the code is accurately predicting experimental trends and the absolute magnitude of the predictions are within 25%.

VII. CONCLUSIONS

APPLICATION OF COMPUTER MODEL

A unified analytical approach to the solution of the shaped charge penetration problem in concrete has been developed. The analytical technique for describing the jet configuration of a generalized shape charge design has been verified and the corresponding penetration of the jet is correlated to experimental results. The penetration time history is predicted when the empirical parameter V_{min} is defined for the short standoff regime and when the nonidealized jet/target interactions are taken into account in the form of a penetration efficiency parameter η. The jet energy/target hole volume method of predicting the hole profile produces adequate results for a target constant $c = 0.0036$ g/cm-μsec^2. The analytical model, developed through correlation to experimental results using the peripherally initiated shaped charge design, can be applied to a wide range of shaped charge designs. Experimental/analytical correlation for liner angles varying from 75 to 120 degrees and for 2 to 8% thick liners indicates the method will work for a generalized shaped charge design. As long as the material properties are known and a mesh of the shaped charge design can be generated and analyzed, the analytical method will work. The overall conclusion is the method developed applies to a unified approach to the penetration problem of a generalized shaped charge design and a concrete target.

LIMITATIONS OF COMPUTER MODEL

1. The appropriate material models for the liner and high explosive must be known. This limitation is not constricting because the equations of state for most metals and explosives are easily obtainable from Refs. 39 and 40.

2. The shaped charge design must be able to be analyzed by a finite element code. This limitation is not constricting as the finite element method is a generalized method which will accept most any design configuration.

3. V_{min} may need to be redefined for jet/target combinations where the jet-to-target density is different than approximately 1. This would involve new penetration-time experiments.

4. The jet energy/hole volume constant will need to be redefined for a new target. This would involve additional shaped charge penetration and hole profile experiments in the new target. Correlation of the experimental results with analytical predictions will define the appropriate target constant.

5. The computer model solves the hydrodynamic portion of the penetration problem but does not consider the spall effects at the target surface. This limitation becomes more pronounced when the function of the shaped charge is to precondition a target for a subsequent projectile that is to follow into the hole.

6. The computer model is not specifically designed to solve nonnormal impact problems, although the hydrodynamic portion of the penetration process should be independent of target impact angle.

RECOMMENDATIONS FOR FURTHER STUDY

1. Penetration -- The current analytical method employs the basic Bernoulli penetration model. More complicated models, such as those proposed by Walters and Majerus, which take into account target viscosity and jet and target flow may provide for a more generalized description of the target. An area of further study would be to incorporate a more complicated penetration model in the code so that empirical target parameters could be replaced by basic target material properties.

2. Hole Profile -- A similar area for further study is the prediction of target hole profile. The current analytical method applies the basic jet energy/hole volume method of determining hole profile. A few more complicated methods discussed in the theory section could be incorporated into the code eliminating the need for the target constant, C, that is required with every target being considered.

3. Target Front Surface Spall -- An analytical method for determining the spall of the target front surface is desirable. A more complicated hole profile method, as

described in 2, is required to incorporate this capability into the code.

4. Oblique Angle Impact -- The effect of large oblique angle impacts is an area for potential study. Specifically, the determination of the typically nonsymmetric spall crater that is evidenced in oblique angle experiments would be useful.

5. Layered Targets -- A layered target capability would be useful for a number of practical targets (spaced armor, roadways or buildings). Incorporation of the layered target capability would make the code a more versatile tool.

VIII. REFERENCES

[1] G. Birkhoff, D. P. McDougal, E. M. Pugh, and G. I. Taylor, "Explosive with Lined Cavities," J. Appl. Phys., 19, 563, 1948.

[2] R. R. Rollings, G. B. Clark, and H. N. Kalia, "Penetration in Granite by Shaped Charge Liners of Various Metals," University of Missouri, Rolla Report RMERC-TR-70-13, April 1971.

[3] F. A. Baum, R. P. Stanykovich, and B. I. Skekter, Physics of an Explosion, (AD 400151), New York, Research Information Service, 546, 1949.

[4] R. J. Eichelberger, "Re-Examination of the Theories of Jet Formation and Target Penetration by Lined Cavity Charges," Doctoral Dissertation, Carnegie Institute of Technology, Pittsburgh, Pa, 1954.

[5] J. Simon, R. DiPersio, "Jet Formation and Utilization," 12th Annual Symposium on Behavior and Utilization of Explosives in Engineering Design, 1972.

[6] J. S. Reinhart and R. D. Cocanower, "Concerning the Design of an Effective Shaped Charge for Oil Well Perforating," J. Appl. Phys., Vol. 30, pp 680-682, May 1959.

[7] C. F. Austin, "Lined Cavity Shaped Charges and Their Use in Rock and Earth Materials," Bulletin 59, New Mexico Inst. Min. and Tech., State Bureau of Mines and Mineral Research, 1959.

[8] C. F. Austin and J. K. Pringle, "Detailed Response of Some Rock Targets to Jets from Lined Cavity Charges, J. Petroleum Tech., January 1964.

[9] C. F. Austin, "Lined Cavity Shaped Charge and Its Use as a Drilling Tool, Trans. AIME, Vol. 220, p. 123, 1961.

[10] Demolition Materials, Bureau of Naval Weapons Ordnance Phamplet, NAVEWPS OP 2212, February 1962.

[11] Applications of Lined Cavity Charges, Navy Bureau of Ordnance, OP 1647, June 1946.

[12] C.M. Cox, "Linear and Conical Shaped Charge Performance," Firestone Tire and Rubber Company, Defense Research Division, Akron, Ohio, April 1964.

[13] W. G. Soper, Performance of Linear Shaped Charge, USNWL, Dahlgren, Virginia, Naval Weapons Laboratory, NWL Report No. 1946, NAVWEPS Report No. 8346, September 1964.

[14] R. G. S. Sewell, "Effects of Velocity and Material Properties on Design Limits for Linear Shaped Charges," U. S. Naval Ordnance Test Station, China Lake, Ca., October 1965.

[15] A. Merendino, J. M. Regan, and S. Kronman, "A Method of Obtaining a Massive Hypervelocity Pellet from a Shaped Charge Jet," Ballistic Research Laboratory, BRLM Report No. 1508, APG, Maryland, August 1963.

[16] E. M. Pugh, R. J. Eichelberger, and N. Rostaker, "Theory of Jet Formation by Charges with Lined Conical Cavities," J. Appl. Phys., 23, 532, 1952.

[17] J. T. Harrison, "Improved Analytical Shaped Charge Code: BASC," Ballistic Research Laboratory, Technical Report ARBRL-TR-02300, March 1981.

[18] Cray Research Incorporated, CRAY-1 Computer System CFT Reference Manual Bloomington, Mn, Publication No. 2240009, 1978.

[19] E. M. Pugh, "A Theory of Target Penetration by Jets," OSRD No. 3752, 1944.

[20] D. C. Pack and W. M. Evans, "Penetration by High-Velocity ('Munroe') Jets: I", Proc. Phys. Soc., 864, 298, 1951.

[21] W. M. Evans and D. C. Pack, "Penetration by High-Velocity ('Munroe') Jets: II," Proc. Phys. Soc., B64, 303, 1951.

[22] G. I. Taylor, "The Use of Flat-Ended Projectiles for Determining Dynamic Yield Stress," Proc. Royal Soc., A194, 287, 1948.

[23] M. A. Cook, "Mechanisms in Cratering in Ultra High Velocity Impacts," J. Appl. Phys., 30, 725, 1958.

[24] A. Tate, "Further Results in the Theory of Long Rod Penetrators," J. Mech. Phys. Solids, 17, 141, 1969.

[25] D. R. Cristman and J. W. Gehring, "Analysis of High-Velocity Projectile Penetration Mechanics," J. Appl. Phys., 37, 1579, 1966.

[26] J. B. Feldman, "Volume-Energy Relation from Shaped Charge Jet Penetrations," Proceedings of the 4th Symposium on Hypervelocity Impact, APGC-TR-60-39 (II), AD 244476, 1960.

[27] C. Riparbelli, "A Method to Calculate the Profile of a Crater Produced by a High Velocity Projectile Impacting a Bulky Target," General Dynamics, Pomona, TM 6-122-44.34-21, 1968.

[28] R. DiPersio, J. Simon, and A. Merendino, "Penetration of Shaped Charge Jets into Metallic Targets," Ballistics

Research Laboratory, BRL Report No. 1296, APG, Maryland, 1965.

[29] W. P. Walters, J. N. Majerus, "Impact Models for Penetration and Hole Growth," Ballistic Research Laboratory, Technical Report ARBRL-TR-02069, 1978.

[30] W. P. Walters and J. N. Majerus, "Hypervelocity Impact Models for Hole Growth and Geometry," Proceedings of the 3rd Annual Vulnerability/Survivability Symposium ADPA, Naval Amphibious Base, Coronada, CA, 1977.

[31] J. N. Majerus and W. P. Walters, "Axial Penetration and Radial Growth for Kinetic Enmergy and Shaped Charge Jet Penetrators," Proceedings of the DEA-G-1060 Ballistic Research and Development Meeting, Naval Surface Weapons Center, Dahlgren, Va, 1978.

[32] J. N. Majerus, W. P. Walters, and G. P. Neitzel, "Impact Models for Penetration and Hole Growth," Proceedings of the 4th International Symposium on Ballistics, Monterey, Ca, 1978.

[33] W. P. Walters and J. N. Majerus, "Shaped Charge Penetration Model, Part I: Monolithic Penetration and Comparison with Experimental Data," Ballistic Research Laboratory, Technical Report ARBRL-TR-02184, AD B041747, 1979.

[34] J. N. Majerus and W. P. Walters, "A Predictive Penetration Model Utilizing an Effective-Flow Viscosity of the Interaction Region," Proceedings of the 6th International Symposium on Ballistics, ADPA, October 1981.

[35] M. van Thiel and L. L. Edwards, "Target Response to High Velocity Penetration," Lawrence Livermore National Laboratory, Report UCRL-85904, October 1981.

[36] L. L. Edwards, R. B. Hickman, J. K. Hobson, and T. C. Michels, "CHAMP: A Coupled HEMP and Multifluid Eulerian Program for Fluid Flow Simulations," Lawrence Livermore National Laboratory, Report UCRL-52444, 1978.

[37] J. O. Hallquist, "MAZE - An Input Generator for DYNA2D and NIKE2D," Lawrence Livermore National Laboratory, Report UCID-19029, Rev. 1, 1982.

[38] J. O. Hallquist, "DYNA2D - An Explicit Two-Dimensional Hydrodynamic Finite Element Code with Interactive Rezoning," Lawrence Livermore National Laboratory, Report UCID-18756, Rev. 1, 1982.

[39] D. J. Steinberg, S. G. Cochran, and M. W. Guinan, "A Constitutive Model for Metals Applicable at High-Strain Rates," J. Appl. Phys., 51(3), March 1980.

[40] B. M. Dobratz, Ed., "Properties of Chemical Explosives and Explosive Simulants," Lawrence Livermore National Laboratory, Report UCRL-51319, Rev. 1, 1974.

[41] S. L. Hancock, "An Hourglass Subtraction Procedure," Physics International Company, Technical Memo TCAM 73-6, May 1973.

[42] J. O. Hallquist, "ORION: An Interactive Post-Processor for the Analysis Codes NIKE2D, DYNA2D, and TACO2D," Lawrence Livermore National Laboratory, Report UCID-19310, 1982.

[43] M. J. Murphy, "MJMPEN: A Code for Predicting the Penetration of a Generalized Shaped Charge Design," Lawrence Livermore National Laboratory, Report UCID-19645, 1982.

[44] M. Blair, "The UXDD80 Graphics System," Lawrence Livermore National Laboratory, Report UCID-30146, January 1977.

[45] M. J. Murphy, "Shaped Charge Penetration in Concrete," Memorandum to R. E. Varosh, 1981.

[46] F. E. Allison and G. M. Bryan, "Cratering by a Train of Hypervelocity Fragments," Proceedings of the 2nd Hypervelocity Impact Effects Symposium, Vol. 1, p. 81, December 1975

[47] F. E. Allison and R. Vitali, "A New Method of Computing Penetration Variables for Shaped Charge Jets," Ballistics Research Laboratory, BRL Report No. 1184, APG, Maryland, 1963.

[48] P. C. Chou, E. Hirsch, and W. P. Walters, "The Virtual Origin Approximation of a Shaped Charge Jet," Proceedings of the 6th International Symposium on Ballistics, ADPA, October 1981.

[49] L. E. Bryant, Jr., "Portable Flash X-Ray Systems: Applications and Techniques," presented at the National Spring Conference of the Americal Society for Nondestructive Testing, March 1975.

[50] R. DiPersio and J. Simon, "The Effect of Target Hardness on the Penetration Capability of Shaped Charge jets," Ballistics Research Laboratory, Report 1408, AD 838991, July 1968.

[51] C. S. Godfrey, "Jet Energy/Target Hole Volume Constant for Concrete," personal conversation with M. J. Murphy, Summer 1981.

GPO 687-002/8043